University of Alberta

Effect of Secondary Structure on Surface Adsorption of Peptides

by

Mojtaba Binazadeh

A thesis submitted to the Faculty of Graduate Studies and Research
in partial fulfillment of the requirements for the degree of

Doctor of Philosophy
in
Chemical Engineering

Department of Chemical and Materials Engineering

Fall 2013
Edmonton, Alberta

ABSTRACT

Protein adsorption at the biomaterial-tissue interface has several detrimental consequences which undermines the widespread application of engineered materials. Herein, it was asked what role protein secondary structures play in the adsorption of peptides, as well as how these structures affect the physicochemical properties of the final adsorbed layer on bare gold (Au) and poly (ethylene glycol) (PEG) modified Au surfaces. To this end, α-helices and β-sheets were induced in poly-L-Lysine (PLL) and persistence of these structures in solution and adsorbed state was confirmed by circular dichroism (CD). PLL adsorption to Au surfaces was monitored using quartz crystal microbalance with dissipation (QCM-D). PLL adsorption on bare Au resulted in higher initial adsorption rates for α-helices as compared to β-sheets but the final adsorbed amount of β-sheets was higher than α-helices regardless of solution salt concentration. Viscosities for films formed from α-helices were ~2x that of β-sheets films, regardless of solution ionic strength. β-sheets have higher zeta potential as compared to α-helices. The interaction energy between PLL and Au surface was found to be driven by electrostatic and van der Waals forces. Presence of PEG grafted brush layers on the Au surface drastically reduced the adsorbed amount of different PLL structures and PLL layers adsorbed on PEG coated surfaces had similar layer viscosities.

To further understand PLL adsorption mechanism and adsorbed layer properties, the interacting forces between PLL-Au, PLL-PLL, PEG-mica, and PEG-PLL surfaces were studied by surface forces apparatus (SFA). SFA results

revealed that the adhesion energy of β-sheet vs. Au and β-sheet vs. β-sheet was considerably more than α-helix vs. Au and α-helix vs. α-helix systems respectively. The substrate surface adhesion energy of β-sheet was more dependent on the solution salt concentration as compared to α-helix due to the higher electrostatic interactions of β-sheet PLL film with Au (higher zeta potential value of β-sheet PLL). It was found that presence of PEG grafted layer eliminated the PLL secondary structure effect on adsorption due to the purely repulsive force that governed the PEG vs. PLL interaction.

ACKNOWLEDGEMENT

I would like to thank my supervisors, Dr. Larry D. Unsworth and Dr. Hongbo Zeng, for their guidance, encouragement and support throughout the course of this study. It was Dr. Unsworth who guided me into the world of biomaterials with his immense knowledge. He has always been supportive and has given me a lot of creative ideas when I was stuck in the middle of the experiment. I am also very grateful to Dr. Zeng, who guided me into the field of surface science and intermolecular forces of polymers. After every discussion with Dr. Zeng about my research work, I had to look back at reference books and previous studies and deeply think about the new aspects of the work that he brought up. It was his unique approach to research which kept me highly interested to my PhD project and intellectually satisfied.

I am also very grateful to the members in my group, especially Ali Faghihejad, for their kind help and valuable discussions. I want to also thank Mr. Ghasem Naddaf for his friendship and support. I would like to specially thank my father, mother, and siblings. Last but not the least, I am very grateful to my wife, Fatemeh, who was with me during the course of my PhD. Without their unconditional love, support, and encouragement, I would never be able to live a good life in Canada and to make my PhD studies so smooth.

Contents

LIST OF TABLES

LIST OF FIGURES

Symbols and Nomenclature

A	Hamaker constant, J
C_M	Concentration of peptide or protein, mg/mL
d, D	Normal distance between two surfaces, m
D_f	Dissipation factor
D_{PEO}	Diffusivity of poly ethylene oxide in aqueous solution, $\mu m^2/s$
du/dy	velocity gradient, s^{-1}
$\Delta l/H$	shear strain
e	Electron charge, 1.602×10^{-19} C
E_L	Circularly polarized light (counter clockwise rotation)
E_R	Circularly polarized light (clockwise rotation)
ΔE	Difference of light absorbance
$E_{dissipated}$	Dissipated energy during oscillation, J/m^2
E_{stored}	Stored energy during oscillation, J/m^2
f, Δf	Frequency and frequency shift, Hz
$F(D)$	The force between two surface, mN
h	Planks constant, 6.626×10^{-34} J.s
k	Boltzman constant, 1.381×10^{-23} $m^2 kgs^{-2} K^{-1}$
L	Adsorbed polymer layer thickness, nm
L_L	Length of the path that light passes in medium
Δm	Adsorbed mass, ng/cm^2
$\ddot{M}$	Mean residue weight of peptide or protein, g
n	overtone

P	Coefficient of atom-atom pair potential
R	Radius of curvature, m
R_f	Flory radius, nm
s	Mean distance between two grafted polymer chains, nm
$W(D)$	Interaction energy between two surfaces, J/m^2
z	Electrolyte ion valence
Z	Geometry dependent electrostatic interaction constant
ZP	Zeta potential, mV
ε_0	Vacuum permittivity, 8.85×10^{-12} $F.m^{-1}$
η	Viscosity, Pa.s
θ	*Tetha* condition
θ_{ell}	degree ellipticity, deg
$[\theta_{ell}]$	Molar ellipticity, deg $cm^{-2}dmol^{-1}$
κ^{-1}	Debye length, m
λ_n	Wavelength of the n'th fringe
τ	shear stress, Pa
μ	Refractive index
v	Main electron adsorption frequency, 3×10^{-15} s^{-1}
ρ	Density, kg/m^3
σ	Shear modulus, Pa
ψ	Surface potential, mV
ω	Circular frequency

1. Introduction[1]

1.1 Non-specific protein and peptide adsorption

Non-specific adsorption of proteins at the tissue-material interface is known to influence a multiplicity of events related directly to the *in vivo* therapeutic efficacy of the tissue contacting biomaterial. Numerous studies have investigated the mechanisms of protein adsorption to surfaces in contact with physiological fluids, where the impetus for protein adsorption is thought to be a variety of forces present between surfaces and macromolecules within aqueous environments. Functional aspects of the therapeutic biomaterial reported to be influenced by non-specific protein adsorption include the initiation of several host responses (thrombosis, inflammation, wound healing), the drug release profile, and the biomaterial degradation [1]. It is well known that shortly after implantation, a layer of plasma proteins will cover the tissue contacting surface [2-6]. Moreover, upon adsorption at the tissue-material interface these proteins may undergo a surface-induced conformational rearrangement. In addition to facilitating an increase in the protein-surface interaction, conformational changes in adsorbed proteins may lead to the exposure of hidden domains that initiate

---

[1] Parts of this chapter were published in:

i) Poly (ethylene glycol) and Poly (carboxy betaine) Based Nonfouling Architectures: Review and Current Efforts**.** *Mojtaba Binazadeh, Maryam Kabiri, and Larry D. Unsworth***, Proteins at Interfaces III State of the Art.** 2012**,** 621-643.

ii) Inhibiting Nonspecific Protein Adsorption: Mechanisms, Methods, and Materials. *Mojtaba Binazadeh, Hongbo Zeng, and Larry D. Unsworth*, **Biomaterials Surface Science**. 2013, 45-55.

adverse reactions such as the accumulation of inflammatory cells, foreign body response, and coagulation [7-11]. It has been shown, for instance, that exposed protein domains may provide ligands that facilitate cell responses directly; for example, conformational changes in fibrinogen have been shown to expose several occult epitopes that interact with immune cells directly [12-14]. Thus, significant effort has been expended in developing surfaces that either inhibit non-specific protein adsorption or minimize the conformational changes proteins undergo upon adsorption.

Surface engineering for the express purpose of inhibiting non-specific protein adsorption, or subsequent protein denaturing, has shown that substrate surface properties can dramatically affect the adsorbed amount of proteins, as well as their final adsorbed conformation [15]. That said, issues surrounding protein adsorption to surfaces have not been resolved and require further attention for the express purpose of developing cost effective, convenient, and versatile strategies for rendering surfaces resistant to non-specific protein adsorption [16]. In order to investigate protein adsorption mechanisms different researchers have conducted experiments with a single- or multi-component protein solution, on a vast variety of surface architectures [17, 18]. In fact too many surface architectures exist to be covered herein. Suffice it to say that despite these efforts, controlling protein adsorption has met with limited success. It is thought that there are two main reasons this has been the case: Firstly, the inherent amphiphilic properties of proteins provide multiple pathways by which proteins may interact with surfaces [19]. Secondly, it is not just the presence of the protein that can initiate a

bioresponse, but also its conformation. Thus, designing surfaces for the express purpose of inhibiting or controlling non-specific adsorption events has been the focus of decades of research, and continues to be both an industrially relevant and a scientifically interesting area of activity.

In order to better understand the interaction between proteins and surfaces some researchers have studied the peptides-surface interaction. The advantage of this approach is that peptides with specified amino acid sequence could be synthesized and different aspects of protein properties on non-specific adsorption could be investigated. The adsorption study of a 14-mer amphiphilic leucine-lysine peptide (LK14) to silica and polystyrene, suggested that the respective hydrophilicity and hydrophobicity of these interacting substrates affects adsorption rates, adsorption extents, adsorbed layer morphologies, and the peptide structural rearrangement [20]. Other works were done using a synthetic oligopeptides composed of hydrophobic leucine (L) and hydrophilic lysine (K) capable of forming α-helix (14-mer, LKα14) and β-sheet (15-mer, LKβ15). Using X-ray photoelectron spectroscopy (XPS) it has been shown that the adsorption of β-sheet forming LKβ15 on well-defined carboxylic acid and methyl-terminated self-assembled monolayer surfaces results in a special orientation of the peptide at the surface due to the electrostatic interactions of the peptide lysine side chains with the carboxyl surface and hydrophobic interactions of the leucine side chains with the methyl surface. The adsorption of α-helix forming LKα14 did not suggest such substrate dependent orientation [21]. It has also been reported that chemisorbed layers of tri (ethylene oxide) alkanethiols on Au significantly

reduced the adsorbed amount of proteins (concanavalin A and bovine serum albumin) and peptides (arginine-glycine-aspartic acid-serine (RGDS), angiotensin, bradykinin) [22]. Finally, Puddu et al. suggest that the prevailing interactions between peptide and surface (*i.e.* electrostatic, hydrogen bonding, and hydrophobic) depend on the identity of the peptide (amino acid sequence), the substrate surface functionality (hydrophobic or hydrophilic), solution pH, and peptide concentration [23].

1.1.1 Fundamental forces leading to non-specific adsorption

There is a relatively low energy barrier between conformational states of various protein domains, which results in an overall native conformation that may be highly susceptible to structural changes induced by environmental disturbances: such as the introduction of a surface (e.g., air or bioimplant surface) [24]. The interaction between a protein and a surface is thought to be the result of a balance between van der Waals, electrostatic, hydrophobic, and hydration forces [25]. In aqueous solutions, London-van der Waals (dispersion) forces, which arise due to the interaction of two instantaneously induced dipoles, may constitute ~95% of all van der Waals types of interactions that exist between a protein and a surface found in aqueous media [26]. Dispersion forces are considered long range and effective within distances <100 Å, decaying with the seventh power of distance between two small molecules [27]. The van der Waals force per unit area between two flat surfaces is given by equation 1.1 where D is the distance between two surfaces. A is the Hamaker constant defined by equation 1.2 which accounts for

the chemical nature of the interacting surfaces. P is the coefficient of atom-atom pair potential, and ρ_1 and ρ_2 are the number of atoms per volume in the two bodies.

$$F(D) = -\frac{A}{6\pi D^3} \tag{1.1}$$

$$A = \pi^2 P \rho_1 \rho_2 \tag{1.2}$$

Introduction of a surface in an ion containing aqueous solution results in the disruption of the ion distribution throughout the aqueous media. To preserve charge neutrality, counter-ions from solution accumulate at the surface, resulting in the formation of the electrical double layer. The region closer to the surface, the Stern layer, is comprised of fixed counter-ions that interact with localized surface charges (Figure 1.1). The layer closer to bulk, the Gouy-Chapman layer, is characterized as having counter-ions (with respect to surface) which can exchange with those in the bulk fluid. This layer extends to the point where homogeneous distribution of ions in the bulk solution exists. The characteristic thickness of the double layer, Debye length κ^{-1}, is a function of bulk ion concentration, ion valence, temperature, and medium permittivity. At a lower ionic strength, double layer thickness increases and is characterized as a more diffuse ion concentration [26]. The potential at the shear plane, between the Stern and Gouy-Chapman layers, is zeta potential. It is known that electrostatic forces influence the surface interaction of charged biomolecules in electrolyte solution which could be either repulsive or attractive. The interacting electrostatic force between two flat surfaces at distance D is given by equation 1.3 where Z is electrostatic interaction

constant for 2 surfaces with different surface potentials (ψ) defined in equation1.4 [28]:

$$F(D) = \frac{\kappa^2}{2\pi} Ze^{-\kappa D} \tag{1.3}$$

$$Z = 64\pi\varepsilon_0\varepsilon_2\left(\frac{kT}{ze}\right)^2 \tanh\left(\frac{ez\psi_3}{4kT}\right)\tanh\left(\frac{ez\psi_1}{4kT}\right) \tag{1.4}$$

and κ, inverse of Debye length, is given by equation 1.5 [28]:

$$\kappa = \sqrt{\left(\sum \frac{\rho_j e^2 z_j^2}{\varepsilon_0\varepsilon_2 kT}\right)} \tag{1.5}$$

In the above equations, k=1.381x10^{-23}m^2.kg.s^{-2}.K^{-1}, is Boltzmann constant; ε_0=8.85x10^{-12} F.m^{-1}, is vacuum permittivity; ε_2= 74.8 at 37°C, is relative permittivity of medium; e=1.602x10^{-19} C, is electron charge; z is electrolyte ion valence, ψ is surface potential, and ρ_j is number density of species j.

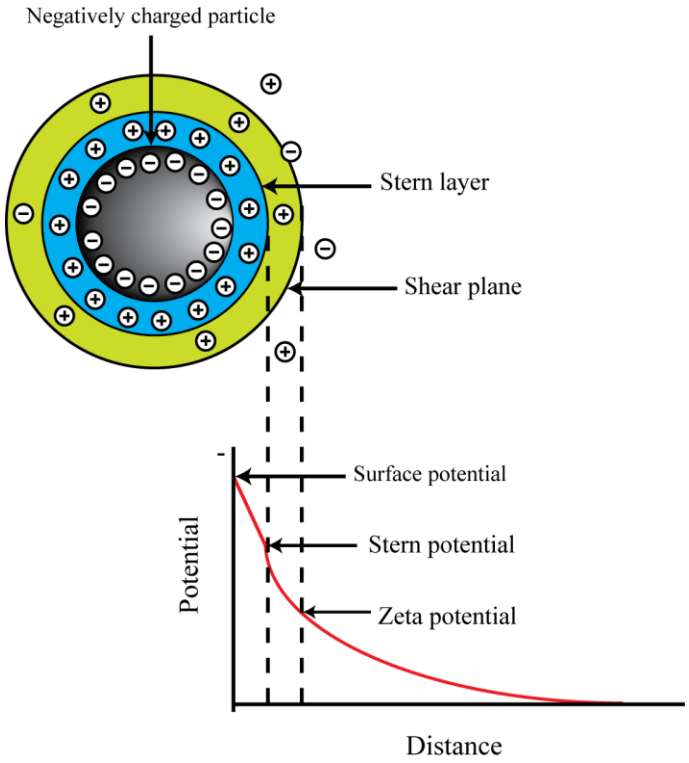

Figure 1.1 Schematic of double layer structure around a negatively charged surface in an electrolyte liquid

Hydrogen bonding, hydrophobic interactions (attractive), and hydration pressure (repulsive) represent interactions that may be a hundred times greater than that of both electrostatic and dispersion forces [26]. The release of highly ordered water molecules from the hydration shell imposed upon two hydrophobic domains is thought to be the driving force for the hydrophobic effect that leads to the spontaneous interaction of these moieties. Whereas, hydration pressure (hydrophilic repulsion) has been described as a result of resistance to the breakdown of the associated water molecules (due to hydrogen bonds) in the hydrated shell around hydrophilic entities [26]. Characteristic decay lengths for hydrophobic interactions and hydration pressures have been reported to be ~13

and ~1 nm, respectively; the repulsive hydration pressure being a short range force compared to attractive hydrophobic interactions. The strength and range of the above-mentioned interactions depends on the protein (conformation, and isoelectric point), solution (pH, and ionic strength) and surface (roughness, and chemical) properties. Ultimately, the adsorption of proteins to surfaces is the result of a combination of these fundamental forces that may affect proteins up to 10 nm away from the surface in question [29].

1.1.2 Effect of secondary structure on adsorption and adsorbed film properties

Protein folding occurs primarily due to the balance between the hydrophobic effect and hydrophilic domains [30]. Depending on the internal coherency state (i.e. softness or hardness) that a protein acquires upon folding its adsorption trends might be influenced: soft proteins may even adsorb to hydrophilic electrostatically repelling surfaces since their structure may easily get rearranged upon coming in contact with the surface; in contrast, hard proteins with a strong internal coherence may not experience a structural rearrangement contribution to their adsorption [31]. Although each protein has a unique structure that is determined by its primary amino acid sequence, several structural features are common. Proteins have a compact three dimensional structure with little internal space. Moreover, there are only a limited number of secondary structures that occur throughout, where ~50% of the protein structure has a defined secondary structure (as opposed to a random coil) [32]. Formation of secondary structure is a result of interactions such as hydrogen bonding between neighbouring amino

acids in the protein's sequence. Secondary structure of a protein influences its physicochemical properties such as shape, size, hydrophobicity, and function in a physiological solution. However, near a surface the interactions between surface and protein might alter the balance of non-covalent interactions (hydrogen bonds, hydrophobic interactions, electrostatic interactions, and van der Waals) and consequently, lead to the non-specific adsorption and denaturing of proteins.

Although the effect of many protein attributes (pI [33, 34], size [35], and hydrophobicity [36]) on non-specific protein adsorption have been studied, there is a dearth in the literature surrounding the effect of secondary structure [37]. Moreover, it is unknown how different secondary structures will interact with the surface in general, important features include surface induced melting of the secondary structure and the resultant change in activity and functionality. Poly-L-Lysine (PLL) was chosen as an appropriate model peptide for investigating the influence of secondary structure on both protein adsorptions. The rationale behind this choice was that using the same molecule (ie. PLL) it is possible to adopt both α-helix and β-sheet structures depending on solution environmental conditions [38].

1.2 Poly (ethylene glycol)

Obviously the literature surrounding protein adsorption to PEG modified surfaces is too vast to summarize within this chapter, especially given that one of the first references to the use of poly ethylene glycol for blood contacting devices was found as early as 1974 [39]. Therefore, attention is paid to the properties of PEG

that may lend itself to providing a low biofouling platform and important papers that have revealed these properties. In general, PEG is a linear polymer with the –CH_2–CH_2–O– monomer that presents an uncharged but polar hydrogen bond accepting group [24]. PEG has both hydrophilic segments (oxygen atoms) and hydrophobic segments (carbon atoms), which makes it soluble in both aqueous and organic solvents. In line with PEG properties, characteristics such as net neutral charge, hydrophilic nature, presence of hydrogen bond acceptors and no hydrogen bond donors are thought to be crucial for the inhibition of non-specific protein adsorption to PEGylated surfaces [40]. In crystalline PEG, the chain adopts a helical structure with 3.5 monomer units per turn [41] and in water it forms a loose coil structure [42]. In aqueous solutions, the ethylene glycol monomer can form up to two hydrogen bonds with water molecules. Finally, hydrogen bonds between PEG and water [43] gradually break upon increasing PEG concentration, solution temperature, and/or solution salt concentration, which reduces PEG solubility in water; resulting in the occurrence of the 'cloud-point' condition for PEG.

1.2.1 Biological applications of poly (ethylene glycol)

PEG has been initially used as a precipitating agent for proteins, viruses, and other biomacromolecules [44, 45]. For many applications, PEG may be conjugated with biomolecules or surfaces of interest. Such conjugations offer enhanced water solubility of the biomacromolecules, reduced toxicity, and reduced kidney clearance [46]. From the time that covalent linkage between PEG and protein [47, 48] was introduced, considerable amount of scientific work has

been done on PEG conjugates. Two examples of PEG-protein conjugates are PEG-asparaginase [49] and PEG-adenosine deaminase [50] for acute lymphoblastic leukemia treatment and adenosine deaminase (ADA) deficiency treatment.

Table 1.1 Important PEG conjugates and their applications

PEG conjugate of	Added properties	Reference
Protein	Reduced immunogenicity, resistance to proteolysis, longevity in blood stream	[50, 51]
Enzyme	Enhanced functionality and stability,	[52]
Peptide	Biologically active, improved solubility	[51]
Liposomes and particulates	Reticuloendothelial system evasion, longevity in blood stream	[53, 54]
Drug	Controlled release, improved solubility, longevity in blood stream, improved permeability	[46, 55]
Nanoparticle	Reduced non-specific interaction with proteins, dispersion and stability in aqueous solution	[56]
Biomaterial	Reduced adsorption of proteins and cells, reduced thrombogenicity	[57]

PEG is also an ideal spacer between two biomolecule or a surface and a biomolecule [58] probably due to well solvation of the ethylene oxide units [43, 59] and repellency of PEG chains in aqueous solutions [60]. Flexibility of the ether bond in an ethylene oxide monomer also contributes to the availability and high activity of PEG-tethered molecules. Heterobifunctional PEGs offer the appropriate end groups which could crosslink two different proteins [51], attach ligands to membrane-forming lipids, graft the polymer onto a solid support [61],

and link receptor to a biomaterial [58, 62]. Biomolecules tethered to a biomaterial surface through a PEG chain could be used as targeting or activating moieties [63]. The activity of surface bounded biomolecules would be maintained due to the elimination of non-specific interactions with the surface by the PEG layer. Moreover, PEG tethered proteins or proteins adsorbed to PEG modified surfaces do not denature by interaction with PEG or surface [64]. A summary of the applications of PEG-conjugate systems is presented in Table 1.1. Multifunctional PEG derivatives could be used to synthesize PEG hydrogels or crosslinked PEG [59] which could be used for wound covering and slow drug release *in vivo* [65, 66]. It had been shown that photochemically reversible PEG hydrogels could be made by use of appropriately substituted PEG derivatives [67]. Moreover, PEG-crosslinked collagen hydrogels may be used for soft tissue replacement due to their benign nature [68, 69].

1.2.2 Applications of poly (ethylene glycol) coating in biomaterials

Although it is known that surface modification with PEG results in lower protein adsorption [40], the mechanisms responsible for such behaviour are not fully understood. In an aqueous solution, flexible ether bonds in a long chain of PEG may confer rotational and conformational mobility to the polymer chain [70]. This molecular mobility is thought to persist even upon chemical tethering of one end to a surface (grafting), which yields a large volume in which a protein is thought to be hindered from entering (excluded volume). It is thought that steric stabilization does not allow the approaching protein to permanently stay in the excluded volume [71] and reach the surface. In combination with this, it has been

shown that for shorter grafted PEG chains strongly associated water molecules (due to hydrogen bonds) in the hydrated shell around the PEG chain [26] may create a repulsive hydration force which repels proteins [72]. Among the interesting studies of PEG properties is the surface forces study by Claesson [73] where repulsive hydration forces between grafted PEG layers were measured directly. It was further confirmed by van Oss [60], *via* measurement of the free energy of repulsion, that soluble PEG molecules in aqueous solution repel each other. These findings are in line with the above mentioned dominant non-fouling mechanism observed for grafted shorter PEG chains [72] where hydration shell around a PEG chain exerts a repulsive force on the adsorbing protein. In addition to these attributes, the presence of a PEG layer either grafted or randomly immobilized chains on a surface forms a pseudo-interface that may attenuate underlying hydrophobic and or electrostatic effects present on the unmodified surface [74].

Some papers of interest have been highlighted (Table 1.2) that have outlined some of the work discussed above. However, an important discussion for anti-fouling efficacy of poly (ethylene glycols) coating involves the chain density effect of chemically end grafted PEG to the surface. Prior to the work of Kingshott, et al. (2002), the discussion of protein adsorption to surfaces modified with grafted PEG largely revolved around understanding the effect of molecular weight, with numerous contradictory results being reported for very similar systems. Kingshott's work was influential in outlining the effect of 'pinning density', and was a work that inspired further study by Unsworth, et al. (2005,

2008). The primary contribution of which was showing that regardless of the grafted PEG molecular weight, when examined as a function of chain density, vastly different molecular weights yielded similar adsorbed amounts of protein from solution. Suggesting that an optimal chain density exists that modulates properties such as hydration and conformational freedom, which directly influences the ability of proteins to interact with the surface [75-77]. Increasing chain density above this critical value may lead to a decrease in the number of water molecules associated with a grafted PEG chain [78], which may play a role in suppressing any associated hydration pressure as the hydration shell around the chain is disturbed and reduced in size. Increased chain density may also lead to a loss of grafted PEG conformational freedom, which may suppress any steric repulsion effects. In addition to this, it has been shown that protein adsorption becomes increasingly affected by distal chemistry effects as the grafted PEG chain density increases [78]. In both cases, with hydroxyl end-group chemistries as well as optimal chain densities, it may be that the hydration state within the layer may play a dominant role in directing the interaction between proteins and surfaces [78]. This was further confirmed by Chang et al. that higher hydration capacity of the polymer film provides a lower protein adsorption [79]; furthermore, it was shown that the bounded water molecules, which form the hydration shell around a grafted PEG chain, contribute more in protein repellency of a PEG modified surface as compared to trapped water molecules which are confined in a network-like PEG layer [80].

Table 1.2 Important papers for PEG antifouling properties and their contribution, [81]

Author, year	Major contribution
Gombotz et al., 1991 [57]	Grafted PEG antifouling mechanism 1: Excluded volume
van Oss, 1994 [26]	PEG antifouling mechanism 2: Repulsive hydration pressure from water shell around PEG chains in solution
Archambault et al., 1998 [82]	Effectiveness of grafted PEG coating on reducing plasma protein adsorption
McPherson et al., 1998 [83]	Identification of influential grafted PEG-surface parameters: Importance of chain density and weak effect of chain length
Sofia et al., 1998 [84]	Higher efficiency of grafted linear PEG compared to star form PEG
Kingshott et al., 2002 [85]	Effect of cloud point grafting on chain density
Unsworth et al., 2005 [18]	Grafting at critical chain density (~0.5 chain/nm^2): Maximum suppression of protein adsorption
Unsworth et al., 2008 [78]	Distal chemistry effect at grafted chain densities greater than critical value

1.3 Objective and techniques

1.3.1 Objective

Through utilizing grafted PEG, it may be possible to further understand the effect that protein structure has upon surface interactions, adsorption, and subsequent film properties. Herein the major question being asked is, how protein secondary structure affects not only adsorption to PEG modified surfaces, but also the subsequent physicochemical properties of the formed film. Through the ubiquitous nature of both the components of proteins (i.e. 22 natural amino acids) and the relatively limited types of secondary structures available, it may be

possible to achieve a better understanding regarding the role protein conformation has on adsorption and the adsorbed film properties.

1.3.2 Circular dichroism (CD)

Circular dichroism (CD) is an optical property of asymmetric molecules which can be used to rapidly determine folding properties and secondary structure of a protein. It occurs when a molecule absorbs left- and right-handed circularly polarized light to different extents [86]. The difference between absorption of left- and right-handed circularly polarized light at different wavelengths can reveal the secondary structure of proteins. Figure 1.2 shows change in the intensity of left- and right- handed circularly polarized lights when they pass through a media exhibiting a circular dichroism effect.

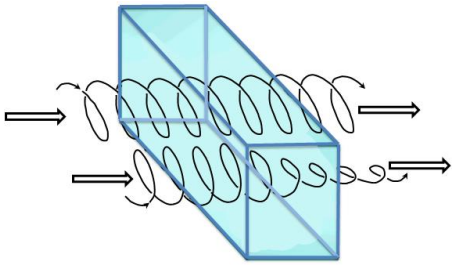

Figure 1.2 Circular dichroism effect

The light source of a CD machine produces a sinusoidal plane polarized light with adjustable wavelengths. A sinusoidal plane polarized light is the resultant of two circularly polarized wave vectors with equal magnitude, one rotates counterclockwise (E_L) and the other rotates clockwise (E_R). After passing

through a medium which exhibits circular dichroism, the light will no longer be plane polarized; it will be elliptically polarized (Figure 1.3) due to preferential absorption of left- and right- handed circularly polarized light and different indices of refraction for each light component. The CD technique yields a difference of absorbance (ΔE) as a function of wavelength, which can be represented as "degrees ellipticity":

$$\theta_{ell} = \tan^{-1} \frac{minor\ axis\ of\ ellipe}{major\ axis\ of\ ellipe} \tag{1.6}$$

The commonly used unit for reporting CD, [θ_{ell}], the molar ellipticity in deg.cm^2/ dmol^{-1} is defined as:

$$[\theta_{ell}] = \frac{\theta_{ell} \times \dot{\ddot{M}}}{L_L \times C_M} \tag{1.7}$$

Where $\dot{\ddot{M}}$ is the mean residue weight of peptide or protein; L_L is the length of the path that light passes in medium; and C_M is concentration of biomolecule.

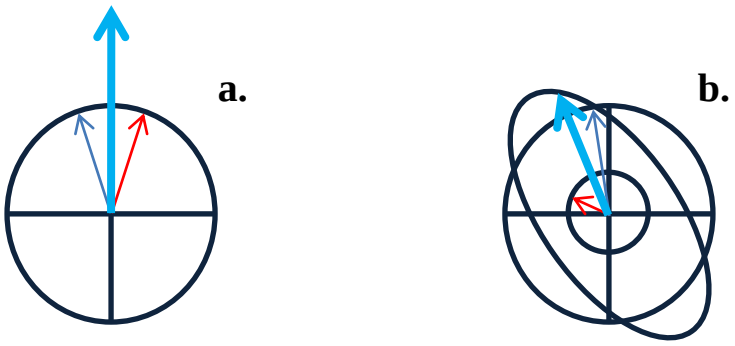

Figure 1.3 Absorption and refraction of circularly polarized light **a.** light before passing medium, **b.** light after passing medium

1.3.3 Quartz Crystal Microbalance with Dissipation monitoring (QCM-D)

Another technique that has gained attention for monitoring protein adsorption to surfaces is QCM-D. The fact that QCM-D can provide highly sensitive real time *in-situ* information about layers adsorbed on a surface makes it a powerful technique for probing protein adsorption on polymeric biomaterial surfaces. The advantage that tracking surface modification using QCM-D has is accurate determination of adsorbed mass. Dissipation factor monitoring also offers unique information about the viscoelastic properties of the surface including layer viscosity. QCM-D study by Weber et al. [87] showed that addition of up to 15% PEG segment to poly(DTE carbonate) decreased human fibrinogen adsorption. Their results suggest that the conformation of surface adsorbed fibrinogen is a function of PEG surface concentration. Yoshikawa et al. [88] also used QCM-D to measure protein adsorption on polymeric surfaces. Their results show that at high grafting density (0.7 chain/nm^2), poly (2-hydroxyethyl methacrylate) brushes show the highest resistance to nonspecific adsorption of proteins of various sizes. QCM-D can be used to track formation and growth of a protein layer on the surface of quartz crystal as a function of time by monitoring changes in the frequency of the quartz oscillation (Δf) and dissipation (ΔD_f) (Figure 1.4) where dissipation factor 'D_f' is defined as [89]:

$$D_f = \frac{E_{dissipated}}{2\pi E_{stored}} \tag{1.8}$$

where '$E_{dissipated}$' and 'E_{stored}' are dissipated and stored energy during oscillation. Adsorption of mass to a quartz crystal will result in a shift in the oscillation

frequency of the quartz crystal toward lower values (negative Δf). Moreover, if a rigid body adsorbs to the surface no change in the dissipation factor will be observed (ie. $\Delta D_f=0$), however, if the adsorbed layer has some viscoelastic properties then the dissipation factor will increase ($\Delta D_f>0$) due to energy loss caused by its oscillating.

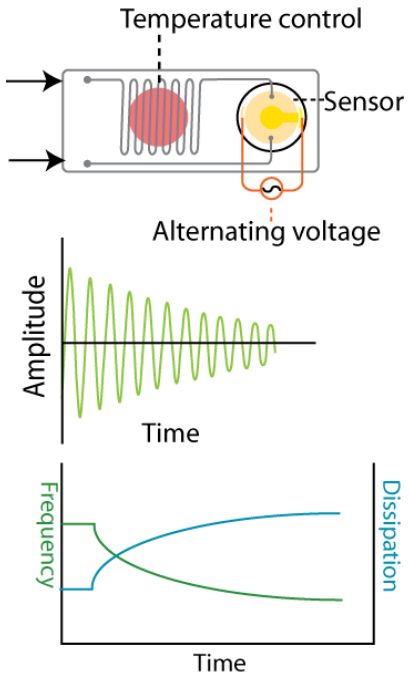

Figure 1.4 Schematic drawing of QCM-D and its working principle

By use of the Sauerbrey equation, adsorbed mass can be calculated as a linear function of frequency change ($\Delta m = -17.7\Delta f$). When dissipation changes observed during the adsorption process is greater than zero (non-rigid adsorbed layer) the Sauerbrey equation underestimates adsorbed mass [90]. Large changes in dissipation are often associated with viscoelastic adsorbed layers; thus, a model that considers the viscoelastic properties of the adsorbed layer is needed for such

systems. QCM-D, coupled with physical models, can be used to understand the kinetic physical properties of the adsorbed protein film including thickness or mass and shear viscosity [91]. The Voight model is the simplest representation of a viscoelastic solid typically used. The model consists of a viscous dashpot (Figure 1.5a.) and an elastic spring (Figure 1.5b.) connected in parallel, which can represent the behaviour of a viscoelastic layer [92]. The viscosity, η, and shear modulus, σ, are defined in equations 1.9 ad 1.10. In these equations τ, du/dy, and Δl/H are shear stress, velocity gradient, and shear strain respectively. Voight model is discussed in detail in chapter 2.

$$\eta = \frac{\tau}{\frac{du}{dy}} \tag{1.9}$$

$$\sigma = \frac{\tau}{\Delta l/_H} \tag{1.10}$$

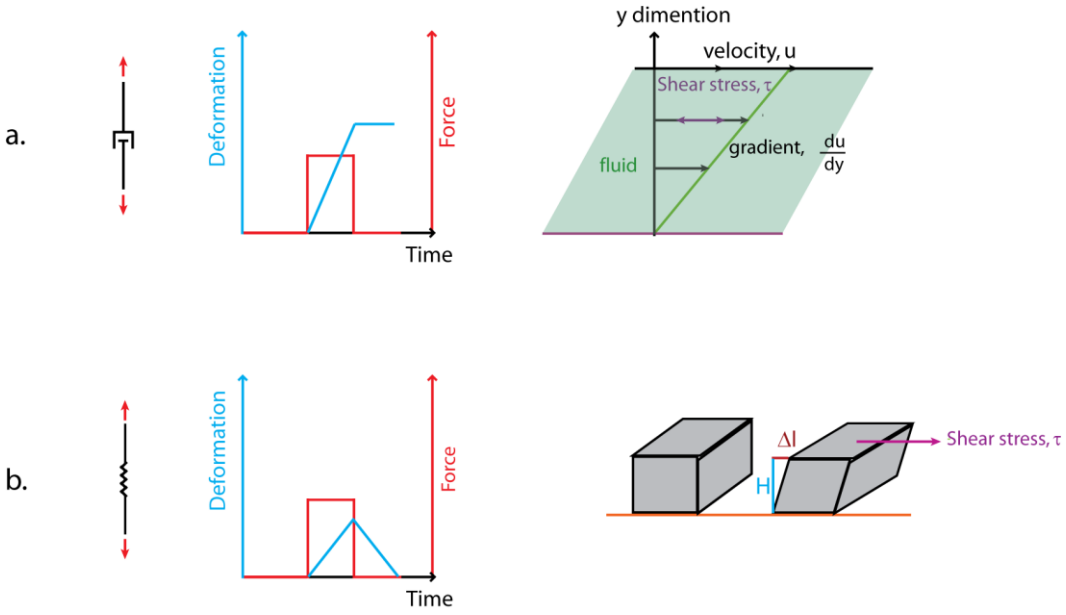

Figure 1.5 schematic of **a.** the basic viscous part and **b**. the elastic part of a viscoelastic element

1.3.4 Surface forces apparatus (SFA)

Surface forces are actively present in systems made/modified by different materials such as nanoparticles [93, 94], hydrocarbons [95], polymers [96, 97], self-assembled monolayers (SAMs) [98], and biomolecules [28, 99]. The surface forces apparatus has been widely used to measure forces of different kinds (including van der Waals, electrostatic forces, capillary and adhesion forces, hydration and solvation forces, hydrophobic and steric interactions, and bio-specific interactions) between surfaces in various liquids and vapors [100]. In the experiments, the surface separation can be monitored through multiple beam interferometry with a theoretical accuracy of <1 Å in real time and in situ, and forces can be determined, with a force sensitivity of <10 nN, by the Hooke's Law by monitoring the difference between the driving distance and real surface separation change [100]. One distinctive advantage of SFA is that surface coverage, size, and orientation of macromolecules and proteins can be determined in a non-perturbative manner [101-105]. Several groups have also developed methods to prepare oriented protein monolayers *via* attaching proteins to functionalized lipid monolayer [106-113].

In SFA experiments, freshly cleaved thin mica sheets (1-5 μm) which is transparent, molecularly smooth with high surface energy is commonly used and other coatings (e.g., SiO_2, Au, TiO_2, and polymers) have also been used as supporting substrates [28, 114-116]. The mica sheets are normally back-coated with a layer of silver (~50 nm) which acts as a mirror surface for the multiple beam interferometry (MBI) in SFA. Mica sheets are glued on two cylindrical glass disks (radii of R_1=R_2=R), and a pair of surfaces is mounted into the SFA

chamber in a crossed–cylinder configuration which is locally equivalent to a sphere-on-flat plate geometry based on the Derjaguin approximation when surface separation D is much smaller than R [28]. The measured force $F(D)$ between the two cylindrically curved surfaces (of radii R_1 and R_2) can be directly related to the interaction energy per unit area between two flat surfaces of the same materials $W_{flat}(D)$ by the Derjaguin approximation shown in equation 1.11, where $R = \sqrt{R_1 R_2}$ is the radius for the equivalent sphere-on-flat geometry.

$$W_{flat}(D) = \frac{F_{curved}(D)}{2\pi\sqrt{R_1 R_2}} = \frac{F_{curved}(D)}{2\pi R} \tag{1.11}$$

Figure 1.6 shows the schematic of typical SFA experiment setup. During the experiment, white light is directed normal to the two surfaces of interest, and the light is reflected back and forth between the silver layers leading to formation of Newton's rings around the closest interaction point. The transmitted light is composed of a particular set of discrete wavelengths which can be separated by a spectrometer, generating so-called fringes of equal chromatic order (FECO) as shown in Figure 1.6b. The change of absolute separation between the two opposing surfaces can be determined *in situ* and in real time by monitoring the wavelength shifts of the FECO fringes. If the two mica sheets have the same thickness, the surface separation D and the fringe wavelength λ_n^D can be correlated by equation 1.12 [117], where '+' refers to odd order fringes (n odd), and '-' refers to even order fringes (n even), λ_n^0 is the wavelength of the nth fringe at reference D=0. $\bar{\mu} = \mu_{mica} / \mu$, where μ_{mica} is the refractive index of mica

at λ_n^D, and μ is the refractive index of the medium between the two mica surfaces at λ_n^D.

$$\tan(2\pi\mu D/\lambda_n^D) = \frac{2\bar{\mu}\sin\left[\pi\left(1-\lambda_n^0/\lambda_n^D\right)/\left(1-\lambda_n^0/\lambda_{n-1}^0\right)\right]}{(1+\bar{\mu}^2)\cos\left[\pi\left(1-\lambda_n^0/\lambda_n^D\right)/\left(1-\lambda_n^0/\lambda_{n-1}^0\right)\right]\pm(\bar{\mu}^2-1)}$$

(1.12)

For the surface interactions of proteins and biopolymers, the medium is normally aqueous solution. Besides using mica as a supporting substrate for the deposition of proteins or polymers, several methods such as deposition of metals and metal oxides [118, 119], plasma treatment [120, 121], Langmuir-Blodgett deposition of surfactants or lipids [122-127] have also been used to modify the mica surface to render the desired properties depending on the applications. Electrical field was also introduced into to SFA by Zeng *et al.* to allow field-sensitive measurements or electrochemical measurements [128]. One can also modify the experimental configurations to meet specific needs of desired measurements, but it should be noted that the corresponding relation between surface separation and wavelengths of interfering fringes must be used accordingly [117, 128].

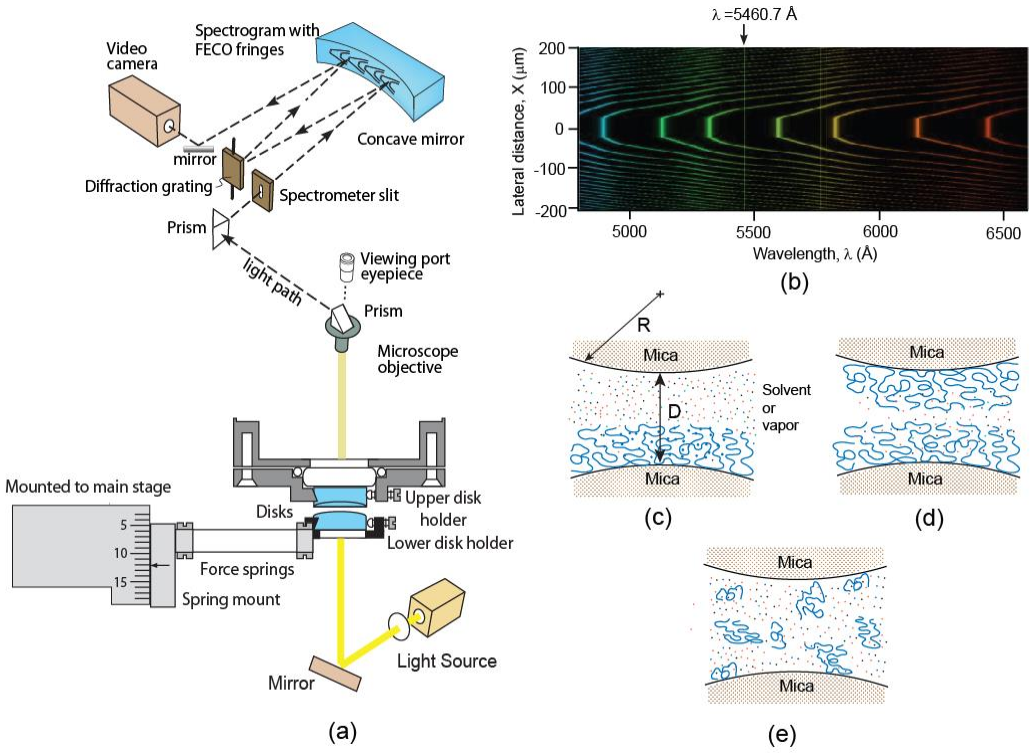

Figure 1.6 Schematic of SFA setup for measuring interaction forces between two surfaces. **a.** schematic of the basic setup of SFA experiments in which multiple beam interferometry is used to monitor the surface separation and deformation in situ and in real time; **b.** a typical image of fringes of equal chromatic order (FECO) for two surfaces in contact obtained in SFA experiments; **c-e.** three typical experimental configurations to measure the interaction forces of polymer/biopolymer surfaces and molecules [129, 130]

SFA technique has also been used to study the molecular and surface interactions in PEG modified systems. Table 1.3 summarized some previous findings regarding PEG related systems and their properties by SFA. These previous studies indicate that the hydration forces and steric interaction play important roles in the antifouling properties of PEG related polymeric systems. SFA can be also used to measure the lateral forces (i.e. friction and lubrication forces) between two interacting surfaces. Several groups have used SFA to study how the presence of a protein or polymer layer lubricates the lateral movement of

two surfaces [131-135]. Drobek et al. reported that presence of a poly (L-Lysine)-*graft*-poly(ethylene glycol) layer results in exceptionally low friction force [136]. The low friction forces could be attributed to the PEG properties: presence of a hydrated flexible neutral PEG layer plays a crucial role in lubricating the surfaces in contact. The unique ability of measuring interaction forces as a function of absolute separation distance makes SFA a powerful tool which provides valuable information regarding the molecular interaction mechanisms of proteins and biopolymers, their adsorption behaviors and impact of various environmental and experimental factors. Other techniques have also been widely used to investigate the intermolecular and/or surface interactions in the related fields, such as atomic force microscope (AFM), total internal reflection microscopy (TIRM), reflectance interference contrast microscopy (RICM). The main features of these techniques and their applications can be found in recent reviews [137].

Table 1.3 Some previous studies on PEG properties and their contributions by SFA

Author, year		**Major contribution**
Claesson et al., 1987	[138]	Direct measurement of steric repulsion force between PEG grafted layers (antifouling mechanism of long PEG chains)
Claesson et al., 1996	[73]	Direct measurement of the repulsive hydration forces between grafted PEG layers (antifouling mechanism of short PEG chains)
Sheth et al., 1997	[139]	PEG can adopt different conformational states in water
Heuberger et al., 2005	[9]	Repulsive and elastic structural forces due to weak network between PEG and water
Zhang et al., 2012	[140]	Direct measurement of steric interaction of comb-type PEG copolymer layers

1.4 Outline of this thesis

This thesis consists of five chapters:

Chapter 1: This chapter provides the research background of the thesis. Non-specific protein adsorption and its contributing factors are discussed. Previous works on design of anti-biofouling surfaces are reviewed and the experimental techniques for this work are outlined. Parts of this chapter was published in: i) Poly (ethylene glycol) and Poly(carboxy betaine) Based Nonfouling Architectures: Review and Current Efforts. Mojtaba Binazadeh, Maryam Kabiri, and Larry D. Unswort, *Proteins at Interfaces III State of the Art.* 2012, 621-643 and ii) Inhibiting Nonspecific Protein Adsorption: Mechanisms, Methods, and Materials. Mojtaba Binazadeh, Hongbo Zeng, and Larry D. Unsworth, *Biomaterials Surface Science*. 2013, 45-55.

Chapter 2: In this chapter, α-helices and β-sheets were induced in Poly-L-Lysine (PLL) at different sodium sulfate concentrations and PLL adsorption to Au surfaces monitored using quartz crystal microbalance with dissipation (QCM-D). Circular dichroism (CD) was used to measure the secondary structure of PLL upon its adsorption on Au. Zeta potential of PLL was measured and the interaction energy between PLL chains and Au surfaces were calculated. This chapter was published in: Effect of peptide secondary structure on adsorption and adsorbed film properties. Binazadeh, M., H. Zeng, and L.D. Unsworth, *Acta Biomaterialia*, 2013. 9(5): p. 6403-6413

Chapter 3: In this chapter, PLL in either α-helix or β-sheet configuration was used to investigate the effect of secondary structures and poly (ethylene glycol) (PEG)

surface coating on protein adsorption events *via* QCM-D. Circular dichroism (CD) was also used to measure the secondary structure of PLL upon its adsorption on Au and PEG surfaces. This chapter accepted for publication in *Acta Biomaterialia.*

Chapter 4: In this chapter, CD was also used to evaluate the persistence of PLL secondary structure upon its adsorption on quartz. PLL in α-helix and β-sheet conformation was adsorbed on mica surfaces and the surface interaction of PLL-PLL, PLL-Au, PEG-mica, and PLL-PEG surfaces was measured using surface forces apparatus (SFA). The interaction of PLL-Au and PLL-PLL layers were explained by Alexander-de Gennes (AdG) and classical Derjaguin-Landdau-Verwey-Overbeek (DLVO) theories. Part of the experiments in this chapter was conducted with the help of Mr. Ali Faghihnejad. This chapter was accepted for publication in *Biomacromolecules.*

Chapter 5: The overall conclusions and future work are outlined in this chapter.

1.5 References

[1] Vladkova, TG. Surface engineered polymeric biomaterials with improved biocontact properties. Int. J. Polym. Sci., 2010;2010:1-22.

[2] Anderson, JM, Bonfield, TL, and Ziats, NP. Protein adsorption and cellular adhesion and activation on biomedical polymers. Int. J. Artif. Organs, 1990;13:375-382.

[3] Andrade, JD and Hlady, V. Plasma protein adsorption: the big twelve. Ann. N. Y. Acad. Sci., 1987;516:158-172.

[4] Nath, N, Hyun, J, Ma, H, and Chilkoti, A. Surface engineering strategies for control of protein and cell interactions. Surf. Sci., 2004;570:98-110.

[5] Pankowsky, DA, Ziats, NP, Topham, NS, Ratnoff, OD, and Anderson, JM. Morphologic characteristics of adsorbed human plasma-proteins on vascular grafts and biomaterials. J. Vasc. Surg., 1990;11:599-606.

[6] Shen, M, Garcia, I, Maier, RV, and Horbett, TA. Effects of adsorbed proteins and surface chemistry on foreign body giant cell formation, tumor necrosis factor alpha release and procoagulant activity of monocytes. J. Biomed. Mater. Res., Part A, 2004;70A:533-541.

[7] Collier, TO and Anderson, JM. Protein and surface effects on monocyte and macrophage adhesion, maturation, and survival. J. Biomed. Mater. Res., 2002;60:487-496.

[8] Evans-Nguyen, KM, Fuierer, RR, Fitchett, BD, Tolles, LR, Conboy, JC, and Schoenfisch, MH. Changes in adsorbed fibrinogen upon conversion to fibrin. Langmuir, 2006;22:5115-5121.

[9] Heuberger, M, Drobek, T, and Spencer, ND. Interaction forces and morphology of a protein-resistant poly(ethylene glycol) layer. Biophys. J., 2005;88:495-504.

[10] Hu, W-J, Eaton, JW, Ugarova, TP, and Tang, L. Molecular basis of biomaterial-mediated foreign body reactions. Blood, 2001;98:1231-1238.

[11] Lu, DR and Park, K. Effect of surface hydrophobicity on the conformational changes of adsorbed fibrinogen. J. Colloid Interface Sci., 1991;144:271-281.

[12] Shiba, E., Lindon, N., J, Kushner, L., Matsueda, R., G, Hawiger, J., Kloczewiak, M., Kudryk, B., Salzman, and W., E. Antibody-detectable changes in fibrinogen adsorption affecting platelet activation on polymer surfaces. Am. J. Physiol., 1991;260:965-974.

[13] Smolarczyk, K, Boncela, J, Szymanski, J, Gils, A, and Cierniewski, CS. Fibrinogen Contains Cryptic PAI-1 Binding Sites That Are Exposed on Binding to Solid Surfaces or Limited Proteolysis. Arterioscler. Thromb. Vasc. Biol., 2005;25:2679-2684.

[14] Ugarova, TP, Budzynski, AZ, Shattil, SJ, Ruggeri, ZM, Ginsberg, MH, and Plow, EF. Conformational changes in fibrinogen elicited by its interaction with platelet membrane glycoprotein GPIIb-IIIa. J. Biol. Chem., 1993;268:21080-21087.

[15] Grinnell, F and Feld, MK. Adsorption characteristics of plasma fibrinectin in relationship to biological-activity. J. Biomed. Mater. Res., 1981;15:363-381.

[16] Dalsin, JL and Messersmith, PB. Bioinspired antifouling polymers. Materials Today, 2005;8:38-46.

[17] Drotleff, S.Polymers and protein-conjugates for tissue engineering. 2006, University of Regensburg: Regensburg, Germany.

[18] Unsworth, LD, Sheardown, H, and Brash, JL. Protein resistance of surfaces prepared by sorption of end-thiolated poly(ethylene glycol) to gold: Effect of surface chain density. Langmuir, 2005;21:1036-1041.

[19] Hlady, V, VanWagenen, RA, and Andrade, JD. Total internal reflection intrinsic fluorescence (TIRIF) spectroscopy applied to protein adsorption, in Surface and Interfacial Aspects of Biomedical Polymers J.D. Andrade, Editor. 1985, Plenum Press, New York, NY, USA, . 81-119.

[20] Mermut, O, Phillips, DC, York, RL, McCrea, KR, Ward, RS, and Somorjai, GA. In Situ Adsorption Studies of a 14-Amino Acid Leucine-Lysine Peptide onto Hydrophobic Polystyrene and Hydrophilic Silica Surfaces Using Quartz Crystal Microbalance, Atomic Force Microscopy, and Sum Frequency Generation Vibrational Spectroscopy. J. Am. Chem. Soc., 2006;128:3598-3607.

[21] Apte, JS, Collier, G, Latour, RA, Gamble, LJ, and Castner, DG. XPS and ToF-SIMS Investigation of alpha-Helical and beta-Strand Peptide Adsorption onto SAMs. Langmuir, 2010;26:3423-3432.

[22] Yoshioka, K, Sato, Y, Tanaka, M, Murakami, T, and Niwa, O. Suppression of Non-specific Adsorption Using Densified Tri(ethylene glycol) Alkanethiols: Monolayer Characteristics Evaluated by Electrochemical Measurements. Anal. Sci., 2010;26:33-37.

[23] Puddu, V and Perry, CC. Peptide Adsorption on Silica Nanoparticles: Evidence of Hydrophobic Interactions. ACS Nano, 2012;6:6356-6363.

[24] Gong, P and Grainger, DW. Nonfouling surfaces: a review of principles and applications for microarray capture assay designs. Methods Mol. Biol., 2007;381:59-92.

[25] Leckband, D and Israelachvili, J. Molecular basis of protein function as determined by direct force measurements. Enzyme Microb. Technol., 1993;15:450-459.

[26] van Oss, CJ. The primary interactions, in Interfacial forces in aqueous media. 1994, CRC Press.

[27] Overbeek, JTG. Colloid science, ed. H.R. Kruyt. Vol. 1. 1952, Amsterdam: Elsevier.

[28] Israelachvili, JN. Force- Measuring Techniques, in Intermolecular and surface forces. 2010, Academic Press: San Diego. 223-252.

[29] Ramsden, JJ. Protein adsorption kinetics, in Biopolymers at interfaces, M. Malmsten, Editor. 2003, Marcel Dekker, Inc.: New York.

[30] Dill, KA. Dominant forces in protein folding. Biochemistry (Mosc.), 1990;29:7133-7155.

[31] Norde, W and Anusiem, ACI. Adsorption, desorption and re-adsorption of proteins on solid surfaces. Colloids Surf., 1992;66:73-80.

[32] Kabsch, W and Sander, C. Dictionary of protein secondary structure: pattern recognition of hydrogen-bonded and geometrical features. Biopolymers, 1983;22:2577-2637.

[33] Chen, S, Li, L, and Zheng, J. Surface Hydration: Principles and Applications toward Lowfouling/Nonfouling Biomaterials. Polymer;In Press, Accepted Manuscript.

[34] Jordan, CE and Corn, RM. Surface plasmon resonance imaging measurements of electrostatic biopolymer adsorption onto chemically modified gold surfaces. Anal. Chem., 1997;69:1449-1456.

[35] Yang, Q, Kaul, C, and Ulbricht, M. Anti-nonspecific protein adsorption properties of biomimetic glycocalyx-like glycopolymer layers: effects of glycopolymer chain density and protein size. Langmuir, 2010;26:5746-5752.

[36] Wang, D, Douma, M, Swift, B, Oleschuk, RD, and Horton, JH. The adsorption of globular proteins onto a fluorinated PDMS surface. J. Colloid Interface Sci., 2009;331:90-97.

[37] Müller, M, Brissová, M, Rieser, T, Powers, AC, and Lunkwitz, K. Deposition and properties of polyelectrolyte multilayers studied by ATR-FTIR spectroscopy. Materials Science and Engineering: C, 1999;8-9:163-169.

[38] Shibata, A, Yamamoto, M, Yamashita, T, Chiou, JS, Kamaya, H, and Ueda, I. Biphasic effects of alcohols on the phase transition of poly(L-lysine) between .alpha.-helix and .beta.-sheet conformations. Biochemistry (Mosc.), 1992;31:5728-5733.

[39] Brash, JL, Uniyal, S, and Samak, Q. EXCHANGE OF ALBUMIN ADSORBED ON POLYMER SURFACES. Transactions American Society for Artificial Internal Organs, 1974;A 20:69-76.

[40] Ostuni, E, Chapman, RG, Holmlin, RE, Takayama, S, and Whitesides, GM. A survey of structure-property relationships of surfaces that resist the adsorption of protein. Langmuir, 2001;17:5605-5620.

[41] Alessi, ML, Norman, AI, Knowlton, SE, Ho, DL, and Greer, SC. Helical and coil conformations of poly(ethylene glycol) in isobutyric acid and water. Macromolecules, 2005;38:9333-9340.

[42] Vennemann, N, Lechner, MD, and Oberthür, RC. Thermodynamics and conformation of polyoxyethylene in aqueous solution under high pressure: 1. Small-angle neutron scattering and densitometric measurements at room temperature. Polymer, 1987;28:1738-1748.

[43] Dormidontova, EE. Role of competitive PEO-water and water-water hydrogen bonding in aqueous solution PEO behavior. Macromolecules, 2002;35:987-1001.

[44] Polson, A. Theory for displacement of proteins and viruses with polyethylene glycol. Prep. Biochem., 1977;7:129-154.

[45] Polson, A, Potgieter, GM, Largier, JF, Joubert, FJ, and Mears, GEF. Fractionation of protein mixtures by linear polymers of high molecular weight. Biochim. Biophys. Acta, 1964;82:463-&.

[46] Veronese, FM and Pasut, G. PEGylation, successful approach to drug delivery. Drug Discov. Today, 2005;10:1451-1458.

[47] King, TP, Kochoumian, L, and Lichtenstein, LM. Preparation and immunochemical properties of methoxypolyethylene glycol-coupled and N-carboxymethylated derivatives of ragweed pollen allergen, antigen-E. Arch. Biochem. Biophys., 1977;178:442-450.

[48] Abuchowski, A, Vanes, T, Palczuk, NC, and Davis, FF. Alteration of immunological properties of bovine serum-albumin by covalent attachment of polyethylene glycol. J. Biol. Chem., 1977;252:3578-3581.

[49] Muller, HJ, Loning, L, Horn, A, Schwabe, D, Gunkel, M, Schrappe, M, von Schutz, V, Henze, G, da Palma, JC, Ritter, J, Pinheiro, JPV, Winkelhorst, M, and Boos, J. Pegylated asparaginase (Oncaspar (TM)) in children with ALL: drug monitoring in reinduction according to the ALL/NHL-BFM 95 protocols. Br. J. Haematol., 2000;110:379-384.

[50] Delgado, C, Francis, GE, and Fisher, D. The uses and properties of PEG-linked proteins. Crit. Rev. Ther. Drug Carrier Syst., 1992;9:249-304.

[51] Roberts, MJ, Bentley, MD, and Harris, JM. Chemistry for peptide and protein PEGylation. Adv. Drug Delivery Rev., 2002;54:459-476.

[52] DeSantis, G and Jones, JB. Chemical modification of enzymes for enhanced functionality. Curr. Opin. Biotechnol., 1999;10:324-330.

[53] Hatakeyama, H, Akita, H, Kogure, K, Oishi, M, Nagasaki, Y, Kihira, Y, Ueno, M, Kobayashi, H, Kikuchi, H, and Harashima, H. Development of a novel systemic gene delivery system for cancer therapy with a tumor-specific cleavable PEG-lipid. Gene Ther., 2007;14:68-77.

[54] Gabizon, A, Horowitz, AT, Goren, D, Tzemach, D, Mandelbaum-Shavit, F, Qazen, MM, and Zalipsky, S. Targeting folate receptor with folate linked to extremities of poly(ethylene glycol)-grafted liposomes: In vitro studies. Bioconjug. Chem., 1999;10:289-298.

[55] Zalipsky, S, Gilon, C, and Zilkha, A. Attachment of drugs to polyethylene glycols. Eur. Polym. J., 1983;19:1177-1183.

[56] Otsuka, H, Nagasaki, Y, and Kataoka, K. PEGylated nanoparticles for biological and pharmaceutical applications. Adv. Drug Delivery Rev., 2003;55:403-419.

[57] Gombotz, WR, Guanghui, W, Horbett, TA, and Hoffman, AS. Protein adsorption to poly(ethylene oxide) surfaces. J. Biomed. Mater. Res., 1991;25:1547-1562.

[58] Zalipsky, S. Chemistry of polyethylene glycol conjugates with biologically active molecules. Adv. Drug Delivery Rev., 1995;16:157-182.

[59] Graham, NB. Poly(ethylene glycol) gels and drug delivery, in Poly (ethylene glycol) chemistry: biotechnical and biomedical applications, J.M. Harris, Editor. 1992, Springer.

[60] Van Oss, CJ. Interfacial forces in aqueous media. 1994: M. Dekker.

[61] Paige, AG, Whitcomb, KL, Liu, J, and Kinstler, O. Prolonged circulation of recombinant human granulocyte-colony stimulating factor by covalent linkage to albumin through a heterobifunctional polyethylene glycol. Pharm. Res., 1995;12:1883-1888.

[62] Wong, JY, Kuhl, TL, Israelachvili, JN, Mullah, N, and Zalipsky, S. Direct measurement of a tethered ligand-receptor interaction potential. Science, 1997;275:820-822.

[63] Hersel, U, Dahmen, C, and Kessler, H. RGD modified polymers: biomaterials for stimulated cell adhesion and beyond. Biomaterials, 2003;24:4385-4415.

[64] Holmberg, K, Bergstrom, K, and Stark, MB. Immobilization of proteins via PEG chains, in Polyethylene Glycol Chemistry: Biotechnical and Biomedical Application, J.M. Harris, Editor. 1992, Plenum Press: New York. 303-324.

[65] Graham, NB. Poly(ethylene oxide) and related hydrogels, in Hydrogels in medicine and pharmacy, N.A. Peppas, Editor. 1987, CRC Press Inc.: Boca Raton, Florida. 95-113.

[66] Sawhney, AS, Pathak, CP, and Hubbell, JA. Bioerodible hydrogels based on photopolymerized poly(ethylen glycol)-co-poly(alpha-hydroxy acid) diacrylate macromers. Macromolecules, 1993;26:581-587.

[67] Andreopoulos, FM, Deible, CR, Stauffer, MT, Weber, SG, Wagner, WR, Beckman, EJ, and Russell, AJ. Photoscissable hydrogel synthesis via rapid photopolymerization of novel PEG-based polymers in the absence of photoinitiators. J. Am. Chem. Soc., 1996;118:6235-6240.

[68] Papavasiliou, G, Sokic, S, and Turturro, M. Synthetic PEG hydrogels as extracellular matrix mimics for tissue engineering applications. 2012.

[69] Rhee, WR, J.; Castro, M.; Schroeder, J.; Rao, PR; Hartner, C.; Berg, RA n vivo stability of poly(ethylene glycol) collagen composites, in Poly (ethylene glycol) chemistry: biotechnical and biomedical applications, J.M. Harris and A. Zalipsky, Editors. 1992, Springer: Washington. 420-440.

[70] Valentini, M, Napoli, A, Tirelli, N, and Hubbell, JA. Precise determination of the hydrophobic/hydrophilic junction in polymeric vesicles. Langmuir, 2003;19:4852-4855.

[71] Lee, JH, Lee, HB, and Andrade, JD. Blood compatibility of polyethylene oxide surfaces. Prog. Polym. Sci., 1995;20:1043-1079.

[72] Li, LY, Chen, SF, Zheng, J, Ratner, BD, and Jiang, SY. Protein adsorption on oligo(ethylene glycol)-terminated alkanethiolate self-assembled monolayers: The molecular basis for nonfouling behavior. J. Phys. Chem. B, 2005;109:2934-2941.

[73] Claesson, PM, Blomberg, E, Paulson, O, and Malmsten, M. Adsorption and interaction of a graft copolymer of poly(ethylene imine) and poly(ethylene oxide). Colloids and Surfaces a-Physicochemical and Engineering Aspects, 1996;112:131-139.

[74] Unsworth, LD.Protein adsorption to chemisorbed polyethylene oxide thin films, in Chemical engineering. 2005, McMaster University: Hamilton, Ontario.

[75] Vanderah, DJ, Vierling, RJ, and Walker, ML. Oligo(ethylene oxide) Self-Assembled Monolayers, with Self-Limiting Packing Densities for the Inhibition of Nonspecific Protein Adsorption. Langmuir, 2009;25:5026-5030.

[76] Alexander, S. Adsorption of chain molecules with a polar head: A scaling description. Journal De Physique, 1977;38:983-987.

[77] Unsworth, LD, Tun, Z, Sheardown, H, and Brash, JL. Chemisorption of thiolated poly(ethylene oxide) to gold: surface chain densities measured by ellipsometry and neutron reflectometry. J. Colloid Interface Sci., 2005;281:112-121.

[78] Unsworth, LD, Sheardown, H, and Brash, JL. Protein-resistant poly(ethylene oxide)-grafted surfaces: chain density-dependent multiple mechanisms of action. Langmuir, 2008;24:1924-1929.

[79] Chang, Y, Ko, CY, Shih, YJ, Quemener, D, Deratani, A, Wei, TC, Wang, DM, and Lai, JY. Surface grafting control of PEGylated poly(vinylidene fluoride) antifouling membrane via surface-initiated radical graft copolymerization. J. Membr. Sci., 2009;345:160-169.

[80] Chang, Y, Shih, YJ, Ko, CY, Jhong, JF, Liu, YL, and Wei, TC. Hemocompatibility of Poly(vinylidene fluoride) Membrane Grafted with Network-Like and Brush-Like Antifouling Layer Controlled via Plasma-Induced Surface PEGylation. Langmuir, 2011;27:5445-5455.

[81] Binazadeh, M, Zeng, H, and Unsworth, LD.Effect of peptide secondary structure on adsorption and adsorbed film properties to PEO modified surfaces, in 62nd Canadian Chemical Engineering Conference. 2012: Vancouver, British Columbia; Canada.

[82] Archambault, JG and Brash, JL. Protein repellent polyurethane surfaces by chemical grafting of PEO: Comparison of amino- and hydroxyl-terminated PEO as grafting reagents. Transactions of the 24th Annual Meeting of the Society for Biomaterials, 1998;21:251.

[83] McPherson, T, Kidane, A, Szleifer, I, and Park, K. Prevention of protein adsorption by tethered poly(ethylene oxide) layers: Experiments and single-chain mean-field analysis. Langmuir, 1998;14:176-186.

[84] Sofia, SJ, Premnath, V, and Merrill, EW. Poly(ethylene oxide) grafted to silicon surfaces: Grafting density and protein adsorption. Macromolecules, 1998;31:5059-5070.

[85] Kingshott, P, Thissen, H, and Griesser, H. Effects of cloud-point grafting, chain length, and density of PEG layers on competitive adsorption of ocular proteins J. Biomaterials, 2002;23:2043.

[86] Greenfield, NJ. Using circular dichroism spectra to estimate protein secondary structure. Nat. Protoc., 2006;1:2876-2890.

[87] Weber, N, Pesnell, A, Bolikal, D, Zeltinger, J, and Kohn, J. Viscoelastic properties of fibrinogen adsorbed to the surface of biomaterials used in blood-contacting medical devices. Langmuir, 2007;23:3298-3304.

[88] Yoshikawa, C, Goto, A, Tsujii, Y, Fukuda, T, Kimura, T, Yamamoto, K, and Kishida, A. Protein repellency of well-defined, concentrated poly(2-hydroxyethyl methacrylate) brushes by the size-exclusion effect. Macromolecules, 2006;39:2284-2290.

[89] Notley, SM, Eriksson, M, and Wagberg, L. Visco-elastic and adhesive properties of adsorbed polyelectrolyte multilayers determined in situ with QCM-D and AFM measurements. J. Colloid Interface Sci., 2005;292:29-37.

[90] Yan, MQ, Liu, CX, Wang, DS, Ni, JR, and Cheng, JX. Characterization of adsorption of humic acid onto alumina using quartz crystal microbalance with dissipation. Langmuir, 2011;27:9860-9865.

[91] Weber, N, Wendel, HP, and Kohn, J. Formation of viscoelastic protein layers on polymeric surf aces relevant to platelet adhesion. J. Biomed. Mater. Res., Part A, 2005;72A:420-427.

[92] Voinova, MV, Rodahl, M, Jonson, M, and Kasemo, B. Viscoelastic acoustic response of layered polymer films at fluid-solid interfaces: Continuum mechanics approach. Phys. Scr., 1999;59:391-396.

[93] Akbulut, M, Alig, ARG, Min, Y, Belman, N, Reynolds, M, Golan, Y, and Israelachvili, J. Forces between surfaces across nanoparticle solutions: role of size, shape, and concentration. Langmuir, 2007;23:3961-3969.

[94] Min, Y, Akbulut, M, Belman, N, Golan, Y, Zasadzinski, J, and Israelachvili, J. Normal and shear forces generated during the ordering (directed assembly) of confined straight and curved nanowires. Nano Lett., 2007;8:246-252.

[95] Israelachvili, J, Maeda, N, and Akbulut, M. Comment on reassessment of solidification in fluids confined between mica sheets. Langmuir, 2006;22:2397-2398.

[96] Zeng, H, Maeda, N, Chen, N, Tirrell, M, and Israelachvili, J. Adhesion and friction of polystyrene surfaces around Tg. Macromolecules, 2006;39:2350-2363.

[97] Chen, N, Maeda, N, Tirrell, M, and Israelachvili, J. Adhesion and friction of polymer surfaces: the effect of chain ends. Macromolecules, 2005;38:3491-3503.

[98] Akbulut, M, Godfrey Alig, AR, and Israelachvili, J. Triboelectrification between smooth metal surfaces coated with self-assembled monolayers (SAMs)†. The Journal of Physical Chemistry B, 2006;110:22271-22278.

[99] Min, Y, Kristiansen, K, Boggs, JM, Husted, C, Zasadzinski, JA, and Israelachvili, J. Interaction forces and adhesion of supported myelin lipid bilayers modulated by myelin basic protein. Proceedings of the National Academy of Sciences, 2009;106:3154-3159.

[100] Israelachvili, J, Min, Y, Akbulut, M, Alig, A, Carver, G, Greene, W, Kristiansen, K, Meyer, E, Pesika, N, Rosenberg, K, and Zeng, H. Recent advances in the surface forces apparatus (SFA) technique. Reports on Progress in Physics, 2010;73:1-16.

[101] Kekicheff, P, Ducker, WA, Ninham, BW, and Pileni, MP. Multilayer adsorption of cytochrome-C on mica around isoelectric pH. Langmuir, 1990;6:1704-1708.

[102] Klein, J and Luckham, PF. Long-range attractive forces between 2 mica surfaces in an aqueous polymer solution. Nature, 1984;308:836-837.

[103] Lee, CS and Belfort, G. Changing activity of ribonuclease-A during adsorption; a molecular explanation. Proc. Natl. Acad. Sci. U. S. A., 1989;86:8392-8396.

[104] Zeng, H, Hwang, DS, Israelachvili, JN, and Waite, JH. Strong reversible Fe3+-mediated bridging between dopa-containing protein films in water. Proc. Natl. Acad. Sci. U. S. A., 2010;107:12850-12853.

[105] Lu, Q, Hwang, DS, Liu, Y, and Zeng, H. Molecular interactions of mussel protective coating protein, mcfp-1, from Mytilus californianus. Biomaterials, 2012;33:1903-1911.

[106] Blankenburg, R, Meller, P, Ringsdorf, H, and Salesse, C. Interaction between biotin lipids and streptavidin in monolayers- formation of oriented two-

dimensional protein domains induced by surface recognition. Biochemistry (Mosc.), 1989;28:8214-8221.

[107] Darst, SA, Ahlers, M, Meller, PH, Kubalek, EW, Blankenburg, R, Ribi, HO, Ringsdorf, H, and Kornberg, RD. 2-dimensional crystals of streptavidin on biotinylated lipid layers and their interactions with biotinylated macromolecules. Biophys. J., 1991;59:387-396.

[108] Darst, SA, Ribi, HO, Pierce, DW, and Kornberg, RD. Two-dimensional crystals of escherichia-coliI RNA-polymerase holoenzyme on positively charged lipid layers. J. Mol. Biol., 1988;203:269-273.

[109] Kalb, E, Engel, J, and Tamm, LK. Binding of proteins to specific target sites in membranes measured by total internal reflection fluorescence microscopy. Biochemistry (Mosc.), 1990;29:1607-1613.

[110] McConnell, HM, Watts, TH, Weis, RM, and Brian, AA. Supported planar membranes in studies of cell-cell recognition in the immune-system. Biochim. Biophys. Acta, 1986;864:95-106.

[111] Pisarchick, ML and Thompson, NL. Binding of a monocolonal-antibody and its FAB fragment to supported phospholipid monolayers measured by total internal reflection fluorescence microscopy. Biophys. J., 1990;58:1235-1249.

[112] Poglitsch, CL and Thompson, NL. Interaction of antibodies with FC-receptors in substrate-supported planar membranes measured by total internal-reflection fluorescence microscopy. Biochemistry (Mosc.), 1990;29:248-254.

[113] Uzgiris, EE. Antibody organization on lipid films- influence of pH and interchain disulfide reduction. Biochem. J., 1990;272:45-49.

[114] Peanasky, J, Schneider, HM, Granick, S, and Kessel, CR. Self-assembled monolayers on mica for experiments utilizing the surface forces apparatus. Langmuir, 1995;11:953-962.

[115] Zeng, H, Tian, Y, Anderson, TH, Tirrell, M, and Israelachvili, JN. New SFA techniques for studying surface forces and thin film patterns induced by electric fields. Langmuir, 2008;24:1173-1182.

[116] Hwang, DS, Harrington, MJ, Lu, Q, Masic, A, Zeng, H, and Waite, JH. Mussel foot protein-1 (mcfp-1) interaction with titania surfaces. J. Mater. Chem., 2012;22:15530-15533.

[117] Israelachvili, JN. Thin film studies using multiple-beam interferometry. J. Colloid Interface Sci., 1973;44:259-272.

[118] Smith, CP, Maeda, M, Atanasoska, L, White, HS, and McClure, DJ. Ultrathin platinum films on mica and the measurement of forces at the platinum-water interface. J. Phys. Chem., 1988;92:199-205.

[119] Horn, RG and Smith, DT. Measuring surface forces to explore surface-chemistry- mica, sapphire, and silica. J. Non-Cryst. Solids, 1990;120:72-81.

[120] Claesson, PM, Cho, DL, Golander, CG, Kiss, E, and Parker, JL. Functionalized mica surfaces obtained by a cold-plasma process. Surfactants and Macromolecules : Self-Assembly at Interfaces and in Bulk, ed. B.R.J.S.P. Lindman. Vol. 82. 1990. 330-336.

[121] Parker, JL, Cho, DL, and Claesson, PM. Plasma modification of mica- forces between fluorocarbon surfaces in water and a nonpolar liquid. J. Phys. Chem., 1989;93:6121-6125.

[122] Marra, J. Direct measurment of the interchain between phosphatidylglycerol bilayers in aqueous-electrolyte solutions. Biophys. J., 1986;50:815-825.

[123] Marra, J and Israelachvili, J. Direct measurments of forces between phosphatidylcholine and phosphatidylethanolamine bilayers in aqueous-electrolyte solutions. Biochemistry (Mosc.), 1985;24:4608-4618.

[124] Claesson, PM, Herder, PC, Berg, JM, and Christenson, HK. The state of fluorocarbon surfactant monolayers at the air-water interface and on mica surfaces. J. Colloid Interface Sci., 1990;136:541-551.

[125] Helm, CA, Israelachvili, JN, and McGuiggan, PM. Molecular mechanisms and forces involved in the adhesion and fusion of amphiphilic bilayers. Science, 1989;246:919-922.

[126] Helm, CA, Israelachvili, JN, and McGuiggan, PM. Role of hydrophobic forces in bilayer adhesion and fusion. Biochemistry (Mosc.), 1992;31:1794-1805.

[127] Israelachvili, J and Marra, J. Direct methods for measuring conformational water forces (hydration forces) between membrane and other surfaces. Methods Enzymol., 1986;127:353-360.

[128] Zeng, H, Tian, Y, Anderson, TH, Tirrell, M, and Israelachvili, JN. New SFA techniques for studying surface forces and thin film patterns induced by electric fields. Langmuir, 2007;24:1173-1182.

[129] Lu, Q, Wang, J, Faghihnejad, A, Zeng, H, and Liu, Y. Understanding the molecular interactions of lipopolysaccharides during E. coli initial adhesion with a surface forces apparatus. Soft Matter, 2011;7:9366-9379.

[130] Zeng, H. Polymer adhesion, friction, and lubrication. 2012: John Wiley & Sons, in press.

[131] Zappone, B, Ruths, M, Greene, GW, Jay, GD, and Israelachvili, JN. Adsorption, lubrication, and wear of lubricin on model surfaces: Polymer brush-like behavior of a glycoprotein. Biophys. J., 2007;92:1693-1708.

[132] Gourdon, D, Lin, Q, Oroudjev, E, Hansma, H, Golan, Y, Arad, S, and Israelachvili, J. Adhesion and stable low friction provided by a subnanometer-thick monolayer of a natural polysaccharide. Langmuir, 2008;24:1534-1540.

[133] Benz, M, Chen, NH, and Israelachvili, J. Lubrication and wear properties of grafted polyelectrolytes, hyaluronan and hylan, measured in the surface forces apparatus. Journal of Biomedical Materials Research Part A, 2004;71A:6-15.

[134] Hwang, DS, Zeng, H, Lu, Q, Israelachvili, J, and Waite, JH. Adhesion mechanism in a DOPA-deficient foot protein from green mussels. Soft Matter, 2012;8:5640-5648.

[135] Hwang, DS, Zeng, H, Srivastava, A, Krogstad, DV, Tirrell, M, Israelachvili, JN, and Waite, JH. Viscosity and interfacial properties in a mussel-inspired adhesive coacervate. Soft Matter, 2010;6:3232-3236.

[136] Drobek, T and Spencer, ND. Nanotribology of surface-grafted PEG layers in an aqueous environment. Langmuir, 2008;24:1484-1488.

[137] Leckband, D and Israelachvili, J. Intermolecular forces in biology. Q. Rev. Biophys., 2001;34:105-267.

[138] Claesson, PM and Golander, CG. Direct measurments of steric interactions between mica surfaces covered with electrostatically bound low molecular weight polyethylene oxide. J. Colloid Interface Sci., 1987;117:366-374.

[139] Sheth, SR and Leckband, D. Measurments of attractive forces between proteins and end-grafted poly(ethylene glycol) chains. Proc. Natl. Acad. Sci. U.S.A., 1997;94:8399-8404.

[140] Zhang, L, Zeng, H, and Liu, Q. Probing molecular and surface interactions of comb-type polymer polystyrene-graft-polyethylene oxide (PS-g-PEO) with an SFA. J. Phys. Chem. C, 2012;116:17554-17562.

2. Effect of Peptide Secondary Structure on Adsorption and Adsorbed Film Properties[2]

2.1. Introduction

Spontaneous and non-specific adsorption of proteins at the interface between physiological fluids and materials is a major problem that continues to challenge the broad application of most biomaterials [1-5]. Specifically, the consequences of protein fouling at the tissue-material interface may include compromised implant performance, adverse host responses (inflammation, immune, and thrombotic), implant failure, and patient infection; situations that ultimately impair patient health, device efficiency, and increase the cost of treatment [6]. Although there are numerous studies investigating protein adsorption and its mechanism, systematic studies of individual aspects of proteins are difficult as each protein has a unique chemical composition as well as secondary and tertiary/quaternary structures that may allow for preferential adsorption at surfaces of different physiochemical properties. Moreover, it is understood that the strength and range of protein-surface interactions are dependent on the protein (amino acid sequence [7], molecular weight [8], and isoelectric point [9, 10]), solution (pH [11], ionic strength [12], and temperature [13]) and surface (roughness [14], structure [15], hydrophobicity [16], and chemical nature [17]) properties. Although the effect of many protein attributes (pI [9, 10], size [8], and hydrophobicity [18]) on non-specific protein adsorption have been investigated, there have been very few

[2] This chapter was published in: Effect of peptide secondary structure on adsorption and adsorbed film properties. *Binazadeh, M., H. Zeng, and L.D. Unsworth*, **Acta Biomaterialia**, 2013. 9 (5): p. 6403-6413.

systematic studies [19] elucidating the effect of secondary structure composition on protein adsorption and the resulting adsorbed layer properties.

Although each protein has a 'unique' physical and chemical structure determined by its amino acid sequence, several structural features are common among all proteins. In general, proteins have a compact three dimensional structure with little internal space. Moreover, there are a relatively limited number of secondary structures (e.g. α-helix, β-sheet, etc.) periodically occurring throughout the main protein chain: where ~50% of the protein sequence is devoted to α-helix and β-sheet formation [20, 21]. Secondary structure formation has been attributed to hydrogen bonding between neighbouring amino acids in the protein's sequence, and can directly influence the protein's physicochemical properties such as shape, size, apparent hydrophobicity, charge, and function. In an α-helix chain each amine group from the backbone forms a hydrogen bond with the carbonyl group of amino acid four places earlier in the primary sequence. In case of β-sheets, two strands form hydrogen bonds *via* the carbonyl group in the backbone of one strand with the amine group from the opposing backbone of a neighbouring strand. The α-helix has a more compact structure than the β-sheet, due to the formation of hydrogen bonds between immediate neighbouring amino acids. For a PLL chain (Figure 2.1), 3.6 residues form a full helical turn with 0.54 nm pitch and 26° pitch angle [22]. The distance between two adjacent strands in a β-sheet motif has been reported to be 10.08 Å [23]. For a given molecular weight of PLL, geometric differences between different secondary structures result in a β-sheet structure that is 2.3 times longer than an α-helix.

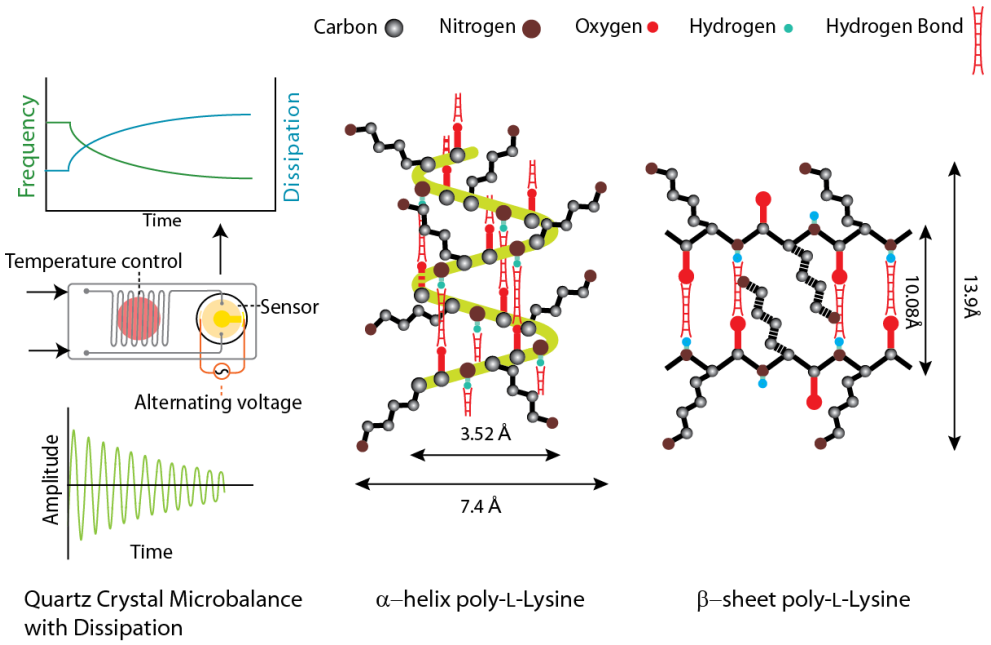

Figure 2.1 Schematic drawing of experimental setup of quartz crystal microbalance with dissipation (QCM-D) and PLL in α-helix[22] and β-sheet[23] conformation.

The protein adsorption literature is too vast to review in its entirety, herein. Suffice it to say that several investigations have looked at protein adsorption mechanisms *via* experiments using a known protein or multi-component protein solutions for a wide variety of surfaces [24, 25]. From bulk solution to a substrate surface, diffusion moves proteins towards the surface and adsorption occurs due to the influence of intermolecular and surface forces that can affect proteins from ~1 to ~10 nm away from the surface [26]. The relatively low energy barrier between conformational states of various protein domains yields an overall native conformation that is highly susceptible to structural changes induced by environmental disturbances, viz., the introduction of a surface [27]. Near a surface the interactions between the surface and protein might alter

the balance of intramolecular non-covalent interactions responsible for secondary structure formation (hydrogen bonds, hydrophobic interactions, electrostatic interactions, and van der Waals) and consequently, lead to non-specific protein adsorption and surface induced denaturing.

In fact, the adsorption of proteins on a surface may cause a perturbation in protein conformation. This conformational change may expose hydrophobic domains of the protein, resulting in the formation of multiple contact points between the proteins and surface that yields a tight adhesion to the biomaterial surface [28-32]. It has been reported that conformational changes of adsorbed proteins can be responsible for adverse host responses such as accumulation of inflammatory cells, foreign body response, and coagulation [28, 33-35]. Despite the apparent influence that secondary structures have on protein properties, very few investigations have tried to systematically evaluate their influence on protein adsorption. Bonekamp reported that the secondary structure of PLL (random coil and α-helix) does not affect its adsorbed amount on polystyrene latex [19]. Further to this, it was reported that these secondary structures were perturbed upon adsorption to polystyrene surface. However, it is important to note that inconsistent solution pH conditions used in these studies convolute the interpretation of the results as PLL secondary structure strongly depends upon solution pH. In this previous work, the conformation of adsorbed PLL was indirectly deduced *via* analysis of proton titration data as opposed to direct determination using techniques like circular dichroism (CD). It is still largely unknown how these secondary structures will interact with the surface, and how it

may lead to surface induced unfolding of the secondary structures, layer viscoelasticity, and adsorbed mass surface-density.

Thus, the purpose of this work is to systematically investigate the influence protein secondary structure has on adsorption and adsorbed film properties. To better understand the effect of secondary structure of proteins on non-specific protein adsorption, Poly-L-Lysine (PLL) was used as a model peptide. The rationale behind this choice is that, while maintaining a constant overall molecular charge profile, PLL can adopt both α-helix and β-sheet structures depending on solution pH and temperature (Figure 2.1) [36]. PLL chains in exactly the same physicochemical solution condition may have a specific, pre-induced secondary structure depending on the solution preparation path (thermal history). It has been reported that 75% α-helix content can be induced in a PLL solution by increasing pH; heating this α-helix PLL solution will transform these chains into β-sheet (i.e. complete transformation of α-helix to β-sheet) [37]. The formation of adsorbed layer in this work will be monitored using a quartz crystal microbalance with dissipation (QCM-D), providing kinetic information about absorbed film thickness, adsorbed mass, and adsorbed film viscoelastic properties (i.e. shear viscosity) [38]. QCM-D allows for the formation and growth kinetics of a protein layer on a quartz crystal sensor to be captured with time by monitoring changes in the frequency (Δf) and dissipation (ΔD_f) (Figure 2.1). A quartz crystal sensor is a thin piezoelectric plate with Au electrodes on each side. Briefly, when mass is added to the sensor, its resonance frequency (f) will decrease due to the piezoelectric effect of quartz, and the

viscoelastic properties of the adsorbed layer can be determined through monitoring the dissipation shift. It is thought that understanding this fundamental effect of a protein's structural subunits will improve our knowledge about influential parameters involved in non-specific protein adsorption and ultimately help us in designing engineered surfaces for biomedical devices.

2.2 Materials and experimental methods

2.2.1 Materials and sample preparation

PLL-HCl, molecular weight range 15-30 kDa, sodium sulfate (anhydrous), potassium phosphate (monobasic and dibasic, anhydrous), and sodium hydroxide were purchased from Sigma- Aldrich Canada Ltd. QCM-D Au sensors and quartz slides were purchased from Biolin Scientific Inc. and GM Aassociates Inc., respectively. 10 mM potassium phosphate solution (PB) with 5, 50, and 500 mM sodium sulphate was used in the experiments. To form α-helix PLL, pH of protein solution was adjusted to 10.6 by adding 50 mM NaOH and in order to transform α-helix to β-sheet, solution sample was heated to 70°C and cooled back to (initial) room temperature (24 °C).

2.2.2 Circular Dichroism (CD)

CD was used to track the formation and persistence of desired secondary structures of PLL in solution as well as in the adsorbed state. Herein, 10 mM potassium phosphate solution (PB) with 5, 50, or 500 mM sodium sulphate without pH adjustment was used to prepare 5 mg/mL PLL stock solution. The

stock solution was diluted 50 times and pH of diluted PLL solution was adjusted to 10.6 with 50 mM NaOH solution to form α-helix structure. In order to transform α-helix to β-sheet, the sample was heated at 70°C for 50 min. All samples were degassed for 20 min using a vacuum pump (Bluffton 1603007404) with liquid nitrogen trap to eliminate any influence of dissolved gases on CD measurement. For time related measurements, in bulk solution, a quartz cuvette (0.2 cm pathlength, International Crystal Lab) was used.

CD measurements of PLL in solution were conducted after sample preparation using a Jasco-J810 equipped with a Julabo AWC100 water bath for temperature control. A background spectrum was obtained using a degassed 10 mM PB with appropriate sodium sulfate concentration (without PLL) at pH 10.6 and 37°C. After formation of desired secondary structure of PLL, its persistence in solution was evaluated at 37°C by measuring its CD spectra for up to 8 hrs. CD spectra for all samples were recorded from 190 to 260 nm and all reported CD spectra are average of three measurements.

In order to measure the CD spectra of PLL in adsorbed state, PLL was first adsorbed on Au coated quartz slides by immersion of the quartz slides in a PLL solution (similar to the solution condition for CD measurements) which possessed specified secondary structure for 1 hr to ensure plateau adsorption. The quartz slides were coated with chromium and Au according to the protocol reported by Sivaraman et al [39]. The adsorbed PLL layer was then rinsed with PB solution (without PLL) ensuring that the CD reading was mainly due to the adsorbed PLL. A 0.12 mm gap was maintained between the two Au sides of

quartz slides by use of a Teflon adhesive film (McMaster-Carr). In this way the adsorbed PLL layer could stay hydrated to avoid drying-induced conformation changes [40]. The CD measurements of adsorbed PLL were also done at 37ºC.

2.2.3 Quartz Crystal Microbalance with Dissipation (QCM-D)

The adsorption of PLL and impact of secondary structure was investigated using a QCM-D with Au coated quartz sensor (fundamental frequency of 4.95 MHz) (Q-sense E4, Q-sense AB, Gothenburg, Sweden), which has the capacity of measuring changes in resonance frequency (Δf) and energy dissipation (ΔD_f) of QCM-D sensors simultaneously. PLL solution with desired secondary structure was prepared and the structure confirmed using CD prior to QCM-D experiments. Bulk PLL solution was kept at 37ºC. A high precision pump (ISMATEC) was used to achieve a solution flow over the Au coated quartz sensor of 0.15 mL/min. Before injection of PLL solution, the PB solution without PLL was first pumped into the QCM-D module to obtain a stable baseline. PLL with the specified secondary structure was then introduced into the QCM-D module and adsorption was allowed to proceed for 20 minutes till the plateau adsorption was reached, viz., the change in frequency and dissipation per minute became less than 0.1 Hz/min and 0.06 min^{-1}, respectively. In this study, the Voigt viscoelastic model in Q-sense Qtools 3.0 was used to correlate the frequency change to mass change (see Theory below).

2.2.4 QCM-D Sensor Cleaning Protocol

QCM-D sensors were cleaned according to manufacturer's protocol. In brief, a sensor was placed in a UV/Ozone Procleaner chamber (Bio Force Nanosciences Inc.) for 10 min, then transferred into ammonium peroxide solution (5:1:1 mixture of MilliQ water, ammonia (25%), and hydrogen peroxide (30%)) at 75ºC for 5 min. The wet sensor surface was rinsed with MilliQ water and dried with purified nitrogen gas. UV/Ozone treatment was repeated again after cleaning with ammonium peroxide.

2.2.5 Molecular size and Zeta potential measurements

Marvern Nano-S Zetasizer was used to measure the zeta potential and dynamic light scattering of PLL chains in solution. 1 mg/mL PLL solution with pre-known secondary structure and salt concentration was used. The cell holder was programmed to maintain the temperature of 37°C and measurement was started at least 10 min after placement of the sample cell to ensure thermal equilibrium. Zeta potential and dynamic light scattering measurements were repeated at least 3 times for each sample.

2.2 Theoretical methods

2.1.1 Voigt model

Adsorption of mass on the QCM-D quartz sensor surface results in a decrease in the resonance frequency (*f*) of sensor due to its piezoelectric effect, which can be monitored in real time. In this study, data modeling and analysis after the experimental measurements were carried out with Q-sense Qtools 3.0, in which

Sauerbrey model and Viscoelastic model could be chosen to correlate frequency shift with mass change. By use of the Sauerbrey equation, adsorbed mass of relatively uniform, rigid, and thin film can be calculated as a linear function of frequency change. However, when the dissipation change associated with adsorption processes is much larger than zero (non-rigid adsorbed layer), the Sauerbrey equation usually underestimates adsorbed mass [41]. Therefore, the Voigt model, which is the simplest representation of a viscoelastic solid, was used here to correlate the mass, thickness, and viscoelastic property of adsorbed layer to the measured shifts in frequency and dissipation [42]. Based on the Voigt model, for a viscoelastic layer (index "1") on quartz slide (index "0") immersed in a bulk Newtonian fluid (index "2") the following equations hold [42]:

$$\Delta f \approx -\frac{1}{2\pi\rho_0 h_0}\left\{\frac{\eta_2}{\delta_2}+\left[H_1\rho_1\omega-2H_1\left(\frac{\eta_2}{\delta_2}\right)^2\frac{\eta_1\omega^2}{\sigma_1^2+\omega^2\eta_1^2}\right]\right\} \tag{2.1}$$

$$\Delta D_f \approx \frac{1}{2\pi f\rho_0 H_0}\left\{\frac{\eta_2}{\delta_2}+\left[2H_1\left(\frac{\eta_2}{\delta_2}\right)^2\frac{\eta_1\omega^2}{\sigma_1^2+\omega^2\eta_1^2}\right]\right\} \tag{2.2}$$

$$\delta_2=\sqrt{\frac{2\eta_2}{\rho_2\omega}} \tag{2.3}$$

where f stands for oscillation frequency, D_f dissipation, ρ density, H thickness, η viscosity, σ shear modulus, and ω is the circular frequency.

By fitting the QCM-D data (frequency and dissipation change as a function of time for n=5 and 7 overtones) with the Voigt model, the thickness (or mass) and shear viscosity of the adsorbed layer can be determined. It should be

noted that the Voigt model necessitates the assumption that the solution flowing over the sensor is viscous and Newtonian. Moreover, uniform density and thickness of the adsorbed layer is also assumed. The adsorbed hydrated layer is considered as a viscoelastic film and quartz crystal is assumed purely elastic. In the Voigt model, it is also assumed that there is no slip between the adsorbed molecules and the Au coated crystal during the experiment. It was reported that the layer density has only a minor influence on the modeling results [43]. In fact, layer thickness and density are paired and changes in layer density result in changes in layer thickness. As a result the adsorbed mass is relatively insensitive to minor differences in the assumed layer density (results not shown). In our data analysis a density of 0.994 g/cm^3 and viscosity of 0.7 cP were chosen for PLL solution in 10 mM potassium phosphate solution with 5 or 50 mM sodium sulfate at 37 ºC [44]. For PLL solution in 10 mM potassium phosphate solution with 500 mM sodium sulfate at 37 ºC, 1.07 g/cm^3 [44] and 0.9 cP [45] were chosen as the density and viscosity, respectively.

2.1.2 Surface interaction energies

α-helix PLL may show a cylinder-like configuration. Thus, the van der Waals and electrostatic interaction energies (per unit length) between α-helix PLL and a flat Au QCM-D sensor surface can be described by equations 2.4 and 2.5, respectively [46]. β-sheet PLL may have more of a rectangular flat geometry, therefore, the van der Waals and electrostatic interaction energies per unit length of rectangular β-sheet PLL with flat Au surface can be described by equations 2.6 and 2.7, respectively [46], where W stands for interaction energy, *vdw*,

electrostatic, α, and β refer to van der Waals interaction, electrostatic interaction, α-helix, and β-sheet respectively, A is Hamaker constant, R=3.7 Å is helix radius (Figure 2.1), d is the distance between α-helix cylinder/ β-sheet surface and Au surface, Z is geometry independent electrostatic interaction constant, κ^{-1} is Debye length, and i=13.9 Å is width of rectangular β-sheet PLL (Figure 2.1).

$$W_{vdw,\alpha} = -\frac{A}{12}\sqrt{\frac{R}{2d^3}} \tag{2.4}$$

$$W_{electrostatic,\alpha} = \sqrt{\frac{\kappa R}{2\pi}} Z e^{-\kappa d} \tag{2.5}$$

$$W_{vdw,\beta} = -\frac{Ai}{12\pi d^2} \tag{2.6}$$

$$W_{electrostatic,\beta} = \frac{\kappa i}{2\pi} Z e^{-\kappa d} \tag{2.7}$$

Hamaker constant of PLL (surface 1) and Au (surface 3) across aqueous solution (medium 2) can be given by equation 2.8 [47]:

$$A_{123} \approx \frac{3h}{8\sqrt{2}} \frac{(n_1^2 - n_2^2)v_1 v_3}{\left(n_1^2 + n_2^2\right)^{1/2}\left(v_1 + \left(n_1^2 + n_2^2\right)^{1/2} v_3\right)} \approx \frac{3hv_e}{8\sqrt{2}} \frac{\left(n_1^2 - n_2^2\right)}{\left(n_1^2 + n_2^2\right)^{1/2}\left(1 + \left(n_1^2 + n_2^2\right)^{1/2}\right)} \tag{2.8}$$

Geometry independent electrostatic interaction constant Z for 2 surfaces with different surface potentials is defined as shown in equation 2.9 [46]:

$$Z = 64\pi\varepsilon_0\varepsilon_2\left(\frac{kT}{ze}\right)^2 \tanh\left(\frac{ez\psi_3}{4kT}\right)\tanh\left(\frac{ez\psi_1}{4kT}\right) \tag{2.9}$$

and κ is given by equation 2.10 [46]:

$$\kappa = \sqrt{\left(\sum \frac{\rho_j e^2 z_j^2}{\varepsilon_0 \varepsilon_2 kT} \right)} \tag{2.10}$$

In the above equations, k=1.381x10^{-23}m^2.kg.s^{-2}.K^{-1}, is Boltzmann constant; ε_0=8.85x10^{-12} F.m^{-1}, is vacuum permittivity; ε_2= 74.8 at 37°C, is relative permittivity of medium; h=6.626x10^{-34} J.s, is Planck constant; υ is the main electronic absorption frequency in the UV (υ_e=3x10^{15} s^{-1}); n is refractive index (n_1=1.48 for PLL [48] and n_2=1.33); e=1.602x10^{-19} C, is electron charge; z is electrolyte ion valence (z=1 for KH_2PO_4 and NaOH and z=2 for Na_2SO_4 and K_2HPO_4), ψ is surface potential (approximate value of ψ_1(i.e. zeta potential) is given in Table 2.3 and ψ_3= -49.4 mV for Au [49] at pH 10.6) and ρ_j is number density of species j (ρ_j=6.022x10^{26} M_j, where M_j is the molarity of species j).

2.2 Results and Discussion

The effect of secondary structures on protein adsorption and subsequent film properties was investigated using PLL based α-helices and β-sheets. It is thought that secondary structures may not only influence the adsorption process of proteins, but also directly impact the physical properties of the formed film through hydrogen bonding, and/or denaturing at the solid interface. Secondary structures are formed *via* several important non-covalent interactions including hydrogen bonds, hydrophobic interactions, electrostatic bonds, and van der Waals forces [50]. The free energies contributed by each of the above interaction types leads to the stabilization of the protein structure, which is affected by protein

molecular composition as well as vicinal solution conditions. Previously, it has been shown that PLL can be transformed into different secondary structures through controlling solution conditions. In order to systematically investigate the effect of secondary structures upon peptide adsorption and subsequently formed layer properties it is thought that through transforming PLL into multiple secondary structures a view on the effect this has on surface charge would be illuminated while allowing for secondary structure influences upon adsorption and film properties to be studied; where conformational differences between different secondary structures may cause differences in surface potential values.

2.2.1 PLL secondary structure determination: in solution

It has been shown that PLL maintains a random coil structure in solution at neutral pH, where other secondary structures can be induced through the manipulation of solution pH and temperature [51], presence of organic solvents [52], salts [53], and phospholipids [54]. Specifically, PLL α-helix conformations were induced by increasing the solution pH from ~7 to 10.6 (37ºC), which has been shown to almost complete transformation of random coiled PLL to α-helices [55]. This solution was then heated to 70°C for 50 min so as to transform α-helix PLL into β-sheet conformations. These secondary structures being confirmed using CD, where α-helices have a maximum peak at ~190 nm and minimum peaks at ~205 and 222 nm, and β-sheets have a respective maximum and minimum peak at ~195 and ~215 nm [56, 57]. Moreover, the intensity of these peaks is directly proportional to relative concentration of the secondary structures within the electromagnetic (EM) beam path. That said, the ultimate goal was to

characterize the adsorption of these structures for comparison to QCM-D experiments. Thus, in order to proceed with adsorption experiments, it was necessary to first determine if the secondary structures formed in solution could be maintained, once formed, at 37°C for long durations (especially β-sheet PLLs).

Figure 2.2 summarizes the CD data corresponding to PLL in solution just after secondary structure induction and normalization of solution temperature to 37^{o}C. In all cases, it was found that α-helix (Figure 2.2a, 2.2c, and 2.2e) and β-sheet (Figure 2.2b, 2.2d, and 2.2f) secondary structures were stable in solution for up to 8 hrs (Table 2.1). Moreover, given that various salt concentrations would be used to evaluate the effect of electrostatic forces on peptide adsorption, the effect of salt concentration on solution peptide conformation was also evaluated. It was found that no meaningful changes in either peak position or peak intensity were observed over the time of this study, suggesting that the respective secondary structures induced through controlling solution conditions persist and adsorption times of <8 hrs could be used for studying PLL adsorption to Au coated surfaces for all solutions presented herein.

2.2.2 PLL secondary structure determination: adsorbed state

PLL adsorption to Au coated quartz slides was conducted so as to determine if the adsorption event ultimately influenced the secondary structure of these peptides (Figure 2.2). Table 2.1 summarizes peak position and intensity of both α-helix and β-sheet conformers in solution at different times and in the adsorbed state on Au for different salt concentrations. Given the minor differences in peak positions between the bulk and adsorbed PLL it is probable that no determinable

denaturation of these peptides has occurred upon adsorption. These peak position differences could be attributed to slight differences in cuvette path-length and/or optical properties of the different cuvettes used. Especially as it has been previously reported that a 3 nm shift in CD peak position does not imply an overall difference in secondary structure [56, 58].

Table 2.1 Position and intensity of peaks in the CD spectra of different PLL conformations in solution and adsorbed state. Data from 0.1mg/mL PLL in 10 mM potassium phosphate solution with 5, 50, or 500 mM Na_2SO_4 at pH 10.6, T 37ºC

Salt concentration	Conformer	Time (hr)	Peak 1 position	Intensity 10^3 [θ]	Peak 2 position	Intensity 10^3 [θ]	Peak 3 position	Intensity 10^3 [θ]
5		Solution	190.0	8.5	203.5	-13.2	223.0	-8.0
	α-helix	8	190.0	10.2	204.0	-13.0	223.0	-8.1
		adsorbed	190.0	15.9	204.0	-29.7	222.0	-18.7
		0	192.0	9.0	214.0	-10.6	-	-
	β-sheet	8	191.5	6.6	213.0	-10.3	-	-
		adsorbed	192.5	19.5	214.0	-32.3	-	-
50		0	191.0	12.7	204.0	-9.9	222.5	-6.2
	α-helix	8	192.0	9.7	205.0	-10.4	221.5	-6.6
		adsorbed	190.0	10.0	204.5	-23.4	223.0	-18.1
		0	192.5	13.4	215.0	-8.5	-	-
	β-sheet	8	191.5	17.6	214.5	-8.2	-	-
		adsorbed	194.5	21.5	215.0	-29.4	-	-
500		0	191.0	17.0	206.5	-9.6	221.0	-7.0
	α-helix	8	190.0	19.3	206.5	-10.0	221.5	-7.5
		adsorbed	190.0	19.2	204.0	-27.1	223.0	-18.9
		0	195.5	11.1	216.0	-9.9	-	-
	β-sheet	8	195.5	6.5	215.0	-10.2	-	-
		adsorbed	192.5	14.4	216.0	-23.9	-	-

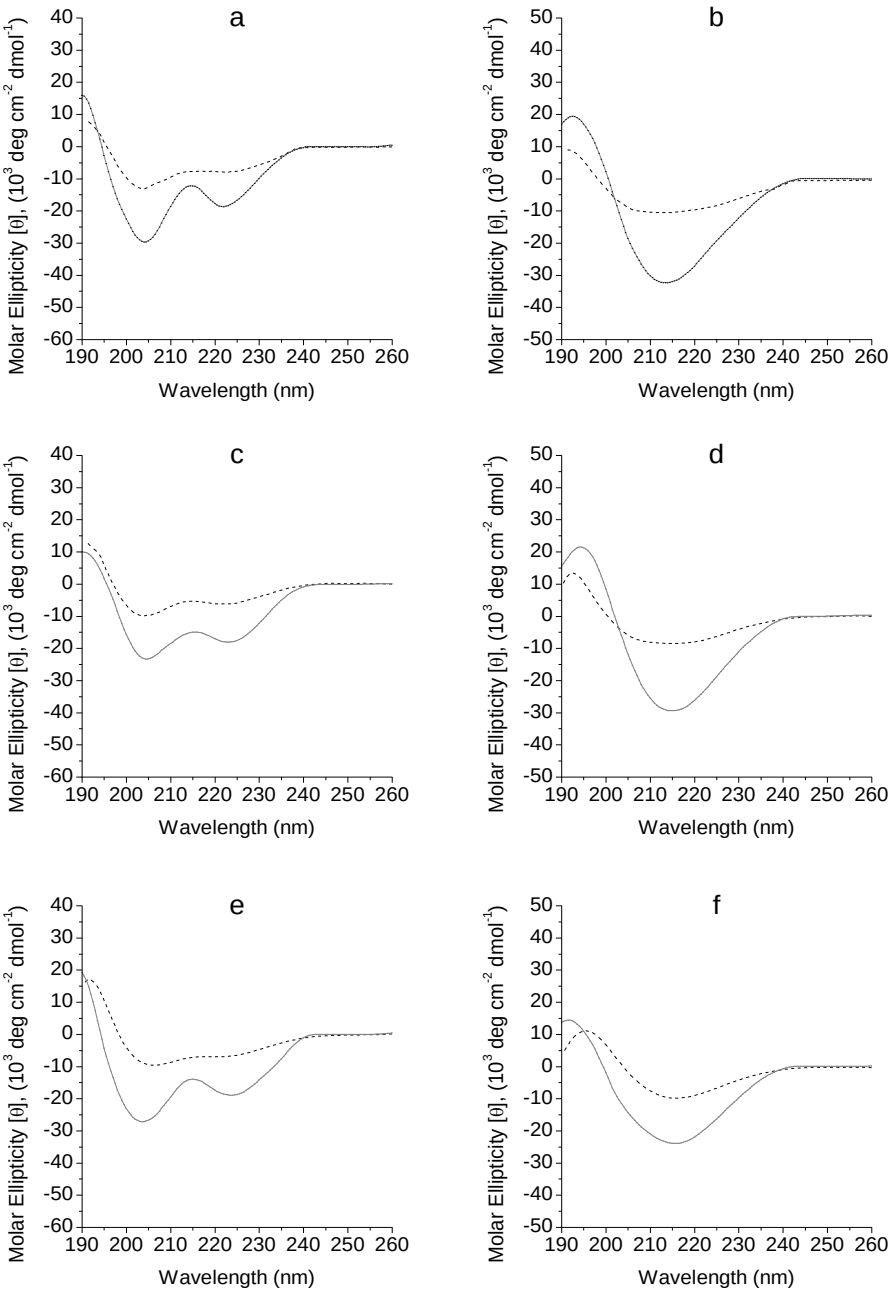

Figure 2.2 CD spectra of PLL in α-helix conformation shown in left subfigures **a**, **c**, **e.** and β-sheet conformation shown in right subfigures **b**, **d**, **f.** in 0.1 mg/mL PLL bulk solution immediately after preperation (…) and after being adsorbed to Au coated quartz slides (—) from 10 mM potassium phosphate solution with **a**, **b.** 5 mM Na_2SO_4 top subfigure; **c**, **d.** 50 mM Na_2SO_4 middle subfigures; and **e**, **f.** 500 mM Na_2SO_4 bottom subfigures; at pH 10.6, T 37ºC. All bulk PLL conformations were stable up to 8 hrs (data not shown), and upon adsorption secondary structures seemed to be retained. Data represent the average of n=3 measurements.

2.2.3 PLL layer properties: mass adsorbed, thickness, and layer viscosity

Through monitoring shifts in the oscillating frequency (Δf) and dissipation (ΔD_f) of a quartz crystal, the thickness, adsorbed mass, and viscoelastic properties of an adsorbed film can be determined with time. Representative QCM-D data (Figure 2.3) details the adsorption profiles for both α-helix and β-sheet adsorption to Au coated sensors from 10 mM PB as a function of Na_2SO_4 concentration. In all systems, the 5 min of PB solution (void of PLL) rinse (t=-5 to 0 min) is included so as to illustrate that the stable baseline was achieved prior to introducing PLL (t=0 min). At the end of the adsorption process (t=20 min), PB solution was injected again to rinse the adsorbed PLL layer (t=20 to 25 min).

The overall change in Δf was significantly larger for β-sheet compared to the α-helix adsorption: β-sheet frequency decrease of -54.5±1.0, -18.1±0.9, and -12.1±0.7 Hz, as opposed to -10.1±0.3, -9.4±0.3, and -6.1±0.2 Hz for α-helix in solutions containing 5, 50, and 500 mM sodium sulfate, respectively. Increasing the sodium sulfate concentration from 5 to 50 and 500 mM led to respective reductions in Δf by ~67 and ~78% for β-sheet adsorption; whereas, a reduction of ~7 and ~40% in Δf was observed for α-helix adsorption upon increasing the salt concentration from 5 to 50 and 500 mM, respectively. It is also notable that the interaction of α-helix PLL with the Au sensor was initially faster than that of β-sheet: α-helix frequency drop of -48.3±4.5, -25.8±3.5, and -21.5±1.8 Hz/min as opposed to -6.4±0.1, -6.5±0.5, and -16.6±0.4 Hz/min frequency drop for β-sheet PLL in solutions with 5, 50, and 500 mM sodium sulfate, respectively. Finally, it has been reported that the absolute value of the ratio of $\Delta D_f/\Delta f$ yields information regarding the adsorbed layer structure. A low $\Delta D_f/\Delta f$ ratio for adsorbed α-helix

PLL layer (~0.06, 0.05, and 0.07 Hz^{-1} for α-helix as opposed to ~0.15, 0.15, and 0.53 Hz^{-1} for β-sheet adsorption from solutions with 5, 50, and 500 mM sodium sulphate, respectively) suggests a relatively low energy dissipation and a stiffer and more compact layer structure [59, 60] for α-helix PLL as compared with β-sheet.

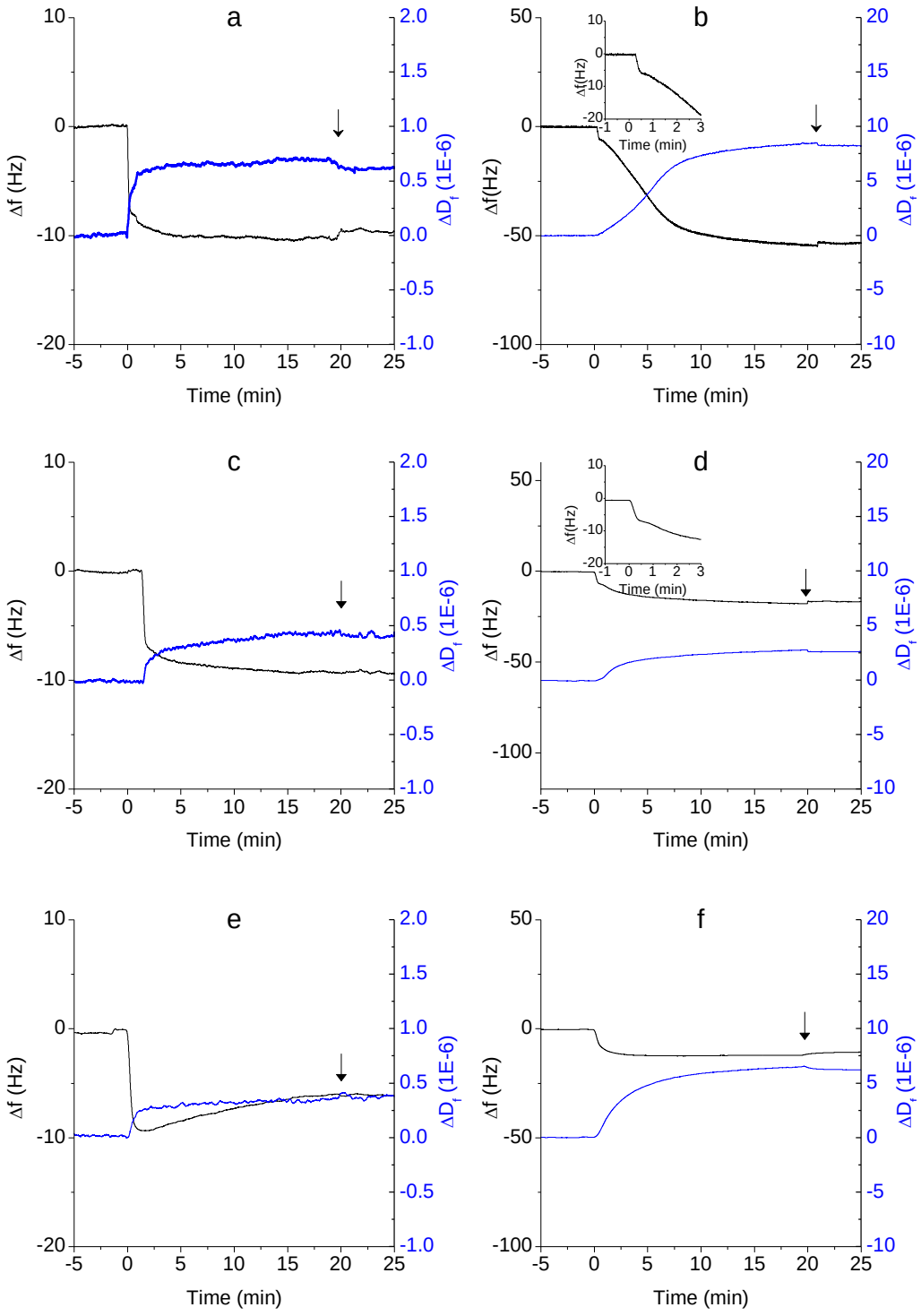

Figure 2.3 Representative time course of Δf and ΔD_f for **a**, **c**, **e.** α-helix; and **b**, **d**, **f.** β-sheet PLL adsorption on QCM-D Au sensor at different salt concentration; 0.15 mL/min flow rate, 0.1 mg/mL PLL in 10 mM potassium phosphate solution with **a**, **b.** 5 mM Na_2SO_4; **c**, **d.** 50 mM Na_2SO_4; and **e**, **f.** 500 mM Na_2SO_4; at pH 10.6, T 37ºC. Time -5 to 0 min and time 20 to 25 min corresponds to the PB wash before and after PLL adsorption. Arrow indicates the PB wash after adsorption process

Modelling results of QCM-D data, using the Voigt model, are presented in Figure 2.4. Left subfigures show time course of mass and thickness growth for both α-helix and β-sheet PLL adsorbed layers as a function of salt concentration. Linear proportionality of thickness and mass of the adsorbed layer is a result of the assumption that the layer density is constant. That said, as mentioned earlier, adsorbed mass is minimally affected by the input modelling value of layer density due to paring of layer thickness and layer density (results not shown). It should be noted that the adsorption parameters obtained by QCM-D experiments (Δf and ΔD_f) represent the hydrated PLL layer properties adsorbed on the pre- PB solution washed Au sensor. In other words, the effect of water molecules participating in the formation of the hydration shells around the PLL chains are imbedded within this analysis. Average values of PLL adsorption parameters are listed in Table 2.2. Initial adsorption rate of α-helix (average rate from beginning until adsorption half time) was always higher than that of β-sheet at each salt concentration. By increasing sodium sulfate concentration from 5 to 50 mM the initial adsorption rate of α-helix increased from 322±30 to 440±60 ng/cm^{2}min. However, further increase of Na_2SO_4 concentration to 500 mM only slightly reduced the initial rate of α-helix adsorption to 385±32 ng/cm^{2}min. In contrast, the initial adsorption rate of β-sheet increased monotonically with an increase of salt concentration. Furthermore, the adsorption half time for both α-helix and β-sheet decreased with an increase in sodium sulfate concentrations, indicating hampered PLL adsorption. In all cases the adsorption half time for β-sheet was much higher than α-helix so that the plateau adsorbed amount of β-sheet was higher than that of α-

helix systems. The final adsorbed amounts for α-helix and β-sheet, from PB solution containing 5 mM Na_2SO_4 were 231±5 ng/cm^2 and 1087±14 ng/cm^2 respectively. Increasing the Na_2SO_4 concentration to 50 mM decreased the adsorbed mass of α-helix and β-sheet to 82.2 and 44.2% of that at 5 mM Na_2SO_4, while for 500 mM Na_2SO_4 the final adsorbed mass of α-helix and β-sheet was further reduced to 51.5 and 26.5%, respectively. The fact that these percent reductions in adsorbed amount do not correspond with the final frequency drop may be due to the viscoelastic behavior of the adsorbed layers.

Using size measurements (Table 2.3) coupled with the Stokes-Einstein equation, aqueous diffusion coefficients for α-helix and β-sheet PLL were calculated. It is evident from Table 2.2 that there is a considerable drop in the diffusion coefficient when the salt concentration increases from 50 to 500 mM, suggesting that solution viscosity is a key parameter influencing the diffusion coefficient values (note that PLL size is almost independent of salt concentration, Table 2.3). The diffusion coefficient ratios of α-helix to β-sheet are 1.5, 1.7, and 1.5 in PLL solutions of 5, 50, and 500 mM Na_2SO_4 respectively. The initial adsorption rate ratios of α-helix to β-sheet are 2.7, 3.1, and 1.8 in PLL solution with 5, 50, and 500 mM Na_2SO_4 respectively. Comparing these diffusion coefficient ratios with the initial adsorption rate ratios suggests that the adsorption process is not diffusion limited, but that its effect on adsorption may increase with ionic strength (note that the solution viscosity increases with ionic strength yielding a decrease in the molecular diffusivity). The above results suggest that

ionic strength has a more pronounced effect on β-sheet PLL adsorption as compared to that on α-helix.

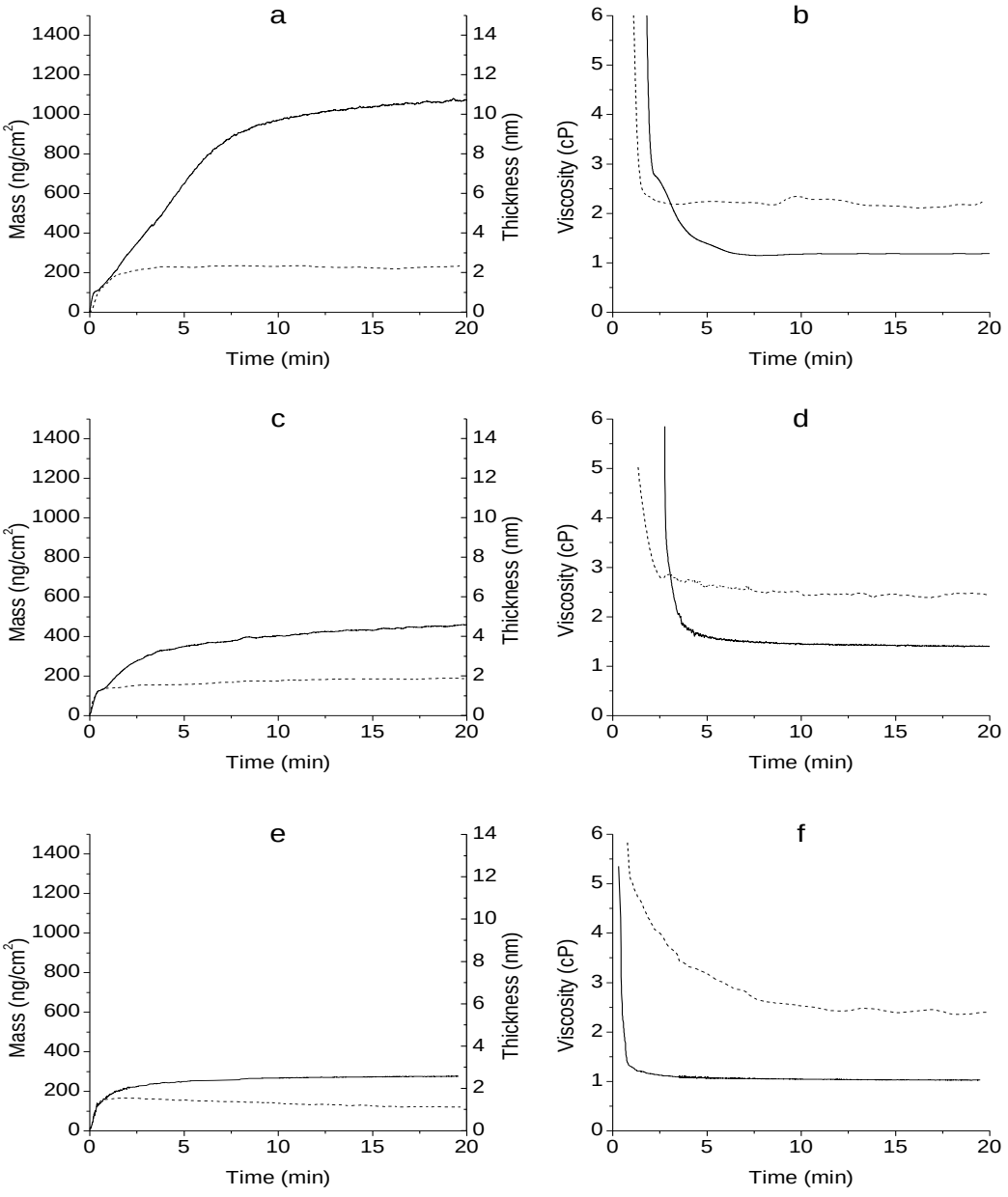

Figure 2.4 Representative QCM-D kinetic profiles of mass adsorption and layer thickness as well as the viscosity as a function of film formation for both α-helix (…) and β-sheet (─) adsorption to Au coated sensors at different salt concentration; 0.15 mL/min flow rate, 0.1 mg/mL PLL in 10 mM PB with **a, b.** 5 mM Na_2SO_4; **c, d.** 50 mM Na_2SO_4; and **e, f.** 500 mM Na_2SO_4.

The viscosity-time profiles associated with the adsorption of α-helix and β-sheet, as a function of salt concentrations, show a similar drastic decrease in initial viscosity (t<1 min, Figure 2.4). The initial sharp decrease in viscosity may be due to the fact that the adsorbing layers are not uniform, thus violating a critical modelling assumption [61]. It is obvious that the α-helix layers yield a plateau layer more viscous than β-sheet layers, regardless of salt concentration. In fact, it appears that layer viscosity remains almost the same for each conformer regardless of the Na_2SO_4 concentration, suggesting that layer viscosity is probably more strongly correlated to peptide structure than solution conditions. Even the 500 mM Na_2SO_4 solution, which corresponds to a solution viscosity of 0.9 cP (as opposed to 5 and 50 mM Na_2SO_4 with 0.7 cP viscosity at 37°C), does not cause a detectable alteration of adsorbed layer viscosity. It has been previously reported that the secondary structures can imbue rigidity to the protein [62-64]. Results of this work suggest that rigidity of PLL α-helix structure is significantly more than β-sheet. This higher viscosity for α-helix layers may arise from the H-bonds between neighbouring amino acids on the same chain that result in a pronounced reduction in chain flexibility [65] as opposed to the H-bonds between amino acids from two adjacent chains used to form β-sheet PLL; a result attested to by the relatively higher $\Delta D_f/\Delta f$ ratio for β-sheet PLL. Arrangement of water molecules *via* hydrogen bonding between free amine groups of lysine residues may be a function of PLL secondary structure and contribute to the higher viscosity of α-helix PLL film.

Table 2.2 Physical properties of α-helix and β-sheet adsorbed layers and their adsorption kinetic parameters at different salt concentrations

Na_2SO_4 concentration [mM]	Conformer	Thickness [nm]	Adsorbed mass [ng/cm^2]	Viscosity [cP]	Aqueous diffusion coefficient [nm^2/s]	Initial adsorption rate [ng/cm^{2}min]	Adsorption half time [s]
5	α-helix	2.3±0.1	231±5	2.3±0.1	47.4	322±30	22±2
	β-sheet	10.9±0.1	1087±14	1.2±0.1	31.2	120±1	274±4
50	α-helix	1.9±0.1	190±5	2.4±0.1	47.7	440±60	13±2
	β-sheet	4.8±0.2	481±22	1.4±0.1	28.5	140±10	102±3
500	α-helix	1.1±0.1	119±3	2.5±0.1	34.1	385±32	13±1
	β-sheet	2.7±0.1	288±14	1.1±0.1	23.3	219±5	40±1

Data are average ± SD.

2.2.4 PLL layer properties: role of surface interaction energy

Our results indicate the secondary structure plays an important role in the adsorption process of a polypeptide. Au is a hydrophilic surface [66] with a water contact angle of 62±2° [67] and PLL consists of one free amine group per residue, which forms hydrogen bonds with the surrounding water molecules in the solution; thus, the interaction between PLL chains and Au is not primarily hydrophobic. The pI value of PLL is around ~12.2, and a PLL chain carries 33.7 positive charges at pH 10.6 [68]. The fact that α-helix and β-sheet structures could exist in the same solution conditions and that the secondary structure formation is primarily a result of hydrogen bonding, not charge profile changes, makes it unlikely that the molecular charge of PLL changes upon secondary structure induction. PLL size determination reveals that α-helix and β-sheet have a size of

13.7±0.9 and 20.8±0.9 nm respectively in PB solution with 5 mM Na_2SO_4, and change of salt concentration does not cause a dramatic change in the size of these conformers (Table 2.3). Although the net charge of a PLL chain remains constant, different PLL conformers appear to have different zeta potential values: 4.6±0.4 and 12.6±0.4 mV for α-helix and β-sheet in PB solution with 5 mM Na_2SO_4. Although the zeta potential value of β-sheet PLL remains higher than α-helix, regardless of solution salt concentration, the zeta potential value for each PLL conformer in solution decreases with increasing ionic strength (as expected). Moreover, it has been reported that the zeta potential of Au surface at pH 10.6 is -49.4 mV [49]. So it is evident that probably electrostatic forces may contribute to the adsorption of these PLL chains. Despite the fact that PLL has a constant charge at each physicochemical condition, higher zeta potential values for β-sheet PLL together with higher final adsorbed amount of β-sheet PLL suggest the secondary structure plays a role in modulating the intensity of electrostatic interactions between PLL and surface through controlling the surface contact area and presentation of charges to the surface.

Table 2.3 α-helix and β-sheet PLL Zeta potential, Debye length, integration energy ratio, and initial adsorption rate ratio in 10 mM PB with different salt concentration

Na_2SO_4 Concentration [mM]	α-helix Size± SD [a] [nm]	β-sheet Size± SD [nm]	α-helix ZP± SD [mV]	β-sheet ZP± SD [mV]	Debye length (κ^{-1}) [nm]	β/α interaction energy ratio at κD=8	β/α initial adsorption rate ratio
5	13.7±0.9	20.8±0.9	4.6±0.4	12.6±0.4	1.49	0.31	0.37
50	14±1	23±1	3.5±0.1	7.4±0.1	0.72	0.43	0.38
500	14.8±0.9	22±1	1.8±0.4	5.6±0.5	0.25	0.72	0.65

a. Size and Zeta potential (ZP) values are average of 3 measurements ± standard deviation (SD).

The interaction energy per unit length of PLL chain versus distance from the surface for both α-helix and β-sheet PLL at different salt concentrations was determined using DLVO theory (Figure 2.5). The Hamaker constant, *A*, used for this system is $3.3x10^{-20}$ J. It can be seen that at large distances from the surface, the α-helix interaction energy is slightly higher than the β-sheets, regardless of the ionic strength. However, within the vicinity of the Au surface it is β-sheet PLL that has a drastically higher interaction with the surface. Ratio of interaction energy of β-sheet to α-helix is also determined, where it was observed that far away from the surface (more than 8 κD) the interaction energy between PLL and Au surface approaches to zero and the ratio of β-sheet to α-helix PLL is almost constant for each ionic strength condition. At long distances the interactions between PLL and the Au surface are governed by electrostatic and van der Waals interactions, with the adsorption rates between conformers thus expected to be

proportional to their corresponding interaction energies (Figure 2.5). It should be noted that at long distances between the Au surface and PLL chains the van der Waals interactions are weaker and inverse power-law dependence of these interactions increases by 1; i.e. $1/d^2$ changes to $1/d^3$ for two surfaces. Furthermore, presence of ions in the solution can screen the zero-frequency contribution to the van der Waals interactions (electrostatic screening) [46]. The interaction energy ratio of β-sheet to α-helix based on DLVO theory at 8 κD (large distance away from the surface where interaction energy is a weak function of distance) and initial adsorption rate ratio of β-sheet to α-helix (Table 2.3) differ by 16, 13, and 10% for 5, 50, and 500 mM Na_2SO_4, respectively. Thus, this correlation between theoretical and experimental results suggests that the adsorption of PLL (β-sheet and α-helix) to Au is largely driven by electrostatic and van der Waals forces, which is expected given the differences in charge between the surface and the PLL.

Figure 2.5 shows that the interaction of β-sheets PLL with the Au surface at small κD is higher than that of α-helices, which is probably due to the larger surface area of β-sheets (Figure 2.1) exposed to the negatively charged Au surface as compared to the α-helix system (Figure 2.1). The differences in zeta potential and interaction energy with Au for β-sheets and α-helix PLL most likely accounts for the differences in initial adsorption rates (Table 2.3) and adsorbed layer properties. The higher adsorbed amount/thickness of the β-sheet PLL film may also be due to the relatively strong intermolecular interaction between β-sheet PLLs. The intermolecular interaction is thought to be weaker than the interaction

between a β-sheet PLL chain and the Au surface, but may consequently drive further adsorption of β-sheet PLL with a slower rate but takes it to a higher extend regardless of solution ionic strength. It has been reported by Grigsby et al [69] that the secondary structure-specific intermolecular interactions of PLL in aqueous solution are mainly due to hydrophobic interactions of uncharged lysine side chains which is greater for β-sheet compared to α-helix conformation due to larger area through which two β-sheet PLLs interact (assuming β-sheet and α-helix conformations as a flat surface and a cylinder respectively). Presence of a Au surface could align PLL chains and cause formation of nuclei on the surface [70]. The strength of the interaction between nuclei on the surface and PLL chains in the solution may determine the adsorption extent. It may be the comparatively strong interaction between β-sheet PLL chains that results in a higher adsorbed amount. These data suggest that secondary structure of the chains play an overriding role in driving adsorption at the interface.

From Figure 2.5, at distances close to the Au surface interaction energy is β-sheet > α-helix and the interaction energy ratio of β-sheet to α-helix drastically increases upon approaching the surface. This comparatively dramatic high interaction energy between β-sheet and Au surface, in the vicinity of the Au, could be the impetus for the high instantaneous adsorption rate at the beginning of the β-sheet adsorption (Figures 2.3 and 2.4). In fact, β-sheet chains in the proximity of the surface will be rapidly adsorbed due to the high interaction energy while those further away need to diffuse toward the interacting Au surface.

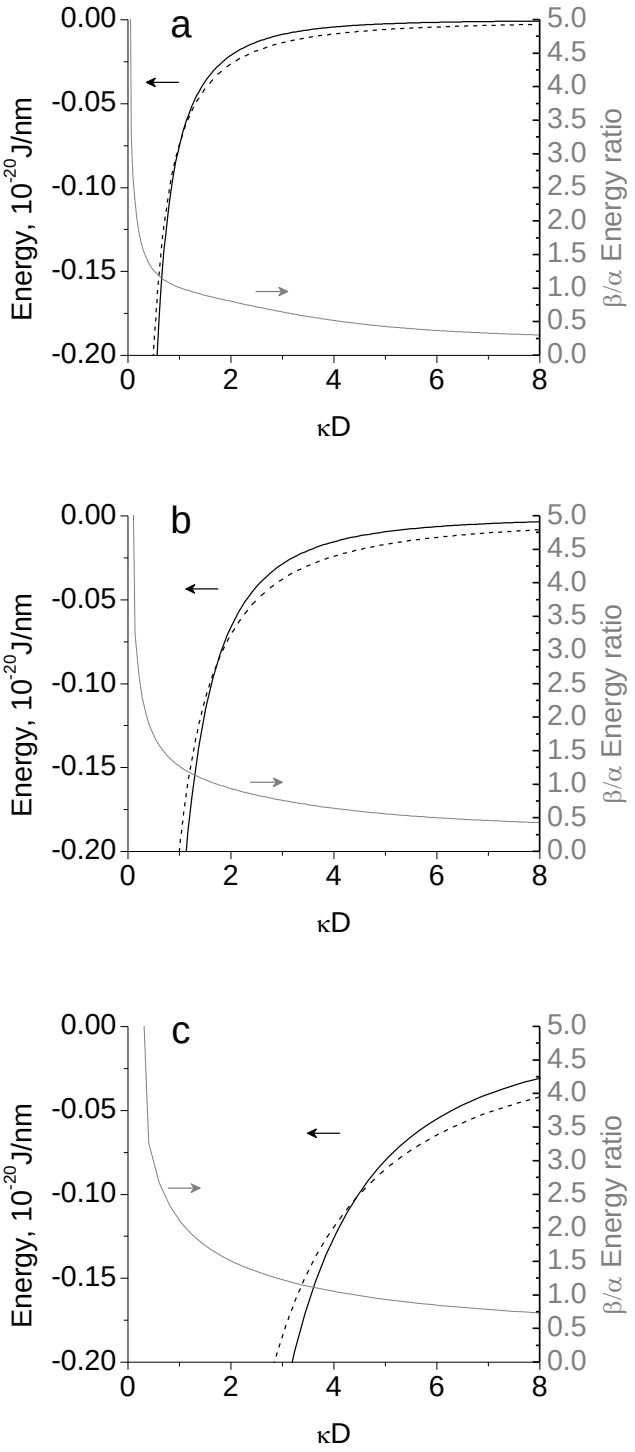

Figure 2.5 Interaction energy per unit length for α-helix (…) and β-sheet (—) PLL with Au surface and the ratio of interaction energies of β-sheet to α-helix PLL (—) in 10 mM PB with **a.** 5 mM Na_2SO_4, **b.** 50 mM Na_2SO_4, and **c.** 500 mM Na_2SO_4 as a function of dimensionless distance from the surface. At large 'D' the α-helix PLL interaction with the surface is stronger. At small 'D' the β-sheet PLL interaction with the surface is stronger and it drastically increase by β-sheet PLL approach to the surface.

2.3 Conclusion

The effect of secondary structure of PLL on its adsorption to a Au surface was investigated. CD results showed that secondary structure of PLL persist upon adsorption from solutions of different ionic strengths to a Au surface. It is evident from QCM-D data that the secondary structures of proteins may play an important role in their adsorption to solid surfaces. Secondary structure modulates conformation of the PLL chain and local charges in solutions, impacting the interaction between the PLL and Au and further affecting adsorption rate, extent, and layer viscosity. The interactions between PLL and Au in aqueous solutions are mainly van der Waals and electrostatic, which reduces upon an increase of the ion concentration and results in a decrease in the adsorbed amount. Higher extent of adsorption in case of β-sheet PLL could be due to stronger intermolecular interactions among β-sheet PLLs. Noticeable differences in the viscosity of layers formed by different secondary structures of PLL, having the same physicochemical condition, give insight about their degree of rigidity and adhesion. Our results provide new insights into the fundamental understanding of adsorption mechanisms of proteins, and can be used for the development of better materials/coatings for controlling the non-specific adsorption of proteins.

2.4 References:

[1] Anderson, JM, Bonfield, TL, and Ziats, NP. Protein adsorption and cellular adhesion and activation on biomedical polymers. Int. J. Artif. Organs, 1990;13:375-382.

[2] Andrade, JD and Hlady, V. Plasma protein adsorption: the big twelve. Ann. N. Y. Acad. Sci., 1987;516:158-172.

[3] Nath, N, Hyun, J, Ma, H, and Chilkoti, A. Surface engineering strategies for control of protein and cell interactions. Surf. Sci., 2004;570:98-110.

[4] Pankowsky, DA, Ziats, NP, Topham, NS, Ratnoff, OD, and Anderson, JM. Morphologic characteristics of adsorbed human plasma-proteins on vascular grafts and biomaterials. J. Vasc. Surg., 1990;11:599-606.

[5] Shen, M, Garcia, I, Maier, RV, and Horbett, TA. Effects of adsorbed proteins and surface chemistry on foreign body giant cell formation, tumor necrosis factor alpha release and procoagulant activity of monocytes. J. Biomed. Mater. Res., Part A, 2004;70A:533-541.

[6] Statz, AR, Meagher, RJ, Barron, AE, and Messersmith, PB. New peptidomimetic polymers for antifouling surfaces. J. Am. Chem. Soc., 2005;127:7972-7973.

[7] Ball, V. Adsorption behavior of different polypeptides in the 3 kDa molecular weight range at an Si0.8Ti0.2O2-aqueous solution interface from low ionic strength solutions. Colloids Surf., B, 2004;33:129-142.

[8] Yang, Q, Kaul, C, and Ulbricht, M. Anti-nonspecific protein adsorption properties of biomimetic glycocalyx-like glycopolymer layers: effects of glycopolymer chain density and protein size. Langmuir, 2010;26:5746-5752.

[9] Chen, SF, Li, LY, Zhao, C, and Zheng, J. Surface hydration: Principles and applications toward low-fouling/nonfouling biomaterials. Polymer, 2010;51:5283-5293.

[10] Jordan, CE and Corn, RM. Surface plasmon resonance imaging measurements of electrostatic biopolymer adsorption onto chemically modified gold surfaces. Anal. Chem., 1997;69:1449-1456.

[11] Elgersma, AV, Zsom, RLJ, Lyklema, J, and Norde, W. Kinetics of single and competitive protein adsorption studied by reflectometry and streaming potential measurements. Colloids Surf., 1992;65:17-28.

[12] Ramsden, JJ and Prenosil, JE. Effect of ionic-strength on protein adsorption-kinetics. J. Phys. Chem., 1994;98:5376-5381.

[13] Norde, W and Lyklema, J. The adsorption of human plasma albumin and bovine pancreas ribonuclease at negatively charged polystyrene surfaces: I. Adsorption isotherms. Effects of charge, ionic strength, and temperature. J. Colloid Interface Sci., 1978;66:257-265.

[14] Deligianni, DD, Katsala, N, Ladas, S, Sotiropoulou, D, Amedee, J, and Missirlis, YF. Effect of surface roughness of the titanium alloy Ti-6Al-4V on human bone marrow cell response and on protein adsorption. Biomaterials, 2001;22:1241-1251.

[15] Ostuni, E, Chapman, RG, Holmlin, RE, Takayama, S, and Whitesides, GM. A survey of structure-property relationships of surfaces that resist the adsorption of protein. Langmuir, 2001;17:5605-5620.

[16] Wong, SY, Han, L, Timachova, K, Veselinovic, J, Hyder, MN, Ortiz, C, Klibanov, AM, and Hammond, PT. Drastically lowered protein adsorption on microbicidal hydrophobic/hydrophilic polyelectrolyte multilayers. Biomacromolecules, 2012;13:719-726.

[17] Meder, F, Daberkow, T, Treccani, L, Wilhelm, M, Schowalter, M, Rosenauer, A, Mädler, L, and Rezwan, K. Protein adsorption on colloidal alumina particles functionalized with amino, carboxyl, sulfonate and phosphate groups. Acta Biomater., 2012;8:1221-1229.

[18] Wang, D, Douma, M, Swift, B, Oleschuk, RD, and Horton, JH. The adsorption of globular proteins onto a fluorinated PDMS surface. J. Colloid Interface Sci., 2009;331:90-97.

[19] Bonekamp, BC. Conformational properties and adsorbed layer structure of adsorbed poly-L-Lysine and poly-DL-Lysine as inferred from adsorption measurements and proton titrations. Colloids Surf., 1989;41:267-286.

[20] Kabsch, W and Sander, C. Dictionary of protein secondary structure: pattern recognition of hydrogen-bonded and geometrical features. Biopolymers, 1983;22:2577-2637.

[21] Martin, J, Gibrat, JF, and Rodolphe, F.Hidden Markov model for protein secondary structure, in International Symposium on Applied Stochastic Models and Data Analysis. 2005: Brest, France.

[22] Andrews, DW and Ottensmeyer, FP. Electron-microscopy of the poly-L-Lysine alpha-helix. Ultramicroscopy, 1982;9:337-348.

[23] Demirdoven, N, Cheatum, CM, Chung, HS, Khalil, M, Knoester, J, and Tokmakoff, A. Two-dimensional infrared spectroscopy of antiparallel beta-sheet secondary structure. J. Am. Chem. Soc., 2004;126:7981-7990.

[24] Drotleff, S.Polymers and protein-conjugates for tissue engineering. 2006, University of Regensburg: Regensburg, Germany.

[25] Unsworth, LD, Sheardown, H, and Brash, JL. Protein resistance of surfaces prepared by sorption of end-thiolated poly(ethylene glycol) to gold: Effect of surface chain density. Langmuir, 2005;21:1036-1041.

[26] Ramsden, JJ. Protein adsorption kinetics, in Biopolymers at interfaces, M. Malmsten, Editor. 2003, Marcel Dekker, Inc.: New York.

[27] Gong, P and Grainger, DW. Nonfouling surfaces: a review of principles and applications for microarray capture assay designs. Methods Mol. Biol., 2007;381:59-92.

[28] Collier, TO and Anderson, JM. Protein and surface effects on monocyte and macrophage adhesion, maturation, and survival. J. Biomed. Mater. Res., 2002;60:487-496.

[29] Evans-Nguyen, KM, Fuierer, RR, Fitchett, BD, Tolles, LR, Conboy, JC, and Schoenfisch, MH. Changes in adsorbed fibrinogen upon conversion to fibrin. Langmuir, 2006;22:5115-5121.

[30] Heuberger, M, Drobek, T, and Spencer, ND. Interaction forces and morphology of a protein-resistant poly(ethylene glycol) layer. Biophys. J., 2005;88:495-504.

[31] Hu, W-J, Eaton, JW, Ugarova, TP, and Tang, L. Molecular basis of biomaterial-mediated foreign body reactions. Blood, 2001;98:1231-1238.

[32] Lu, DR and Park, K. Effect of surface hydrophobicity on the conformational changes of adsorbed fibrinogen. J. Colloid Interface Sci., 1991;144:271-281.

[33] Absolom, DR, Zingg, W, Policova, Z, and Neumann, AW. Determination of the surface tension of protein coated materials by means of the advancing solidification front technique. ASAIO J., 1983;29:146-151.

[34] Andrade, JD, Hlady, VL, and Vanwagenen, RA. Effects of plasma-protein adsorption on protein conformation and activity. Pure Appl. Chem., 1984;56:1345-1350.

[35] Dadsetan, M, Jones, JA, Hiltner, A, and Anderson, JM. Surface chemistry mediates adhesive structure, cytoskeletal organization, and fusion of macrophages. J. Biomed. Mater. Res., Part A, 2004;71A:439-448.

[36] Shibata, A, Yamamoto, M, Yamashita, T, Chiou, JS, Kamaya, H, and Ueda, I. Biphasic effects of alcohols on the phase transition of poly(L-lysine) between .alpha.-helix and .beta.-sheet conformations. Biochemistry (Mosc.), 1992;31:5728-5733.

[37] Chittchang, M, Salamat-Miller, N, Alur, HH, Vander Velde, DG, Mitra, AK, and Johnston, TP. Poly (L-Lysine) as a model drug macromolecule with which to investigate secondary structure and microporous membrane transport, part 2: diffusion studies. J. Pharm. Pharmacol., 2002;54:1497-1505.

[38] Weber, N, Wendel, HP, and Kohn, J. Formation of viscoelastic protein layers on polymeric surf aces relevant to platelet adhesion. J. Biomed. Mater. Res., Part A, 2005;72A:420-427.

[39] Sivaraman, B, Fears, KP, and Latour, RA. Investigation of the effects of surface chemistry and solution concentration on the conformation of adsorbed proteins using an improved circular dichroism method. Langmuir, 2009;25:3050-3056.

[40] Wolkers, WF, van Kilsdonk, MG, and Hoekstra, FA. Dehydration-induced conformational changes of poly--lysine as influenced by drying rate and carbohydrates. Biochim. Biophys. Acta, Gen. Subj., 1998;1425:127-136.

[41] Yan, MQ, Liu, CX, Wang, DS, Ni, JR, and Cheng, JX. Characterization of adsorption of humic acid onto alumina using quartz crystal microbalance with dissipation. Langmuir, 2011;27:9860-9865.

[42] Voinova, MV, Rodahl, M, Jonson, M, and Kasemo, B. Viscoelastic acoustic response of layered polymer films at fluid-solid interfaces: Continuum mechanics approach. Phys. Scr., 1999;59:391-396.

[43] de Kerchove, AJ and Elimelech, M. Structural growth and viscoelastic properties of adsorbed alginate layers in monovalent and divalent salts. Macromolecules, 2006;39:6558-6564.

[44] Green, DW and Perry, RH. Perry's Chemical Engineers' Handbook (8th Edition). 2008: McGraw-Hill. 2-96, 2-449.

[45] Correia, RJ and Kestin, J. Viscosity and density of aqueous sodium sulfate and potassium sulfate solutions in the temperature range 20-90 .degree.C and the pressure range 0-30 MPa. J. Chem. Eng. Data, 1981;26:43-47.

[46] Israelachvili, JN. Force- Measuring Techniques, in Intermolecular and surface forces. 2010, Academic Press: San Diego. 223-252.

[47] Kristiansen, K, Zeng, H, Wang, P, and Israelachvili, JN. Microtribology of Aqueous Carbon Nanotube Dispersions. Adv. Funct. Mater., 2011;21:4555-4564.

[48] Vörös, J. The Density and Refractive Index of Adsorbing Protein Layers. Biophys. J., 2004;87:553-561.

[49] Giesbers, M, Kleijn, JM, and Stuart, MAC. The electrical double layer on gold probed by electrokinetic and surface force measurements. J. Colloid Interface Sci., 2002;248:88-95.

[50] van Oss, CJ. The primary interactions, in Interfacial forces in aqueous media. 1994, CRC Press.

[51] Chittchang, M, Alur, HH, Mitra, AK, and Johnston, TP. Poly(L-lysine) as a model drug macromolecule with which to investigate secondary structure and membrane transport, part I: physicochemical and stability studies. J. Pharm. Pharmacol., 2002;54:315-323.

[52] Arunkumar, AI, Kumar, TKS, Sivaraman, T, and Yu, C. Acetonitrile-induced conformational transitions in poly-L-lysine. Int. J. Biol. Macromol., 1997;21:299-305.

[53] Tiffany, ML. Circular-dichroism study of charged polypeptides interaction with salts. Physiol. Chem. Phys., 1975;7:191-207.

[54] Fukushima, K, Sakamoto, T, Tsuji, J, Kondo, K, and Shimozawa, R. The transition of alpha-helix to beta-structure of poly-L-Lysine induced by phosphatidic-acid vesicles and its kinetics at alkaline pH. Biochim. Biophys. Acta, Biomembr., 1994;1191:133-140.

[55] Chiou, J-S, Tatara, T, Sawamura, S, Kaminoh, Y, Kamaya, H, Shibata, A, and Ueda, I. The [alpha]-helix to [beta]-sheet transition in poly(L-lysine): Effects of anesthetics and high pressure. Biochim. Biophys. Acta, Protein. Struct. Mol. Enzymol., 1992;1119:211-217.

[56] Parson, WW. Circular Dichroism, in Modern Optical Spectroscopy: With Exercises and Examples from Biophysics and Biochemistry. 2009, Springer: New York. 307-334.

[57] Miles, AJ, Whitmore, L, and Wallace, BA. Spectral magnitude effects on the analyses of secondary structure from circular dichroism spectroscopic data. Protein Sci., 2005;14:368-374.

[58] Greenfield, NJ. Using circular dichroism spectra to estimate protein secondary structure. Nat. Protoc., 2006;1:2876-2890.

[59] Dutta, AK and Belfort, G. Adsorbed gels versus brushes: Viscoelastic differences. Langmuir, 2007;23:3088-3094.

[60] Notley, SM, Eriksson, M, and Wagberg, L. Visco-elastic and adhesive properties of adsorbed polyelectrolyte multilayers determined in situ with QCM-D and AFM measurements. J. Colloid Interface Sci., 2005;292:29-37.

[61] Liu, SX and Kim, J-T. Application of Kevin–Voigt Model in quantifying whey protein adsorption on polyethersulfone using QCM-D. Journal of Laboratory Automation, 2009;14:213-220.

[62] Kaiser, ET and Kezdy, FJ. Secondary structures of proteins and peptides inamphiphilic environments (a review). Proc. Natl. Acad. Sci. U. S. A. Phys. Sci., 1983;80:1137-1143.

[63] Cocinero, EJ, Stanca-Kaposta, EC, Gamblin, DP, Davis, BG, and Simons, JP. Peptide secondary structures in the gas phase: consensus motif of N-linked glycoproteins. J. Am. Chem. Soc., 2009;131:1282-1287.

[64] Wells, SA, Jimenez-Roldan, JE, and Romer, RA. Comparative analysis of rigidity across protein families. Phys. Biol., 2009;6.

[65] Chittchang, M, Mitra, A, and Johnston, T. Interplay of secondary structure and charge on the diffusion of a polypeptide through negatively charged aqueous Pores. Pharm. Res., 2007;24:502-511.

[66] Smith, T. The hydrophilic nature of a clean gold surface. J. Colloid Interface Sci., 1980;75:51-55.

[67] Mattiuzzi, A, Jabin, I, Mangeney, C, Roux, C, Reinaud, O, Santos, L, Bergamini, JF, Hapiot, P, and Lagrost, C. Electrografting of calix 4 arenediazonium salts to form versatile robust platforms for spatially controlled surface functionalization. Nat. Commun., 2012;3.

[68] Putnam, C. Protein calculator v3.3 2006 March 28, 2006; Available from: http://www.scripps.edu/~cdputnam/protcalc.html.

[69] Grigsby, JJ, Blanch, HW, and Prausnitz, JM. Effect of secondary structure on the potential of mean force for poly--lysine in the [alpha]-helix and [beta]-sheet conformations. Biophys. Chem., 2002;99:107-116.

[70] Ogi, H, Fukunishi, Y, Yanagida, T, Yagi, H, Goto, Y, Fukushima, M, Uesugi, K, and Hirao, M. Seed-Dependent Deposition Behavior of Aβ Peptides Studied with Wireless Quartz-Crystal-Microbalance Biosensor. Anal. Chem., 2011;83:4982-4988.

3. Effect of Secondary Structure on Peptide Adsorption on End-grafted Polyethylene Glycol Layers[3]

3.1 Introduction

Non-specific protein adsorption, which spontaneously occurs upon introduction of a biomaterial surface into a physiological fluid, challenges the widespread application of most biomedical devices [1-5]. The presence of adsorbed protein itself may directly influence cell-surface interactions. Moreover, the surface-induced structural rearrangement of proteins [6] may further yield an increase in protein-surface binding through multiple contact points and possibly expose normally occult epitopes that further facilitate cellular events at the biointerface [7-11]. All of which may initiate adverse host responses (thrombotic and immune) and accumulation of inflammatory cells; adversely affecting patient health and treatment costs directly [7, 12-15]. Although adsorption-induced conformational changes of the proteins play an important role in patient health, there is a dearth in the literature surrounding the role protein secondary structures play in directing protein adsorption and subsequent surface-induced denaturing. The development of surface engineering strategies for rendering blood contacting surfaces resistant to both adsorption and denaturing of proteins [16, 17] is essential and may not be possible without a detailed understanding of the protein-surface interactions at the molecular level.

[3] This chapter was published in: Effect of Secondary Structure on Peptide Adsorption on End-grafted Polyethylene Oxide Layers. *Binazadeh, M., H. Zeng, and L.D. Unsworth,* **Acta Biomaterialia**. In press.

Polyethylene glycol (PEG) surface modification is considered the gold-standard strategy for inhibiting non-specific adsorption of proteins [18]. Neutral charge, hydrophilic nature, with hydrogen bond acceptors and no hydrogen bond donors, are some properties thought to imbue PEG coatings with non-fouling attributes [19]. Each ethylene glycol (EG) segment in PEG can form up to two hydrogen bonds with water molecules in an aqueous solution, resulting in the formation of a loose coil structure [20]. An increase in aqueous PEG concentration, solution temperature, and/or ion concentration results in a reduction of PEG solubility, where hydrogen bonds between PEG and H_2O decreases to the point of PEG precipitation (θ condition) [21, 22]. It has been previously reported that the hydration number of an EG segment is ~2.0 in a good solvent [23]. For a dilute PEG solution (less than 5% PEG vol/vol), in θ solvents, the hydration number of an EG segment was reported to decrease to ~1.7 [22]. Surface grafting of PEG from its θ solution may result in the increase of PEG volume fraction in the vicinity. For example, a tethered PEG layer (5000 MW) with a chain density of ~0.4 chain/nm^2 corresponded to a layer with ~20% PEG vol/vol with an estimated ~1.5 hydrogen bonds per EG unit; a lower PEG hydration state compared to that in the bulk θ solutions [24]. In addition to suppressing the electrical and van der Waals interactions between proteins in the bulk solution and the virgin surface modified with PEG, two long standing mechanisms have been proposed for non-fouling properties of PEG surfaces. The hydrated flexible ether bonds in a uniformly end-tethered long PEG chain confer conformational and rotational mobility to the polymer chain [25] resulting in a

large volume that proteins are excluded from [26]. And for shorter end-tethered PEG chains hydrogen bonded water molecules in the hydration shell around the PEG chain [27] lead to a stabilized hydration state that inhibits protein adsorption [28]. That said, it has been found that these two modes of inhibiting protein adsorption may be unified by the effect of chain density within the formed PEG layer [29].

It is known that the surface interaction strength of proteins and peptides depends on properties of interacting surfaces (hydrophobicity [30], chemical nature [31] and roughness [32]), proteins (isoelectric point [33, 34], molecular weight [35], and amino acid sequence [36]), and solution conditions (ionic strength [37], pH [38], and temperature [39]). Although it has been reported that ~50% of the amino acids in a proteins' sequence are involved in the formation of α-helices and β-sheets [40, 41], it is evident that the effects of protein secondary structure on adsorption and conformational changes have not been widely discussed. Protein secondary structure is determined by its amino acid sequence and is thought to influence the protein's physicochemical (shape, size, apparent charge, and hydrophobicity) and biofunctional properties. Moreover, these structural subunits may dictate the extent of protein unfolding at interfaces [42, 43]. The impact secondary structures have on protein adsorption remains limited. Previous reports include the adsorption of amphiphilic leucine-lysine peptide (LK) capable of forming α-helix and β-sheet structures [44-50]. Adsorption of a 14-mer amphiphilic leucine-lysine peptide (LK14) to hydrophilic silica and hydrophobic polystyrene revealed that the hydrophilicity and hydrophobicity of

interacting substrates affected adsorption rates, adsorption extents, surface morphologies, and the peptide structural rearrangement [46]. Other works regarding peptide secondary structure and its influence on surface adsorption were done using a synthetic oligopeptides composed of hydrophobic leucine (L) and hydrophilic lysine (K) capable of forming α-helix (14-mer, LKα14) and β-sheet (15-mer, LKβ15) with hydrophobic periodicities of 3.5 and 2, respectively. Using X-ray photoelectron spectroscopy (XPS) it has been shown that the adsorption of β-sheet forming LKβ15 on well-defined carboxylic acid and methyl-terminated self-assembled monolayer surfaces results in electrostatic interactions of the peptide lysine side chains bond with the carboxyl surface and hydrophobic interactions of the leucine side chains bond to the methyl surface while the adsorption of α-helix forming LKα14 did not suggest such substrate dependent orientation [44]. It was also reported that the secondary structure of both peptides persist upon adsorption on carboxylic acid and methyl-terminated self-assembled monolayer surfaces [48]. Finally, Puddu et al. suggest that the contribution of prevailing interactions between peptide and surface (*i.e.* electrostatic, hydrogen bonding, and hydrophobic) depend on the identity of the peptide (amino acid sequence), the substrate surface functionality (hydrophobic or hydrophilic), solution pH, and peptide concentration [51]. It has also been reported that chemisorbed layers of tri (ethylene glycol) alkanethiols on Au significantly reduced the adsorbed amount of proteins (concanavalin A and bovine serum albumin) and peptides (arginine-glycine-aspartic acid-serine (RGDS),

angiotensin, bradykinin) [52]; however, no discussion regarding peptide adsorption mechanisms were reported.

It still remains largely unknown how different secondary structures interact with engineered surfaces. Understanding the effect protein secondary structures have on protein adsorption behaviour is both fundamentally and practically important, and may aid further design of engineered surfaces. In this work, we have systematically investigated the formation of a chemisorbed PEG layer to Au, as well as utilized a model peptide (Poly-L-Lysine, PLL) formed into different secondary structures [53] (i.e., α-helices and β-sheets (Figure 3.1) while maintaining a constant molecular charge profile [54]). The formation of chemisorbed PEG and adsorbed PLL layers in this work was monitored using QCM-D, which provides real time information about mass or thickness evolution of the adsorbed protein layer and its shear viscosity [55]. PEG layers on QCM-D Au sensor was formed *via* chemisorption of end thiolated PEG chains (750 and 2000 MW) from a 5 mM aqueous θ solution to obtain a dense polymer brush layer [21]. The bulk and adsorbed layer secondary structure of PLL was measured by CD for both adsorption to Au and PEG-Au systems. Our results provide new insight into the fundamental understanding of surface adsorption mechanisms of peptides to PEG modified substrates: focusing on fundamental properties of these systems.

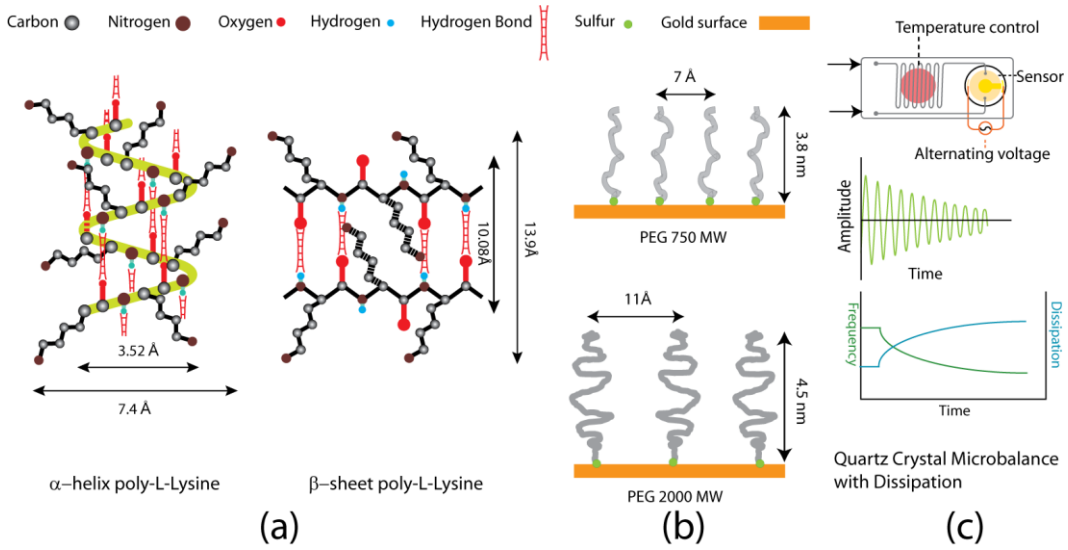

Figure 3.1 Schematic drawing of **a.** PLL in α-helix [56] and β-sheet [57] conformations, b**.** chemisorbed PEG 750 and PEG 2000 layers on Au surface, and **c.** experimental setup and working principle of QCM-D.

3.2 Materials and experimental methods

PEG methyl ether (MW 750 and 2000), deuterated chloroform (99.9% grade), PLL-HCl, molecular weight range 15-30 kDa, mercaptoacetic acid, isopropyl ether, hydrogen peroxide, ammonium hydroxide, and toluene were purchased from Sigma Aldrich (Canada). QCM-D Au sensors and quartz slides were purchased from Biolin Scientific Inc. and GM Associates Inc., respectively. 10 mM potassium phosphate solution (PB) with 5 mM sodium sulphate and sodium phosphate buffered saline (PBS) at pH 7.4 with ionic strength (IS) 3.5 M was used in the experiments. pH adjustment was done using 50 mM NaOH solution. All experiments were done at 37°C.

3.2.1 Thiolation of PEG

PEG was chain-end thiolated by reaction with mercaptoacetic acid as described in detail elsewhere [58, 59]. Briefly, a 100 mL three-necked flask was coupled to a distillation trap prefilled with toluene that was connected to a water cooled condenser. 10 millimole PEG 750 or 2000 was added with 50 mL toluene to the flask. Upon heating the flask to 110°C using an oil bath, mercaptoacetic acid (2.76 g, 30 millimole) was added and the reaction started *via* addition of 2 drops of concentrated sulphuric acid. The reaction was allowed to proceed for 2 hrs and thiolated PEG was purified *via* three times precipitation in ether and then dried under vacuum at 40°C overnight. Proton nuclear magnetic resonance (^{1}HNMR) was used to determine reaction conversion *via* obtaining the spectrum of purified reaction products, taken in deuterated chloroform. ^{1}HNMR results indicated 93 and 91% yield of thiolated PEG 750 and 2000 respectively (results not shown). By ultraviolet-visible spectroscopy (UV-VIS) measurements at 355 nm wavelength it was determined that 5 mM PEG in PBS at 37°C approaches the θ condition when IS has reached 3.5 M (results not shown).

3.2.2 Circular dichroism (CD)

It has been shown that PLL maintains a random coil structure in solution at neutral pH, where other secondary structures can be induced through the manipulation of solution pH and temperature [60] or addition of organic solvents [61], salts [62], and phospholipids [63]. In this work CD was used to track the formation and persistence of desired secondary structures of PLL in solution as well as in the adsorbed state. Herein, 10 mM PB with 5 mM sodium sulphate,

without pH adjustment, was used to prepare 5 mg/mL PLL stock solution. α-helices were formed using well established methods [64], where the stock solution was diluted (50x) and the pH adjusted to 10.6 (Figure 3.1.a). α-helices in this solution were transformed to β-sheets using established methods [60], where the sample was heated at 70°C for 50 min (Figure 3.1.a). All samples were degassed for 20 min using a Fisher Scientific vacuum pump with liquid nitrogen trap to eliminate any influence of dissolved gases on CD measurement. In order to measure PLL secondary structure in bulk solution, a quartz cuvette (0.2 cm pathlength, International Crystal Lab) was used. CD measurements were obtained using a Jasco-J810 equipped with a Julabo AWC100 water bath for temperature control. A background spectrum was collected using a degassed 10 mM PB with 5mM sodium sulphate concentration (without PLL) at pH 10.6 and 37°C. CD spectra for all samples were recorded from 190 to 260 nm and all reported CD spectra are average of three measurements.

CD spectra of adsorbed PLL on Au was obtained after coating quartz slides with Cr and Au as reported elsewhere [65]. Two coated slides were sandwiched together using a Teflon film (McMaster-Carr) with a separation distance of 0.12 mm. Thiolated PEG was chemisorbed by immersion of Au coated quartz slides in PEG solution at θ condition for 40 min. Background spectra for all systems without PLL were recorded using degassed 10 mM PB with 5 mM sodium sulphate concentration (without PLL) at pH 10.6 and 37°C. PLL was then adsorbed to Au coated quartz slides, PEG 750 and 2000 chemisorbed-Au surfaces *via* immersion of quartz slides in a well stirred PLL solution of pre-known

secondary structure. PLL adsorption was allowed to continue for 1 hr to ensure plateau adsorbed amounts. Care was taken so that adsorbed PLL layer stays hydrated to avoid drying induced conformation changes [66]. PLL incubation and CD experiments were done at 37°C.

3.2.3 Quartz Crystal Microbalance with Dissipation (QCM-D)

A quartz crystal sensor is a thin piezoelectric plate sandwiched between two Au electrodes. When a mass is adsorbed on the sensor, its resonance frequency (*f*) changes and the viscoelastic properties of the adsorbed layer can be determined through monitoring the dissipation increase (Figure 3.1.c). Before QCM-D experiments the standard cleaning protocol was employed where the sensor was placed in a UV/Ozone cleaner chamber (Bio Force Nanosciences Inc.) for 10 min, transferred into ammonium peroxide (5:1:1 mixture of milliQ water, ammonia (25%), and hydrogen peroxide (30%)) at 75ºC for 5 min, and rinsed with copious amounts of MilliQ water and dried with purified nitrogen gas. UV/Ozone treatment was repeated again after cleaning with ammonium peroxide.

Chemisorption of thiolated PEG and adsorption of PLLs with different secondary structures was monitored using a QCM-D (Q-sense E4, Q-sense AB, Gothenburg, Sweden) with the capacity of measuring changes in resonance frequency (Δf) and energy dissipation (ΔD_f) of QCM-D sensors (fundamental frequency of 4.95 MHz) simultaneously. In this work thiolated PEG 750 and 2000 at θ solution was used for chemisorption. PLL solution with desired secondary structure was prepared and its secondary structure was confirmed using CD prior to QCM-D experiments. Before chemisorption of PEG or adsorption of PLL, the

buffer without PEG or PLL was first pumped into the QCM-D module to obtain a stable baseline. After the adsorption or chemisorption step, the QCM-D sensor was rinsed with the appropriate solution. In this study, the Voigt viscoelastic model [67] in Q-sense Qtools 3.0 was used to correlate the frequency and dissipation as a function of time (for n=5 and 7 overtones) to mass and shear viscosity of the developing layer. The Voigt model correlates f oscillation frequency, D_f dissipation, h thickness, ρ density, η viscosity, μ shear modulus, and ω the circular frequency, for a viscoelastic layer (index "1") on quartz slide (index "0") immersed in a bulk Newtonian fluid (index "2") as follows [67]:

$$\Delta f \approx -\frac{1}{2\pi\rho_0 h_0}\left\{\frac{\eta_2}{\delta_2}+\left[h_1\rho_1\omega-2h_1\left(\frac{\eta_2}{\delta_2}\right)^2\frac{\eta_1\omega^2}{\mu_1^2+\omega^2\eta_1^2}\right]\right\} \tag{3.1}$$

$$\Delta D_f \approx \frac{1}{2\pi f\rho_0 h_0}\left\{\frac{\eta_2}{\delta_2}+\left[2h_1\left(\frac{\eta_2}{\delta_2}\right)^2\frac{\eta_1\omega^2}{\mu_1^2+\omega^2\eta_1^2}\right]\right\} \tag{3.2}$$

$$\delta_2=\sqrt{\frac{2\eta_2}{\rho_2\omega}} \tag{3.3}$$

3.3 Results and Discussion

3.3.1 PEG layer properties: mass adsorbed, thickness, and layer viscosity

The chemisorption of end-thiolated PEG to Au sensors was conducted from θ solutions and film formation was monitored using QCM-D. Representative QCM-D data (Figure 3.2) details that prior to PEG chemisorption (time: -10 to 0 min) the Au sensor was washed with the θ solution (PEG free) and shows that ion adsorption to, or desorption from, the Au surface was at steady state prior to

introducing PEG. PEG within the θ solution was introduced (time: 0 min) and the oscillation frequency decreased with an initial rate of -156.5 and -281.1 Hz/min for PEG 750 and 2000, respectively. This rapid drop in frequency (Δf) indicated that the PEG interacted with the surface. Flow of PEG in θ solution continued for 40 min, although it is evident that after only ~ 2.5 min the frequency drop reached a maximum of -29.9 and -45.3 Hz for PEG 750 and 2000, respectively. The slight increase in Δf during the remainder of the adsorption process perhaps indicated a reorientation of PEG chains on the surface and possibly desorption of unbounded PEG chains [68, 69]. After 40 min of chemisorption, θ solvent devoid of PEG was injected to rinse the surface for 30 min, at which point Δf reached a plateau amount of -20.2 and -24.8 Hz for PEG 750 and 2000, respectively. These extents of frequency drop are in agreement with previous finding of -17.0 Hz frequency drop upon chemisorption of end-thiolated PEG 600 [70] from its 100 µg/mL solution in PBS on Au sensors at 23°C [71].

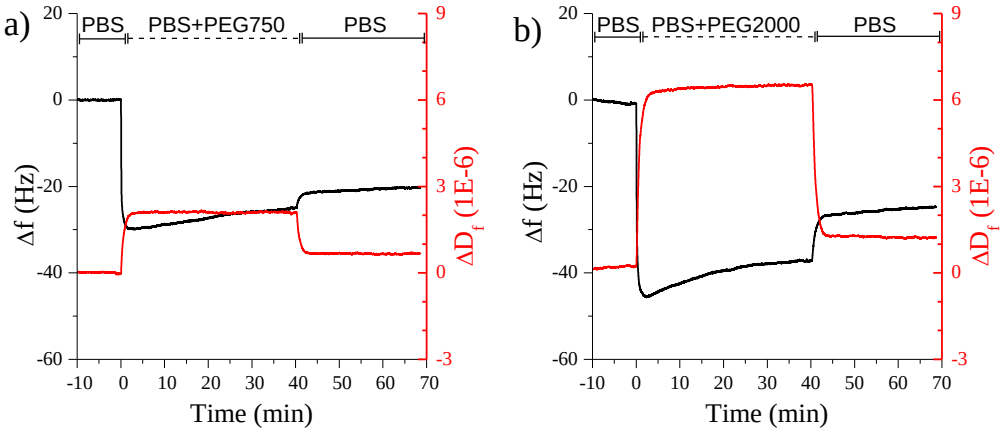

Figure 3.2 Representative Δf and ΔD_f time course of end-thiolated PEG **a.** 750 and **b.** 2000 chemisorption to QCM-D Au sensor from 5 mM PEG solution in PBS buffer at IS 3.5 M and 37 °C (θ solution) with a flow rate of 0.15 mL/min.

A dissipation change of $2.1x10^{-6}$ and $6.5x10^{-6}$ was measured during chemisorption, and $0.7\ x10^{-6}$ and $1.2x10^{-6}$ upon rinsing in θ solvent devoid of PEG for chemisorbed PEG 750 and 2000 layers respectively. These data suggest that higher energy dissipation may be associated with the chemisorbed PEG 2000 layer (Figure 3.2), suggesting the PEG 750 layer may be more rigid than the PEG 2000 layer. Finally, it has been reported that the absolute value of the ratio of $\Delta D_f/\Delta f$ yields information regarding the adsorbed layer structure [72, 73]. A lower $\Delta D_f/\Delta f$ value suggests a relatively stiffer adsorbed layer. Respective $\Delta D_f/\Delta f$ ratios of 0.035 and 0.048 Hz^{-1} for PEG 750 and 2000 layers suggest that the PEG 750 system exhibits a relatively lower energy dissipation, indicating the presence of a stiffer and more compact layer structure [72, 73]. Similar value of $\Delta D_f/\Delta f$ = 0.042 Hz^{-1} for chemisorption of thiolated PEG 500 from its 1 mM solution in ethanol at 24°C was reported previously [74].

Representative modelling results of QCM-D data (Figure 3.3) shows time course development of mass and thickness of PEG 750 and 2000 layers. For modelling purposes, it was assumed that PEG concentration in these solutions were low enough so as to not significantly affect solution density and viscosity. Thus, 1.15 g/cm^3 and 1.05 cP where chosen as density [75] and viscosity [76] of PBS (IS 3.5M) at 37°C, respectively. Density of $1.15g/cm^3$ was chosen for hydrated, chemisorbed PEG layer solutions assuming grafted PEG concentration was low enough so as to not significantly affect layer density. Due to the assumption of constant layer density, thickness and mass of the adsorbed layer are linearly proportional. It has been previously reported that adsorbed mass is

minimally affected by the input modelling value of layer density [77] due to pairing of layer thickness and layer density. Average values of PEG chemisorption parameters are listed in Table 3.1. Initial chemisorption rates of 520±20 and 1180±60 ng/(cm^2 min) for PEG 750 and 2000 suggest that the initial chemisorption rate is almost proportional to the PEG MW. Flory radius was calculated as $R_F=aN^{\upsilon}$ where a is the monomer length (0.*35* nm) [78], N is number of monomers in a polymer chain, and υ is 0.6 and 0.5 for a good solvent and θ condition, respectively [79]. At the θ condition PEG chains start to desolvate and eventually precipitate from solution where the volume occupied by the PEG chain is greatly reduced compared to a good solvent. Consequently, chemisorption of PEG from a solution at θ condition results in the formation of closely packed PEG brushes. Flory radii for PEG chains at θ condition (PBS buffer) and a good solvent (PB solution) are listed in Table 3.1. To obtain the average number of water molecules present per EG unit, the chain density of PEG 750 and 2000 was assumed to be similar to the previously reported values of 2.3 and 1.0 chain/ nm^2, respectively [80]; thus, the average number of water molecules per EG segment was calculated using the chemisorbed PEG wet mass. It was found that ~0.9 and ~1.2 water molecules per EG segment were associated with chemisorbed PEG 750 and 2000 chains, when within the θ solvent, respectively. Diffusivity of PEG 750 and 2000 chains at θ condition based on Stokes-Einstein relation was also reported in the Table 3.1. The ratio of initial chemisorption rates (chain/cm^2 s) and the ratio of diffusivities of PEG 750 to 2000 are 1.3 and 1.6. The fact that

these two values are reasonably close suggests that at the beginning of the chemisorption of PEG from θ solutions, chemisorption was diffusion limited.

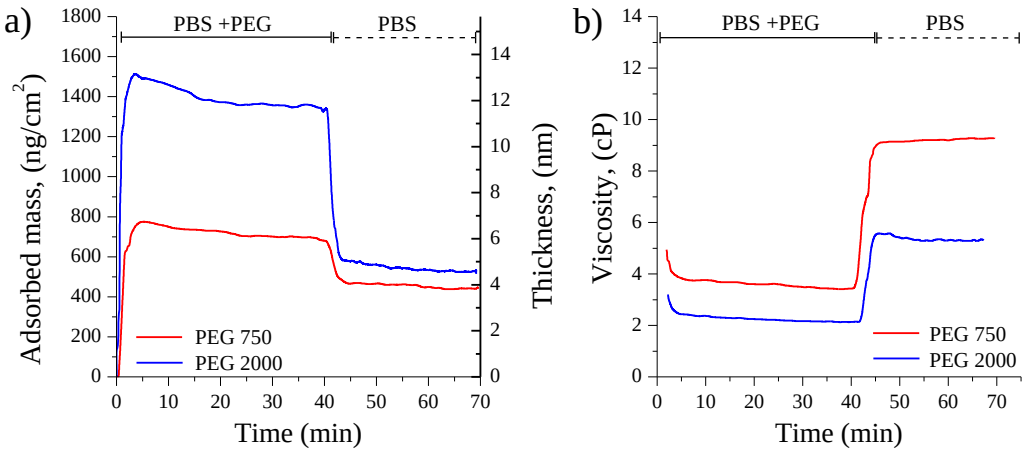

Figure 3.3 Representative time course of **a.** chemisorbed layer mass and thickness and **b.** chemisorbed layer viscosity of PEG 750 and 2000 on QCM-D Au sensor from 5 mM PEG solution in PBS buffer at IS 3.5 M and 37 °C (θ solution) with a flow rate of 0.15 mL/min.

Final chemisorbed amount of PEG remaining post-rinse was 436±6 and 518±6 ng/cm^2 which corresponds to the layer thickness of 3.8±0.1 and 4.5±0.1 nm for PEG 750 and 2000, respectively. Chemisorbed PEG layer regime could be obtained by comparing R_F and mean distance between two PEG grafted points, S, where S>>2R_F defines the dilute nonoverlapping mushroom regime, S~2R_F the semidilute overlapping mushrooms, S<2R_F the dilute brush regime, and S<<2R_F the dense brush regime [81]. In this study, the chemisorbed PEG 750 and 2000 layers form highly extended chains and present a dense brush regime in both θ and good solvents (note that R_F value is solvent dependent). The PEG layer thickness could also be calculated using the scaling theory developed by Alexander [82] for highly extended chains (i.e. dense brush regime):

$$L = N\frac{a^{5/3}}{S^{2/3}} \quad (3.4)$$

where L, N, a, and S are brush length, number of monomer per chain, monomer length, and the mean distance between two neighbouring grafted chains, respectively. Using Alexander scaling relation, the brush lengths of 3.9±0.1 and 7.8±0.1 nm were predicted for PEG 750 and 2000, respectively. The theoretical brush length based on the Alexander relation (3.9±0.1 nm) is in good agreement with the QCM-D result (3.8±0.1 nm) for PEG 750. However for PEG 2000 there is a considerable deviation between predicted (7.8±0.1 nm) and experimental (4.5±0.1 nm) data, which may indicate that the PEG 2000 layer formed a comparatively less extended brush conformation of PEG chains which may lead to increased error in the modelling results.

The change in the viscosity of chemisorbed PEG 750 and 2000 layers at different times (Figure 3.3) suggested that PEG 750 formed a chemisorbed layer more viscous than PEG 2000. Higher viscosity of chemisorbed PEG 750 layer may be due to its higher chain density, shorter chain length, lower $\Delta D_f/\Delta f$ ratio, and ultimately lower layer thickness which constructively resulted in reduced mobility of PEG 750 chains and enhanced layer stiffness. After buffer wash with θ solution devoid of PEG, there is a sudden increase in the viscosity of both chemisorbed PEG 750 and 2000 layers. Such increase in the viscosity of the chemisorbed PEG layers may be due to the removal of loosely bonded PEG chains (as seen in the mass results). It can be seen from Figure 3.3b that final viscosity of chemisorbed PEG 750 layer is almost twice that of chemisorbed PEG 2000 layer. Such differences in the viscosity of chemisorbed PEG 750 and 2000

layers may be a result of the difference in packing density of these chains. In fact, arrangement of water molecules *via* hydrogen bonding between the ether group of each EG segment can be a function of PEG chain density [83] and lesser conformational freedom of hydration shell around closely packed brushes in chemisorbed PEG 750 layer may contribute to its higher viscosity [84].

Table 3.1 Properties of chemisorbed PEG layer on Au QCM-D sensors from 5 mM PEG solution at IS 3.5 M and 37 °C flowing at 0.15 mL/min. Data are average of two measurments ± standard deviation (SD).

	PEG 750	PEG 2000
Initial chemisorption rate, [ng/cm^2 min]	520±20	1180±60
Viscosity, [cP]	9.2±0.8	4.8±0.5
Thickness, [nm]	3.8±0.1	4.5±0.1
Final chemisorbed mass, [ng/cm^2]	436±6	518±6
Chain density, [chain/nm^2]	2.3±0.1	1.0±0.1
Contour length, [nm]	5.9	15.9
Flory radius at θ condition, R_F [nm]	1.4	2.3
Diffusivity, D_{PEG}, [μm^2/s]	154	94
Flory radius in a good solvent, R_F [nm]	1.9	3.4
Mean distance, S [nm]	0.7±0.1	1.0±0.1

The effect of buffer change (a necessary step before PLL adsorption study) on the chemisorbed PEG layer conformation and hydration was studied. For this purpose, the PB solution used for preparation of PLL solution, which was

a good solvent for PEG, was flowed over the QCM-D Au sensor before and after the PEG chemisorption and associated buffer rinses. The frequency drop (Figure 3.4) due to the chemisorption of PEG 750 and 2000 chains are shown by Δf_{PEG750} and $\Delta f_{PEG2000}$, respectively. Frequency drop due to the combined effect of PEG 750 and 2000 chains chemisorbed from θ solution and ion desorption and rehydration of the chemisorbed PEG layer after switching the buffer to a good solvent are denoted by $\Delta f_{PEG750+H2O}$ and $\Delta f_{PEG2000+H2O}$, respectively. The difference between $\Delta f_{PEG+H2O}$ and Δf_{PEG} arose from an increased number of water molecules in the hydration shell of the PEG chain and potential desorption of ions from the Au sensor (Figure 3.4). The fact that the drastic difference in the ion concentration between the good solvent (used for PLL solution preparation) and the θ solvent (used for PEG chemisorption) changes the solution viscosity (from 0.7 to 1.05 cP) makes it impossible to delineate the contribution of ion desorption from the film upon moving to the good solvent. Furthermore, water molecules form hydrogen bonds with the PEG chains resulting in a specific interaction with the PEG layer. To this end, it was assumed that the -4.5 ±0.2 and -7.0±0.3 Hz difference between $\Delta f_{PEG+H2O}$ and Δf_{PEG} for PEG 750 and 2000 comes primarily from added water molecules to the hydration shell of the grafted PEG chains. Using the Sauerbrey equation [85], the added mass of water to the layer was calculated as 79.6±3.5 and 123.9±5.3 ng/cm^2 for chemisorbed PEG 750 and 2000 layers, respectively. This increase in the adsorbed mass values corresponded to addition of ~0.6 and ~0.8 water molecules per EG segment in the hydration shell of chemisorbed PEG 750 and 2000 chains, respectively. However, it should be noted that due to the fact

that more ions probably leave the PEG-Au surface upon introduction of good solvent (which has a considerable lower ionic strength compared with θ solvent), the estimated amount of water incorporated in the film is an underestimation. Rehydration of the chemisorbed PEG chains upon buffer change increased the total number of water molecules per EG segment to ~1.5 and ~2.0 for chemisorbed PEG 750 and 2000 chains in PB solution at pH 10.6. It is probable that some of the water molecules are within the vicinity of the chains and cannot freely move to the bulk solution; thus these water molecules are also accounted for in the QCM-D characterization. The PEG 750 hydration level suggests that this layer remains close to its minimum solubility, which is probably due to the PEG concentration directly in the film. The ~2.0 water molecules per EG segment in the chemisorbed PEG 2000 layer may seem to suggest a hydration state corresponding to a PEG chain in a good solvent; however, the mean distance of 1.0±0.1 nm between chemisorbed PEG 2000 chains suggests a brush regime of highly extended chains; thus, ~2.0 water molecules per EG segment in the hydration shell of the PEG chains may not be present merely due to hydrogen bonding with the oxygen atom in EG segment of polymer.

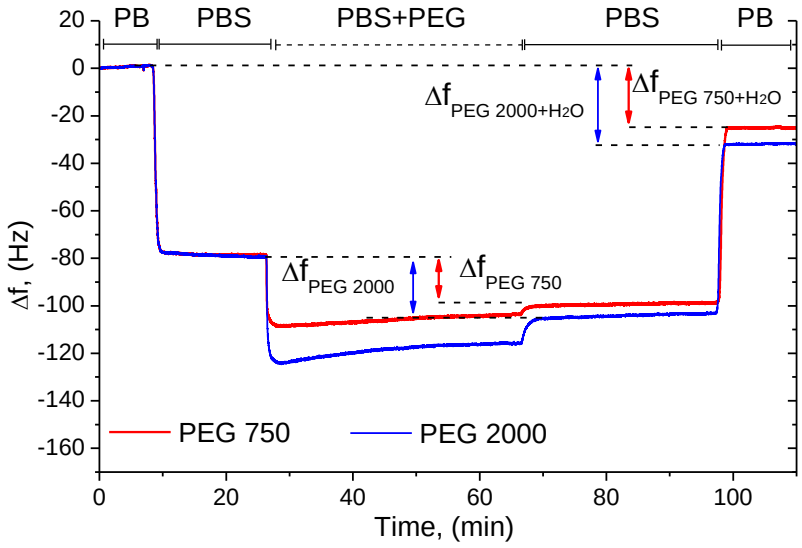

Figure 3.4 Representative *Δf* vs. time for 0.15 mL/min flow of 10 mM PB + 5 mM Na_2SO_4 at pH 10.6 (good solvent) followed by PEG chemisorption from 5 mM PEG solution at IS 3.5 M (*θ* solution) and again good solvent on QCM-D Au sensor at 37°C.

3.3.2 PLL adsorption: secondary structure evaluation

It has been shown that a minimum of 75% α-helix content can be induced in a PLL solution by increasing pH; heating this α-helix PLL solution completely transforms these into β-sheets [53]. As could be seen from Figure 3.1, in an α-helix PLL chain each amine group in the backbone forms a hydrogen bond with the carbonyl group of four residues earlier in the primary sequence, and 3.6 residues form a full helical turn with 26° pitch angle and 0.54 nm pitch [56]. β-sheet structure results when two PLLs form hydrogen bonds *via* the carbonyl group in the backbone of one strand with the amine group from a neighbouring strand. The distance between two adjacent strands in a β-sheet motif is 10.08 Å [57]. For a PLL chain consisting of the same number of lysine residues, geometric differences between different secondary structures make the β-sheet structure 2.3

times longer than α-helix, which shows the less compact structure of β-sheet as compared with α-helix. Compactness of α-helix structure is due to hydrogen bonds between immediate neighbouring amino acids in the same sequence. It should also be noted that pI value of PLL is around 12.2 and at solution pH of 10.6 a PLL chain carries 33.7 positive charges [86]. As mentioned earlier, secondary structure formation is a result of hydrogen bonding, not any change of the charge profile. Thus, it is unlikely that PLL charge change after induction of β-sheet structure by heating α-helix PLL and further cooling. It should be noted that α-helix and β-sheet structure could exist in the same physicochemical condition (same solution; pH 10.6, and 37ºC) although a difference in the thermal history of α-helix and β-sheet PLL solutions exists.

PLL with different secondary structures in solution and adsorbed to Au, chemisorbed PEG 750 and 2000 layers were characterized using CD to determine if the secondary structure altered upon adsorption (Figure 3.5). CD results have previously shown that α-helices have a maximum peak at ~190 nm and minimum peaks at ~205 and 222 nm, while β-sheets have a respective maximum and minimum peak at ~195 and ~215 nm [87, 88]. Table 3.2 summarizes the peak positions and intensities of both α-helix and β-sheet conformations in solution and in adsorbed state for different systems. It has been previously reported that less than a 3 nm shift in peak position does not represent an overall difference in secondary structure [87, 89]. Given the minor differences in peak positions between the bulk and adsorbed PLL for all systems in this study, it is probable that no measurable denaturation of these peptides occurred upon adsorption.

Hydrophilic surfaces have been previously reported to prevent conformation change of biomolecules upon adsorption [90]; thus, persistence of PLL secondary structure upon adsorption on Au could be due to the hydrophilic nature of Au surface. Persistence of PLL structure upon adsorption onto PEG layers may be due to this as well as the structure stabilizing property of PEG chains [91, 92].

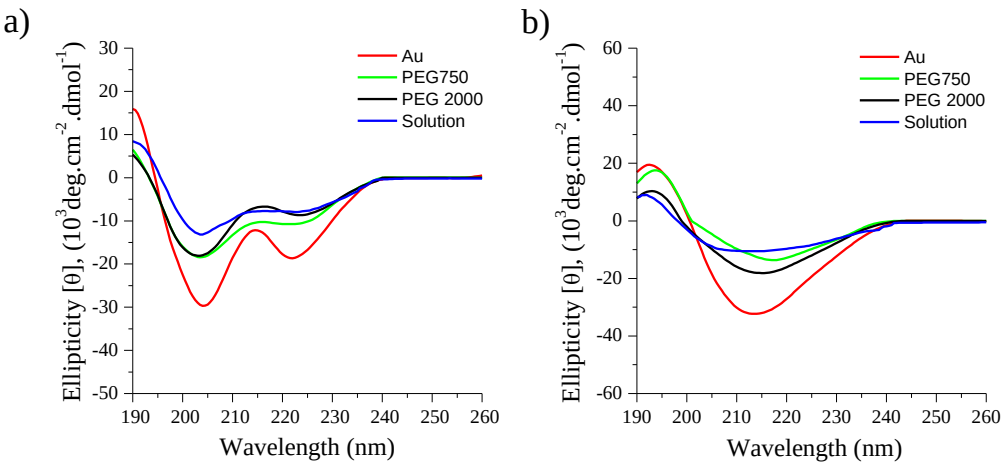

Figure 3.5 CD spectra of PLL in **a.** α-helix and **b.** β-sheet conformation in solution, adsorbed to Au coated quartz slides, PEG 750 and 2000 layer from 10 mM PB with 5 mM Na_2SO_4 at pH 10.6, and 37ºC. Data represent the average of n=3 measurements.

Table 3.2 Position and intensity of peaks in the CD spectra of different secondary structures of PLL in solution and adsorbed state. Data from 0.1 mg/mL PLL in 10 mM PB with 5mM Na_2SO_4 at pH 10.6 and 37ºC. Data represent the average of n=3 measurements.

Conformer		Peak 1 position [nm]	Intensity 10^3 [θ]	Peak 2 position [nm)]	Intensity 10^3 [θ]	Peak 3 position [nm)]	Intensity 10^3 [θ]
α-helix	Solution	190.0	8.5	203.5	-13.2	223.0	-8.0
	Bare Au	190.0	15.9	204.0	-29.7	222.0	-18.7
	PEG 750	190.0	6.5	203.5	-18.4	221.5	-10.7
	PEG 2000	190.0	5.4	204.0	-18.0	223	-8.7
β-sheet	Solution	192.0	9.0	214.0	-10.6	-	-
	Bare Au	192.5	19.5	214.0	-32.3	-	-
	PEG 750	192.0	17.3	215.0	-20.5	-	-
	PEG 2000	193.0	10.3	216.0	-18.1	-	-

3.3.3 PLL layer properties: mass adsorbed, thickness, and layer viscosity

Representative QCM-D data (Figure 3.6) details Δf and ΔD_f profiles for both α-helix and β-sheet adsorption to Au QCM-D sensors from 0.1 mg/mL PLL solution for different surface coatings. The last 5 min of PB solution rinse in each system is included (-5 to 0 min) so as to illustrate that the ion adsorption to, or desorption from, the surface was at steady state prior to introducing PLL (t=0). The overall frequency drop for β-sheet adsorption (-54.5±1.0 Hz) was greater than the α-helix (-10.1±0.3 Hz). However, the initial frequency drop rate of -48.3±4.5 Hz/min for α-helix was much larger than -6.4±0.1 Hz/min for β-sheet PLL. It has been reported that the adsorption of random coil PLL (MW 300,000) from a 300 μg/mL solution (PBS, pH 7.4 and 24°C) on Au sensor resulted in -14

Hz frequency drop [93]. Adsorption of random coil PLL (MW 15,000-30,000) from its 12.5 mg/mL solution in PBS buffer at pH 7.4 and 20°C on silica and polystyrene coated sensors was also reported to reach a plateau after -21 and -17 Hz frequency drop, respectively [94]; a similar trend considering the differences in secondary structure and molecular weight of PLL, solution, and temperature used in these studies. Such differences in the final frequency drop in the above mentioned studies could partially be due to the chemical nature of the surface and its influence on the PLL-surface interaction.

The presence of chemisorbed PEG 750 layer (Figure 3.6c and 3.6d) decreased the final frequency drop to -0.9±0.1 and -6.2±0.6 Hz for α-helix and β-sheet PLL, respectively. For chemisorbed PEG 2000 layers (Figure 3.6e and 3.6f), final frequency drop was -1.2±0.1 and -2.0±0.2 Hz for α-helix and β-sheet PLL, respectively. The initial frequency drop rate was -1.6±0.2 and -5.5±0.1 Hz/min for α-helix and β-sheet PLL adsorbed on chemisorbed PEG 750 and -1.5±0.1 and -3.5±0.2 Hz/min for α-helix and β-sheet PLL adsorbed on chemisorbed PEG 2000. Unlike PLL adsorption on Au, the initial rate of frequency drop for β-sheet PLL adsorption to chemisorbed PEG 750 or 2000 systems was higher than α-helix PLL.

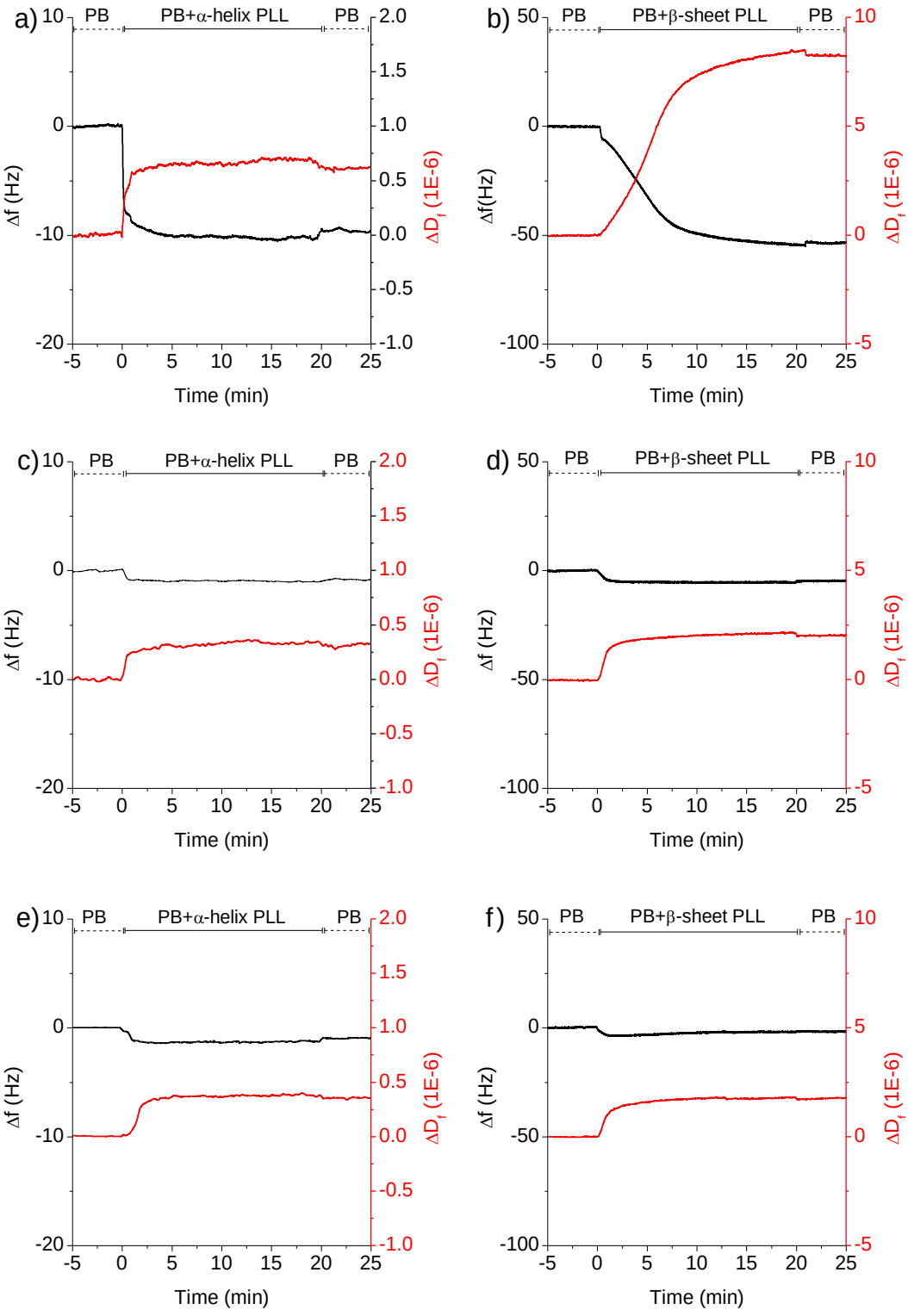

Figure 3.6 Representative time course of Δf and ΔD_f for **a, c, e.** α-helix and **b, d, f.** β-sheet PLL adsorption on QCM-D Au sensor from 0.15 mL/min flowing 0.1 mg/mL PLL in 10 mM potassium phosphate solution with 5 mM Na_2SO_4 at 37°C on **a, b.** bare Au surface, **c, d.** chemisorbed PEG 750, and **e, f.** chemisorbed PEG 2000 layers.

The final $\Delta D_f/\Delta f$ ratio for adsorbed α-helix PLL layer on Au was ~0.06 Hz^{-1}, which is considerably lower than the 0.15 Hz^{-1} value for β-sheet PLL. This lower $\Delta D_f/\Delta f$ ratio for adsorbed α-helix PLL layer on bare Au surface suggests a relatively low energy dissipation, (i.e. stiffer and more compact adsorbed α-helix PLL layer structure) [72, 73] as compared with adsorbed β-sheet PLL to this surface. For all PLL adsorbed layers on PEG, regardless of PLL secondary structure, the $\Delta D_f/\Delta f$ ratio (based on the maximum frequency drop) was ~0.5 Hz^{-1} which does not reflect any statistically significant change in the viscoelastic properties of the PLL films. This could be due to the mobility of the underlying chemisorbed PEG chains.

Representative modelling of QCM-D results of PLL adsorption on Au and PEG chemisorbed surfaces are presented in Figure 3.7 and corresponding adsorption parameters are summarised in Table 3.3. For modelling purpose, it was assumed that PLL concentration is low enough not to influence the solution density and viscosity. Thus, 0.994 g/cm^3 and 0.7 cP were used as solution density and viscosity of 10 mM PB with 5 mM Na_2SO_4 at 37°C containing 0.1 mg/mL PLL respectively [75]. Density of 1.06 g/cm^3 was chosen for the PLL hydrated layer density as reported elsewhere [95]. Left subfigures in Figure 3.7 show time course of mass and thickness growth of adsorbed α-helix and β-sheet PLL layers on QCM-D sensor for different surface coatings. As mentioned earlier, linear proportionality of thickness and mass of the adsorbed layer is due to the assumption of constant layer density. As a result the adsorbed mass is relatively insensitive to minor differences in the assumed layer density. PEG coating caused

a significant drop in initial rate of α-helix mass adsorption from 322±30 ng/cm^{2}min on bare Au to 11±1 and 10±1 ng/cm^{2}min for chemisorbed PEG 750 and 2000 layers, respectively. For β-sheet PLL adsorption on Au the initial adsorption rate was 120±1 ng/cm^2 min. PEG chemisorption caused a gradual drop in initial adsorption rate of β-sheet PLL to 103±2 and 66±3 ng/cm^2 min for chemisorbed PEG 750 and 2000 layers, respectively. It seems that initially chemisorbed PEG 2000 layer adsorbed some β-sheet PLL chains, but a desorption process started after ~2.5 min (Figure 3.7e). The final adsorbed amounts of α-helix and β-sheet PLL on bare Au surface was 231±5 ng/cm^2 and 1087±14 ng/cm^2, respectively. Chemisorption of PEG 750 and 2000 reduced the adsorbed amount of α-helix PLL to ~10 and ~12% of the α-helix PLL adsorbed on bare Au resulting in an average thickness of 0.2±0.1 and 0.3±0.1 nm for α-helix PLL layer adsorbed on PEG 750 and 2000 respectively. The adsorption half time increased from 21.7±1.6 s for α-helix PLL adsorption on Au, to 57.3±5.4 s and 81.0± 6.0 s for α-helix PLL adsorption on chemisorbed PEG 750 and 2000 layers, respectively. In the case of β-sheet PLL adsorption, the presence of chemisorbed PEG 750 and 2000 layers reduced the total adsorbed amount to 12% and 4% of the β-sheet PLL layer on bare Au surface. Adsorption half time for β-sheet PLL dramatically decreased from 271.8 ±4.2 s for β-sheet PLL adsorption on Au, to 36.1±2.6 s and 18.2± 1.4 s for β-sheet PLL adsorption on chemisorbed PEG 750 and 2000 layers, respectively.

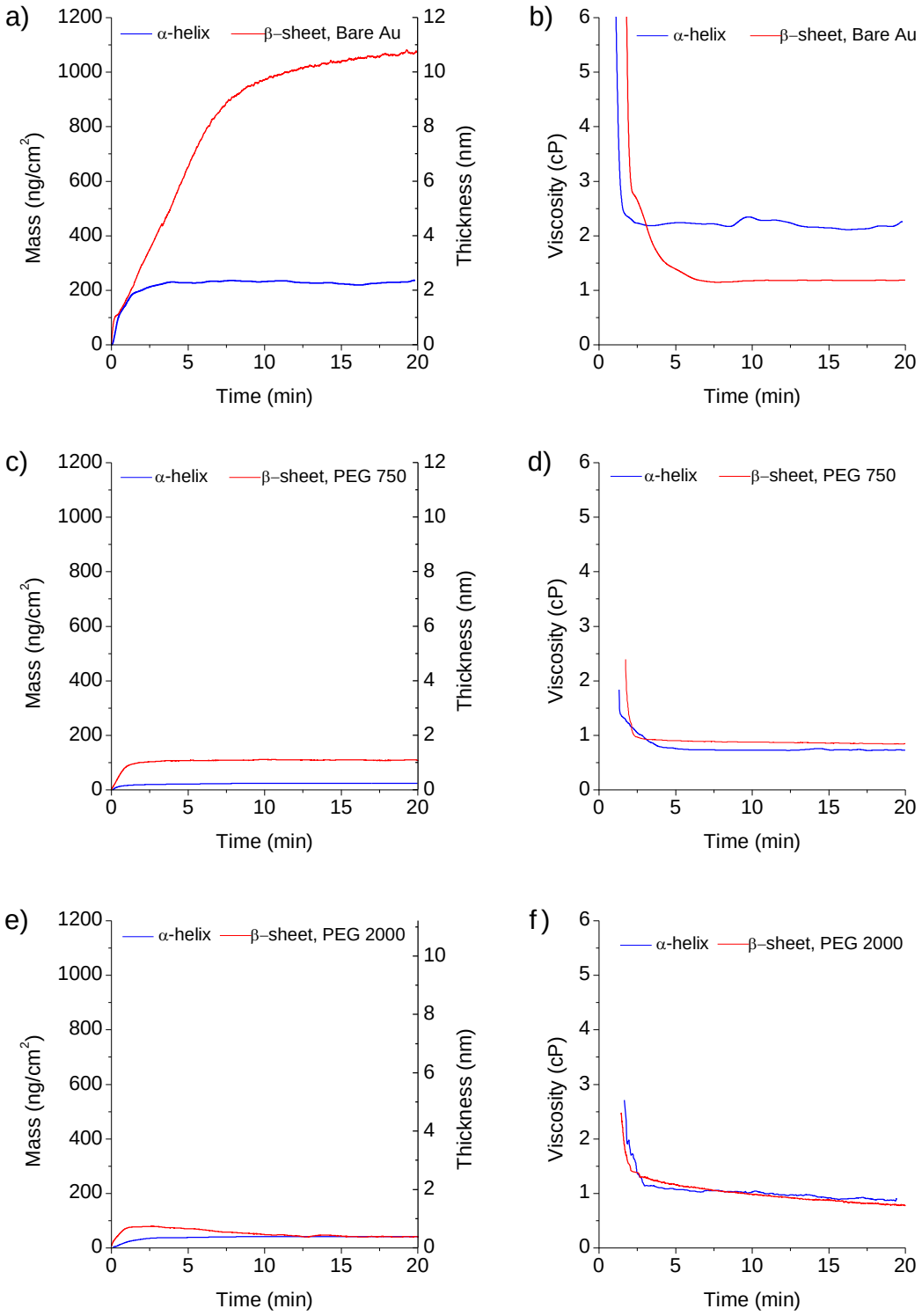

Figure 3.7 Representative QCM-D kinetic profiles of mass adsorption and layer thickness (left subfigures) as well as the viscosity (right subfigures) of α-helix and β-sheet PLL adsorption from 0.15 mL/min flowing 0.1 mg/mL PLL in 10 mM potassium phosphate solution with 5 mM Na_2SO_4 at 37°C on **a, b.** bare Au sensors, **c, d.** chemisorbed PEG 750, and **e, f.** PEG 2000 layer.

Clearly, a decrease in the initial adsorption rate or an increase in the final adsorbed amount increases the adsorption half time. For α-helix PLL adsorption, the drastic drop of the initial adsorption rate upon PEG chemisorption (322±20 ng/cm^2 min on bare Au, to 11±1 and 10±1 ng/cm^2 min on chemisorbed PEG 750 and 2000 respectively) played the main role in increasing the adsorption half time. In contrast, for β-sheet PLL the presence of PEG chemisorbed layers resulted in a gradual decrease in the initial adsorption rate (from 120±2 ng/cm^2.min bare Au, to 103±2 and 66±3 ng/cm^2.min on chemisorbed PEG 750 and 2000 respectively) but the drastic reduction of total adsorbed amount of β-sheet PLL upon PEG chemisorption (from 1087±14 ng/cm^2 on bare Au, to 124±9 and 40±3 ng/cm^2 on chemisorbed PEG 750 and 2000 respectively) could effectively decrease adsorption half time after PEG chemisorption.

The viscosity profiles for the developing α-helix and β-sheet layers on different surfaces are shown in Figure 3.7. It is obvious that the α-helix layer yielded a plateau layer viscosity almost double the viscosity of the β-sheet on Au. However, it appears that the layer viscosity of PLL adsorbed on chemisorbed PEG layers remains almost the same regardless of its secondary structure. Significantly higher viscosity of α-helix PLL compared to β-sheet PLL layers adsorbed on Au may be due to relative rigidity of the PLL chains in α-helix form. Hydrogen bonds between neighbouring amino acids responsible for formation of α-helix have a more pronounced effect on reduction of chain flexibility [96] as opposed to the hydrogen bonds between amino acids from two adjacent chains in β-sheet PLL. Arrangement of water molecules *via* hydrogen bonding between free

amine group of each lysine residue and relative orientation of chains may also be a function of PLL secondary structure. Similar viscosity values of PLL adsorbed on chemisorbed PEG layers, regardless of PEG MW and PLL secondary structure were observed and could be due to mobility of chemisorbed PEG chains which modulates the interaction and preferred orientation of PLL chains and their associated water molecule (i.e. hydration shell) responsible for regulating the layer viscosity. The other important parameter which potentially modulates the viscosity of the adsorbed PLL layer is the adsorbed amount of PLL. Clearly in the case of PLL adsorption on PEG layer, the number of adsorbed PLL chains per unit area is drastically reduced resulting in a larger hydration shell around each PLL chain which may ultimately reduce layer viscosity toward the viscosity of the PLL solution. It should also be noted that upon PLL adsorption the viscosity of the underlying PEG film may change due to PEG layer perturbation, potential desolvation, and intermolecular interactions with PLL. Therefore, the reported viscosity may reflect both the effects of the PLL itself as well as the effect the adsorbed PLL may have upon the PEG film.

Higher adsorbed amount/thickness of the β-sheet PLL layer as compared with α-helix PLL film may also be due to the strong interaction of β-sheet PLL chains with each other. The effect of secondary structure on the intermolecular interaction strength was first reported by Grigsby et al. [97] who found that the interactions between PLL chains in aqueous solution are hydrophobic in nature and greater for β-sheet as compared with α-helix conformation. By considering β-sheet and α-helix conformations as a flat surface and a cylinder respectively,

Grigsby et al. attributed the interaction between PLL chains to be a function of surface to surface contact area [97]. Thus, it may be that the higher adsorbed amount of β-sheet PLL on Au as compared with α-helix is due to further β-sheet incorporation with pre-adsorbed β-sheet structures. Presence of a mobile end-grafted PEG layer weakens the interaction between Au and PLL so that the PLL chains cannot further efficiently interact with pre-adsorbed β-sheets. In fact, reduced immobilization of PLL at the interface has a more pronounced effect on hampering constructive and relatively stronger interactions between β-sheet PLL chains [97] (as compared with α-helix PLL) responsible for increase of the adsorbed β-sheet PLL mass. Higher conformational mobility of the chemisorbed PEG 2000 as compared with chemisorbed PEG 750 chains (i.e. lower viscosity of chemisorbed PEG 2000 layer as compared with chemisorbed PEG 750 layer) further reduced the adsorbed amount of β-sheet PLL.

Table 3.3 Physical properties of α-helix and β-sheet adsorbed layers on different surfaces. Data are average of two measurments ± SD.

		Bare Au	PEG 750	PEG 2000
Initial adsorption rate [ng/cm^2.min]	α-helix	322±30	11±1	10±1
	β-sheet	120±2	103±2	66±3
Adsorption half time [s]	α-helix	21.7±1.6	57.3±5.4	81.0±6.0
	β-sheet	271.8±4.2	36.1±2.6	18.2±1.4
Adsorbed mass[ng/cm^2]	α-helix	231±5	21±2	27±2
	β-sheet	1087±14	124±9	40±3
Thickness [nm]	α-helix	2.3±0.1	0.2±0.1	0.3±0.1
	β-sheet	10.9±0.1	1.2±0.1	0.4±0.1
Viscosity [cP]	α-helix	2.3±0.1	0.8±0.1	0.8±0.1
	β-sheet	1.2±0.1	0.9±0.1	0.8±0.1

3.4 Conclusion

The results of this work suggested that at θ condition it is diffusion which limited chemisorption rates of end-thiolated PEG chains and, within ~2.5 min, PEG chemisorption reached its highest extent. Both chemisorbed PEG 750 and 2000 layers formed brush regime with highly extended chains. It is evident from the final chemisorbed amount of PEG that chemisorbed PEG mass was almost independent of the polymer MW; in other words, chain density values were inversely proportional to the PEG MW. PEG hydration study showed that changing buffer from PBS (3.5 M, pH 7.4) to 10mM PB (5 mM Na_2SO_4, pH 10.6) further hydrated the chemisorbed PEG chains. However, the chemisorbed PEG chains in the PB solution had hydration values similar to that expected for higher

concentrations of PEG chains in the surface vicinity. It is probable that some non-hydrogen bonded water molecules were associated with the polymers and incorporated into the calculation without being directly bonded to the polymer chains.

CD results showed that secondary structure of PLL may persist upon adsorption from solution to Au, and chemisorbed PEG 750 and 2000 surfaces; which could be due to the hydrophilic nature of Au and PEG surfaces and structure stabilizing property of PEG chains. PLL adsorption study revealed that secondary structure regulated the interaction between the PLL and Au surface and further affected adsorption rate, extent, and layer viscosity. Higher extent of adsorption in case of β-sheet PLL could be due to stronger interactions between β-sheet PLL chains. It was found that viscosity of α-helix PLL adsorbed on Au is almost twice as high as β-sheet PLL adsorbed layer, suggesting a stiffer and more compact α-helix PLL adsorbed layer structure which could be due to the secondary structure specific hydrogen bonding patterns between the amino acids residues of the PLL chain. Unlike PLL adsorption on Au surface, the initial adsorption rate of β-sheet PLL on chemisorbed PEG 750 and 2000 brush layers was higher than α-helix PLL. Passivation of Au surface *via* chemisorption of PEG 750 and 2000 drastically suppressed rigidity of the adsorbed layer by elimination of direct interaction between unmodified Au surface and peptide chains resulting in similar layer viscosity for adsorbed PLL layers regardless of PLL secondary structure. Surfaces prepared by chemisorption of PEG 2000 from its θ solution showed a better inhibition of non-specific protein adsorption and final adsorbed

amount of PLL chains onto chemisorbed PEG 2000 layer was almost independent of the secondary structure. It is thought lower viscosity of chemisorbed PEG 2000 layer (as compared with chemisorbed PEG 750 layer) contributes to its better overall performance by reducing the viscosity difference between PLL solution and PEG chemisorbed layer. The inability of PLL to adsorb to the chemisorbed PEG interface may suggest that PEG has a pronounced effect on hampering relatively strong constructive interactions between β-sheet PLL chains responsible for higher adsorbed mass of β-sheet PLL on Au. Results of this work provide new information about the influence of secondary structure on the adsorption of the proteins and could be used to develop better materials/coatings to control the non-specific adsorption of proteins.

3.5 References

[1] Anderson, JM, Bonfield, TL, and Ziats, NP. Protein adsorption and cellular adhesion and activation on biomedical polymers. Int. J. Artif. Organs, 1990;13:375-382.

[2] Andrade, JD and Hlady, V. Plasma protein adsorption: the big twelve. Ann. N. Y. Acad. Sci., 1987;516:158-172.

[3] Nath, N, Hyun, J, Ma, H, and Chilkoti, A. Surface engineering strategies for control of protein and cell interactions. Surf. Sci., 2004;570:98-110.

[4] Pankowsky, DA, Ziats, NP, Topham, NS, Ratnoff, OD, and Anderson, JM. Morphologic characteristics of adsorbed human plasma-proteins on vascular grafts and biomaterials. J. Vasc. Surg., 1990;11:599-606.

[5] Shen, M, Garcia, I, Maier, RV, and Horbett, TA. Effects of adsorbed proteins and surface chemistry on foreign body giant cell formation, tumor necrosis factor alpha release and procoagulant activity of monocytes. J. Biomed. Mater. Res., Part A, 2004;70A:533-541.

[6] Hlady, V, VanWagenen, RA, and Andrade, JD. Total internal reflection intrinsic fluorescence (TIRIF) spectroscopy applied to protein adsorption, in Surface and Interfacial Aspects of Biomedical Polymers J.D. Andrade, Editor. 1985, Plenum Press, New York, NY, USA, . 81-119.

[7] Collier, TO and Anderson, JM. Protein and surface effects on monocyte and macrophage adhesion, maturation, and survival. J. Biomed. Mater. Res., 2002;60:487-496.

[8] Evans-Nguyen, KM, Fuierer, RR, Fitchett, BD, Tolles, LR, Conboy, JC, and Schoenfisch, MH. Changes in adsorbed fibrinogen upon conversion to fibrin. Langmuir, 2006;22:5115-5121.

[9] Heuberger, M, Drobek, T, and Spencer, ND. Interaction forces and morphology of a protein-resistant poly(ethylene glycol) layer. Biophys. J., 2005;88:495-504.

[10] Hu, W-J, Eaton, JW, Ugarova, TP, and Tang, L. Molecular basis of biomaterial-mediated foreign body reactions. Blood, 2001;98:1231-1238.

[11] Lu, DR and Park, K. Effect of surface hydrophobicity on the conformational changes of adsorbed fibrinogen. J. Colloid Interface Sci., 1991;144:271-281.

[12] Absolom, DR, Zingg, W, Policova, Z, and Neumann, AW. Determination of the surface tension of protein coated materials by means of the advancing solidification front technique. ASAIO J., 1983;29:146-151.

[13] Andrade, JD, Hlady, VL, and Vanwagenen, RA. Effects of plasma-protein adsorption on protein conformation and activity. Pure Appl. Chem., 1984;56:1345-1350.

[14] Dadsetan, M, Jones, JA, Hiltner, A, and Anderson, JM. Surface chemistry mediates adhesive structure, cytoskeletal organization, and fusion of macrophages. J. Biomed. Mater. Res., Part A, 2004;71A:439-448.

[15] Statz, AR, Meagher, RJ, Barron, AE, and Messersmith, PB. New peptidomimetic polymers for antifouling surfaces. J. Am. Chem. Soc., 2005;127:7972-7973.

[16] Dalsin, JL and Messersmith, PB. Bioinspired antifouling polymers. Materials Today, 2005;8:38-46.

[17] Vladkova, TG. Surface engineered polymeric biomaterials with improved biocontact properties. Int. J. Polym. Sci., 2010;2010:1-22.

[18] Unsworth, LD.Protein adsorption to chemisorbed polyethylene oxide thin films, in Chemical engineering. 2005, McMaster University: Hamilton, Ontario.

[19] Ostuni, E, Chapman, RG, Holmlin, RE, Takayama, S, and Whitesides, GM. A survey of structure-property relationships of surfaces that resist the adsorption of protein. Langmuir, 2001;17:5605-5620.

[20] Vennemann, N, Lechner, MD, and Oberthür, RC. Thermodynamics and conformation of polyoxyethylene in aqueous solution under high pressure: 1. Small-angle neutron scattering and densitometric measurements at room temperature. Polymer, 1987;28:1738-1748.

[21] Kingshott, P, Thissen, H, and Griesser, H. Effects of cloud-point grafting, chain length, and density of PEG layers on competitive adsorption of ocular proteins J. Biomaterials, 2002;23:2043.

[22] Dormidontova, EE. Role of competitive PEO-water and water-water hydrogen bonding in aqueous solution PEO behavior. Macromolecules, 2002;35:987-1001.

[23] Matsuyama, A and Tanaka, F. Theory of solvation-induced reentrant phase separation in polymer solutions. Phys. Rev. Lett., 1990;65:341-344.

[24] Ren, CL, Nap, RJ, and Szleifer, I. The Role of Hydrogen Bonding in Tethered Polymer Layers. J. Phys. Chem. B, 2008;112:16238-16248.

[25] Valentini, M, Napoli, A, Tirelli, N, and Hubbell, JA. Precise determination of the hydrophobic/hydrophilic junction in polymeric vesicles. Langmuir, 2003;19:4852-4855.

[26] Lee, JH, Lee, HB, and Andrade, JD. Blood compatibility of polyethylene oxide surfaces. Prog. Polym. Sci., 1995;20:1043-1079.

[27] van Oss, CJ. The primary interactions, in Interfacial forces in aqueous media. 1994, CRC Press.

[28] Li, LY, Chen, SF, Zheng, J, Ratner, BD, and Jiang, SY. Protein adsorption on oligo(ethylene glycol)-terminated alkanethiolate self-assembled monolayers: The molecular basis for nonfouling behavior. J. Phys. Chem. B, 2005;109:2934-2941.

[29] Unsworth, LD, Sheardown, H, and Brash, JL. Protein resistance of surfaces prepared by sorption of end-thiolated poly(ethylene glycol) to gold: Effect of surface chain density. Langmuir, 2005;21:1036-1041.

[30] Wong, SY, Han, L, Timachova, K, Veselinovic, J, Hyder, MN, Ortiz, C, Klibanov, AM, and Hammond, PT. Drastically lowered protein adsorption on microbicidal hydrophobic/hydrophilic polyelectrolyte multilayers. Biomacromolecules, 2012;13:719-726.

[31] Meder, F, Daberkow, T, Treccani, L, Wilhelm, M, Schowalter, M, Rosenauer, A, Mädler, L, and Rezwan, K. Protein adsorption on colloidal alumina particles functionalized with amino, carboxyl, sulfonate and phosphate groups. Acta Biomater., 2012;8:1221-1229.

[32] Deligianni, DD, Katsala, N, Ladas, S, Sotiropoulou, D, Amedee, J, and Missirlis, YF. Effect of surface roughness of the titanium alloy Ti-6Al-4V on human bone marrow cell response and on protein adsorption. Biomaterials, 2001;22:1241-1251.

[33] Chen, SF, Li, LY, Zhao, C, and Zheng, J. Surface hydration: Principles and applications toward low-fouling/nonfouling biomaterials. Polymer, 2010;51:5283-5293.

[34] Jordan, CE and Corn, RM. Surface plasmon resonance imaging measurements of electrostatic biopolymer adsorption onto chemically modified gold surfaces. Anal. Chem., 1997;69:1449-1456.

[35] Yang, Q, Kaul, C, and Ulbricht, M. Anti-nonspecific protein adsorption properties of biomimetic glycocalyx-like glycopolymer layers: effects of glycopolymer chain density and protein size. Langmuir, 2010;26:5746-5752.

[36] Ball, V. Adsorption behavior of different polypeptides in the 3 kDa molecular weight range at an Si0.8Ti0.2O2-aqueous solution interface from low ionic strength solutions. Colloids Surf., B, 2004;33:129-142.

[37] Ramsden, JJ and Prenosil, JE. Effect of ionic-strength on protein adsorption-kinetics. J. Phys. Chem., 1994;98:5376-5381.

[38] Elgersma, AV, Zsom, RLJ, Lyklema, J, and Norde, W. Kinetics of single and competitive protein adsorption studied by reflectometry and streaming potential measurements. Colloids Surf., 1992;65:17-28.

[39] Norde, W and Lyklema, J. The adsorption of human plasma albumin and bovine pancreas ribonuclease at negatively charged polystyrene surfaces: I. Adsorption isotherms. Effects of charge, ionic strength, and temperature. J. Colloid Interface Sci., 1978;66:257-265.

[40] Kabsch, W and Sander, C. Dictionary of protein secondary structure: pattern recognition of hydrogen-bonded and geometrical features. Biopolymers, 1983;22:2577-2637.

[41] Martin, J, Gibrat, JF, and Rodolphe, F.Hidden Markov model for protein secondary structure, in International Symposium on Applied Stochastic Models and Data Analysis. 2005: Brest, France.

[42] Raut, VP, Agashe, MA, Stuart, SJ, and Latour, RA. Molecular Dynamics Simulations of Peptide−Surface Interactions. Langmuir, 2005;21:1629-1639.

[43] Kent, MS, Yim, H, Murton, JK, Sasaki, DY, Polizzotti, BD, Charati, MB, Kiick, KL, Kuzmenko, I, and Satija, S. Synthetic polypeptide adsorption to Cu-IDA containing lipid films: a model for protein-membrane interactions. Langmuir, 2008;24:932-942.

[44] Apte, JS, Collier, G, Latour, RA, Gamble, LJ, and Castner, DG. XPS and ToF-SIMS Investigation of alpha-Helical and beta-Strand Peptide Adsorption onto SAMs. Langmuir, 2010;26:3423-3432.

[45] Collier, G, Vellore, N, Yancey, J, Stuart, S, and Latour, R. Comparison Between Empirical Protein Force Fields for the Simulation of the Adsorption Behavior of Structured LK Peptides on Functionalized Surfaces. Biointerphases, 2012;7:1-19.

[46] Mermut, O, Phillips, DC, York, RL, McCrea, KR, Ward, RS, and Somorjai, GA. In Situ Adsorption Studies of a 14-Amino Acid Leucine-Lysine Peptide onto Hydrophobic Polystyrene and Hydrophilic Silica Surfaces Using Quartz Crystal Microbalance, Atomic Force Microscopy, and Sum Frequency Generation Vibrational Spectroscopy. J. Am. Chem. Soc., 2006;128:3598-3607.

[47] Phillips, DC, York, RL, Mermut, O, McCrea, KR, Ward, RS, and Somorjai, GA. Side Chain, Chain Length, and Sequence Effects on Amphiphilic Peptide Adsorption at Hydrophobic and Hydrophilic Surfaces Studied by Sum-Frequency Generation Vibrational Spectroscopy and Quartz Crystal Microbalance. J. Phys. Chem. C, 2006;111:255-261.

[48] Weidner, T, Apte, JS, Gamble, LJ, and Castner, DG. Probing the Orientation and Conformation of alpha-Helix and beta-Strand Model Peptides on Self-Assembled Monolayers Using Sum Frequency Generation and NEXAFS Spectroscopy. Langmuir, 2010;26:3433-3440.

[49] Weidner, T, Breen, NF, Li, K, Drobny, GP, and Castner, DG. Sum frequency generation and solid-state NMR study of the structure, orientation, and dynamics of polystyrene-adsorbed peptides. Proc. Natl. Acad. Sci. U. S. A., 2010;107:13288-13293.

[50] Weidner, T, Samuel, NT, McCrea, K, Gamble, LJ, Ward, RS, and Castner, DG. Assembly and structure of alpha-helical peptide films on hydrophobic fluorocarbon surfaces. Biointerphases, 2010;5:9-16.

[51] Puddu, V and Perry, CC. Peptide Adsorption on Silica Nanoparticles: Evidence of Hydrophobic Interactions. ACS Nano, 2012;6:6356-6363.

[52] Yoshioka, K, Sato, Y, Tanaka, M, Murakami, T, and Niwa, O. Suppression of Non-specific Adsorption Using Densified Tri(ethylene glycol) Alkanethiols:

Monolayer Characteristics Evaluated by Electrochemical Measurements. Anal. Sci., 2010;26:33-37.

[53] Chittchang, M, Salamat-Miller, N, Alur, HH, Vander Velde, DG, Mitra, AK, and Johnston, TP. Poly (L-Lysine) as a model drug macromolecule with which to investigate secondary structure and microporous membrane transport, part 2: diffusion studies. J. Pharm. Pharmacol., 2002;54:1497-1505.

[54] Shibata, A, Yamamoto, M, Yamashita, T, Chiou, JS, Kamaya, H, and Ueda, I. Biphasic effects of alcohols on the phase transition of poly(L-lysine) between .alpha.-helix and .beta.-sheet conformations. Biochemistry (Mosc.), 1992;31:5728-5733.

[55] Weber, N, Wendel, HP, and Kohn, J. Formation of viscoelastic protein layers on polymeric surf aces relevant to platelet adhesion. J. Biomed. Mater. Res., Part A, 2005;72A:420-427.

[56] Andrews, DW and Ottensmeyer, FP. Electron-microscopy of the poly-L-Lysine alpha-helix. Ultramicroscopy, 1982;9:337-348.

[57] Demirdoven, N, Cheatum, CM, Chung, HS, Khalil, M, Knoester, J, and Tokmakoff, A. Two-dimensional infrared spectroscopy of antiparallel beta-sheet secondary structure. J. Am. Chem. Soc., 2004;126:7981-7990.

[58] Barbosa, RV, Moraes, MAR, Gomes, AS, and Soares, BG. EVA-based graft-copolymers as compatibilizing agents for polymer blends. J. Macromol. Sci., Part A: Pure Appl. Chem., 1995;A32:663-669.

[59] Du, YJ and Brash, JL. Synthesis and characterization of thiol-terminated poly(ethylene oxide) for chemisorption to gold surface. J. Appl. Polym. Sci., 2003;90:594-607.

[60] Chittchang, M, Alur, HH, Mitra, AK, and Johnston, TP. Poly(L-lysine) as a model drug macromolecule with which to investigate secondary structure and membrane transport, part I: physicochemical and stability studies. J. Pharm. Pharmacol., 2002;54:315-323.

[61] Arunkumar, AI, Kumar, TKS, Sivaraman, T, and Yu, C. Acetonitrile-induced conformational transitions in poly-L-lysine. Int. J. Biol. Macromol., 1997;21:299-305.

[62] Tiffany, ML. Circular-dichroism study of charged polypeptides interaction with salts. Physiol. Chem. Phys., 1975;7:191-207.

[63] Fukushima, K, Sakamoto, T, Tsuji, J, Kondo, K, and Shimozawa, R. The transition of alpha-helix to beta-structure of poly-L-Lysine induced by phosphatidic-acid vesicles and its kinetics at alkaline pH. Biochim. Biophys. Acta, Biomembr., 1994;1191:133-140.

[64] Chiou, J-S, Tatara, T, Sawamura, S, Kaminoh, Y, Kamaya, H, Shibata, A, and Ueda, I. The [alpha]-helix to [beta]-sheet transition in poly(L-lysine): Effects of

anesthetics and high pressure. Biochim. Biophys. Acta, Protein. Struct. Mol. Enzymol., 1992;1119:211-217.

[65] Sivaraman, B, Fears, KP, and Latour, RA. Investigation of the effects of surface chemistry and solution concentration on the conformation of adsorbed proteins using an improved circular dichroism method. Langmuir, 2009;25:3050-3056.

[66] Wolkers, WF, van Kilsdonk, MG, and Hoekstra, FA. Dehydration-induced conformational changes of poly--lysine as influenced by drying rate and carbohydrates. Biochim. Biophys. Acta, Gen. Subj., 1998;1425:127-136.

[67] Voinova, MV, Rodahl, M, Jonson, M, and Kasemo, B. Viscoelastic acoustic response of layered polymer films at fluid-solid interfaces: Continuum mechanics approach. Phys. Scr., 1999;59:391-396.

[68] Song, J, Yamagushi, T, Silva, DJ, Hubbe, MA, and Rojas, OJ. Effect of Charge Asymmetry on Adsorption and Phase Separation of Polyampholytes on Silica and Cellulose Surfaces. The Journal of Physical Chemistry B, 2009;114:719-727.

[69] Schreiber, F. Structure and growth of self-assembling monolayers. Prog. Surf. Sci., 2000;65:151-256.

[70] Reimhult, K, Petersson, K, and Krozer, A. QCM-D Analysis of the Performance of Blocking Agents on Gold and Polystyrene Surfaces. Langmuir, 2008;24:8695-8700.

[71] Naderi, A, Iruthayaraj, J, Pettersson, Tr, Makuška, Ra, and Claesson, PM. Effect of Polymer Architecture on the Adsorption Properties of a Nonionic Polymer. Langmuir, 2008;24:6676-6682.

[72] Dutta, AK and Belfort, G. Adsorbed gels versus brushes: Viscoelastic differences. Langmuir, 2007;23:3088-3094.

[73] Notley, SM, Eriksson, M, and Wagberg, L. Visco-elastic and adhesive properties of adsorbed polyelectrolyte multilayers determined in situ with QCM-D and AFM measurements. J. Colloid Interface Sci., 2005;292:29-37.

[74] Dubacheva, GV, Van der Heyden, A, Dumy, P, Kaftan, O, Auzely-Velty, R, Coche-Guerente, L, and Labbe, P. Electrochemically Controlled Adsorption of Fc-Functionalized Polymers on beta-CD-Modified Self-Assembled Monolayers. Langmuir, 2010;26:13976-13986.

[75] Green, DW and Perry, RH. Perry's Chemical Engineers' Handbook (8th Edition). 2008: McGraw-Hill. 2-96, 2-449.

[76] Kestin, J and Shankland, IR. Viscosity of aqueous NaCl solutions in the temperature range 25–200 °C and in the pressure range 0.1–30 MPa. Int. J. Thermophys., 1984;5:241-263.

[77] de Kerchove, AJ and Elimelech, M. Structural growth and viscoelastic properties of adsorbed alginate layers in monovalent and divalent salts. Macromolecules, 2006;39:6558-6564.

[78] Hansen, PL, Cohen, JA, Podgornik, R, and Parsegian, VA. Osmotic properties of poly(ethylene glycols): Quantitative features of brush and bulk scaling laws. Biophys. J., 2003;84:350-355.

[79] Teraoka, I. Thermodynamics of Dilute Polymer Solutions, in Polymer Solutions: An Introduction to Physical Properties. 2002, John Wiley & Sons, Inc.: New York. 69-89.

[80] Unsworth, LD, Sheardown, H, and Brash, JL. Protein-resistant poly(ethylene oxide)-grafted surfaces: chain density-dependent multiple mechanisms of action. Langmuir, 2008;24:1924-1929.

[81] Unsworth, LD, Tun, Z, Sheardown, H, and Brash, JL. Chemisorption of thiolated poly(ethylene oxide) to gold: surface chain densities measured by ellipsometry and neutron reflectometry. J. Colloid Interface Sci., 2005;281:112-121.

[82] Alexander, S. Adsorption of chain molecules with a polar head a scaling description. Journal De Physique, 1977;38:983-987.

[83] Pasche, S, De Paul, SM, Vörös, J, Spencer, ND, and Textor, M. Langmuir, 2003;19:9216.

[84] Muller, MT.Aqueous Lubrication by Maens of Surface-Bound Brush-Like Copolymers, in Department of Materials. 2005, Swiss Federal Institute of Technology Zurich: Zurich.

[85] Hook, F, Voros, J, Rodahl, M, Kurrat, R, Boni, P, Ramsden, JJ, Textor, M, Spencer, ND, Tengvall, P, Gold, J, and Kasemo, B. A comparative study of protein adsorption on titanium oxide surfaces using in situ ellipsometry, optical waveguide lightmode spectroscopy, and quartz crystal microbalance/dissipation. Colloids and Surfaces B-Biointerfaces, 2002;24:155-170.

[86] Putnam, C. Protein calculator v3.3 2006 March 28, 2006; Available from: http://www.scripps.edu/~cdputnam/protcalc.html.

[87] Parson, WW. Circular Dichroism, in Modern Optical Spectroscopy: With Exercises and Examples from Biophysics and Biochemistry. 2009, Springer: New York. 307-334.

[88] Miles, AJ, Whitmore, L, and Wallace, BA. Spectral magnitude effects on the analyses of secondary structure from circular dichroism spectroscopic data. Protein Sci., 2005;14:368-374.

[89] Greenfield, NJ. Using circular dichroism spectra to estimate protein secondary structure. Nat. Protoc., 2006;1:2876-2890.

[90] Roach, P, Farrar, D, and Perry, CC. Interpretation of protein adsorption: Surface-induced conformational changes. J. Am. Chem. Soc., 2005;127:8168-8173.

[91] van Oss, CJ. Long-range and short-range mechanisms of hydrophobic attraction and hydrophilic repulsion in specific and aspecific interactions. J. Mol. Recognit., 2003;16:177-190.

[92] Holmberg, K, Bergstrom, K, and Stark, MB. Immobilization of proteins via PEG chains, in Polyethylene Glycol Chemistry: Biotechnical and Biomedical Application, J.M. Harris, Editor. 1992, Plenum Press: New York. 303-324.

[93] Dutta, AK, Nayak, A, and Belfort, G. Viscoelastic properties of adsorbed and cross-linked polypeptide and protein layers at a solid-liquid interface. J. Colloid Interface Sci., 2008;324:55-60.

[94] York, RL, Holinga, GJ, and Somorjai, GA. Investigation of the Influence of Chain Length on the Interfacial Ordering of L-Lysine and L-Proline and Their Homopeptides at Hydrophobic and Hydrophilic Interfaces Studied by Sum Frequency Generation and Quartz Crystal Microbalance. Langmuir, 2009;25:9369-9374.

[95] Porus, M, Maroni, P, and Borkovec, M. Structure of Adsorbed Polyelectrolyte Monolayers Investigated by Combining Optical Reflectometry and Piezoelectric Techniques. Langmuir, 2012;28:5642-5651.

[96] Chittchang, M, Mitra, A, and Johnston, T. Interplay of secondary structure and charge on the diffusion of a polypeptide through negatively charged aqueous Pores. Pharm. Res., 2007;24:502-511.

[97] Grigsby, JJ, Blanch, HW, and Prausnitz, JM. Effect of secondary structure on the potential of mean force for poly--lysine in the [alpha]-helix and [beta]-sheet conformations. Biophys. Chem., 2002;99:107-116.

4. Understanding the Effect of Secondary Structure on Molecular Interactions of Poly- L-Lysine with Different Substrates by SFA[4]

4.1 Introduction

Spontaneous and non-specific adsorption of proteins on biomaterial surfaces in contact with a physiological fluid is known to adversely affect the performance of biomaterials and biomedical devices [1-5]. Consequences of such adsorption include structural rearrangement of proteins [6] responsible for: exposure of occult epitopes that facilitate protein-substrate binding through multiple contact points, accumulation of inflammatory cells [7-11], adverse host responses (thrombotic and immune), patient infection, and implant failure [7, 12-15]. The stability of a protein's secondary structure may influence its adsorption profile and the extent of surface induced denaturation. The surface induced rearrangement of adsorbed proteins can also ultimately modify the secondary, tertiary, and/or quaternary structure of the protein. A fundamental understanding of the protein-substrate interactions, at the molecular level, is essential for developing biomaterials resistant to the non-specific adsorption of proteins [16, 17]. Previous studies have shown that three classes of parameters play important roles in the interaction of proteins with substrates: protein properties (amino acid sequence [18], modification of the main polypeptide chain with sugar, lipids, and other functional groups, molecular weight [19], and isoelectric point [20, 21]),

[4] This chapter was published in: Understanding the Effect of Secondary Structure on Molecular Interactions of Poly- L-Lysine with Different Substrates by SFA. *Binazadeh, M., A. Faghihnejad, H. Zeng, and L.D. Unsworth*, **Biomacromolecules**. In press.

solution conditions (ionic strength [22], presence of multivalent ions in solution, temperature [23], and pH [24]), and properties of interacting substrate (surface charge density, chemical nature [25], hydrophobicity [26], and roughness [27]).

Various forces, such as hydration, hydrophobic, electrostatic, and van der Waals [28-30] are involved in the protein-substrate interaction. One commonly used approach to reduce the non-specific adsorption of proteins is to coat a non-fouling layer on the substrate surface. It has been previously shown that a grafted poly (ethylene glycol) (PEG) layer on biomaterial surface can greatly reduce the adsorbed amount of proteins *via* creation of a pseudo interface (polymer layer-solution interface) which attenuates interacting forces between the proteins and the unmodified substrate surface [31]. The non-fouling properties of the PEG layer are thought to be conferred by the conformational mobility of surface-grafted long PEG chains in aqueous solution due to flexible ether bonds [32] (i.e. large excluded volume [33]). For shorter PEG chains, it was reported that the repulsive force from the hydration shell around PEG chains hinders protein adsorption [34]. It has been previously reported that these two non-fouling modes of PEG may be unified by the effect of the grafted chain density of the PEG layer [31] suggesting that hydration shells are very important to long PEG chains as well.

Secondary structure is largely determined by hydrogen-bonding interaction between the neighboring amino acids in the protein and can influence the protein's physicochemical properties such as size, shape, hydrophobicity, apparent charge, and function. Previous studies have shown that the peptide

secondary structure determines the short-range steric repulsion between two interacting poly (L-glutamic acid) (PLGA) layers [35-37]. Repulsive forces were reported between two adsorbed PLL layers in random coil structure [38, 39]. Recently, our lab has shown that the secondary structure of poly-L-Lysine (PLL) can significantly affect its adsorption process and the viscoelastic properties of adsorbed PLL films to Au [40]. However, a mechanistic understanding of the surface forces involved in the adsorption event of different secondary structures to the modified surfaces is required for both fundamental and practical purposes [41]. In this work, PLL was chosen as a model peptide, and a surface forces apparatus (SFA) was used to directly measure the forces between PLL of different secondary structures (i.e., α-helices and β-sheets) and various substrates (e.g., Au, mica, grafted PEG) to systematically investigate the influence of secondary structures on peptide-substrate interaction mechanisms. Our results shed new light on the fundamental understanding of the interaction between peptides and proteins with a substrate surface.

4.2 Materials and Experimental Methods

PLL-HCl (MW~ 15-30 kDa), poly(ethylene glycol) methyl ether (MW=750 and 2000), mercaptoacetic acid, toluene, concentrated sulfuric acid, deuterated chloroform (99.9% grade) and isopropyl ether were purchased from Sigma Aldrich (Canada). Quartz slides and Ruby mica sheets were purchased from AdValue Technology (Tucson, AZ) and S & J Trading Inc. (Glen Oaks, NY) respectively. PEG was chain-end thiolated by reaction with mercaptoacetic acid

using concentrated sulfuric acid as catalyst as described in detail elsewhere. [42, 43] The conversion rates of 93% and 91% were obtained for PEG 750 (MW=750) and PEG 2000 (MW=2000) respectively (results not shown) as confirmed by proton nuclear magnetic resonance (^{1}HNMR). 10 mM potassium phosphate solution (PB) with 5, 50, and 500 mM sodium sulfate was used to prepare PLL solutions. The PLL concentration used in all experiments was 0.1 mg/mL prepared by 50 times dilution of the 5 mg/mL PLL stock solution. α-helices were formed by adjusting the pH of PLL solution to 10.6 using 50 mM NaOH solution in the potassium phosphate solution with the appropriate sodium sulphate concentration [44]. β-sheets structure was induced by heating α-helices solution at 70°C for 50 min [40]. It is known that an increase in PEG concentration, solution temperature, and/or ion concentration in an aqueous solution results in gradual breakage of hydrogen bonds between H_2O and PEG and causes a reduction of PEG solubility (*theta* condition) [45, 46]. Chemisorption of PEG was conducted in its *theta* solution condition to obtain a dense PEG layer. In this work 5 mM PEG was added into sodium phosphate buffered saline (PBS) at pH 7.4 with ionic strength of 3.5 M to form a PEG solution at *theta* condition. All experiments were conducted at 37°C.

4.2.1 Circular Dichroism (CD)

It is known that PLL maintains a random coil structure in aqueous solutions at neutral pH and other secondary structures (α-helices and β-sheets) can be induced via manipulation of solution pH and temperature [47]. In this work CD was used to track the induction and persistence of desired PLL secondary structures in

solution and in the adsorbed wet state. Herein, 5 mg/mL PLL stock solution was prepared using 10 mM PB with 5, 50, and 500 mM sodium sulfate, with no pH adjustment. α-helices were formed using previously described methods [44], where the stock solution was diluted (50x) and the pH was increased to 10.6. It is known that heating PLL solution transforms α-helices to β-sheets [47]. In this work the α-helices solution was heated at 70°C for 50 min to induce β-sheets structure of PLL. It is known that α-helix and β-sheet PLL structures are stable for at least 8 hrs under the experimental conditions investigated [40] which is longer than the time required for the different measurements (i.e., CD and SFA) in this study. To eliminate any influence of dissolved gases, prior to CD measurements all solutions and samples were degassed for 20 mins under vacuum (10 mm Hg) using a Fisher Scientific vacuum pump with liquid nitrogen trap. Measurement of PLL secondary structure in bulk solution was done using a quartz cuvette (0.2 cm pathlength, International Crystal Lab). The CD equipment was a Jasco-J810 equipped with a Julabo AWC100 water bath for temperature control. A background spectrum was first collected for each sample using 10 mM PB with appropriate sodium sulfate concentration (without PLL) at pH 10.6. CD measurement of each sample was performed at least three times from 185 to 260 nm and all reported CD spectra are the average of three measurements.

Due to the anisotropic optical properties of mica, it is impossible to track the secondary structure of adsorbed PLL on mica using CD. Thus quartz slides, which have a similar chemical composition as mica basal plane, similar surface hydrophilicity (water contact angle <10° for mica [48], and ~10° for quartz [49]),

and vacuum Hamaker constant (8.5×10^{-20} and 6.5×10^{-20} J for mica and quartz respectively [50]) were used to study the secondary structure of PLL in the wet adsorbed state. CD spectra of adsorbed PLL on quartz were obtained using a detachable quartz cuvette with 0.1 mm pathlength. Background spectra for all systems were first recorded using 10 mM PB with 5, 50, and 500 mM sodium sulfate concentration (without PLL) at pH 10.6 and 37°C. PLL was then adsorbed to quartz slides *via* immersion of slides in a well stirred PLL solution of pre-known secondary structure. The adsorption process was allowed to continue for 1 hr to ensure sufficient PLL adsorption for CD measurements. Prior to the CD measurement, quartz slides were rinsed with the PB solution to remove the loosely bounded PLL. Care was taken so that adsorbed PLL layer remains hydrated to avoid drying induced conformation changes [51]. After measuring the CD spectrum of adsorbed hydrated PLL in 10 mM PB with 5 mM sodium sulfate concentration at pH 10.6, the solution was replaced with 10 mM PB with 50 and 500 mM sodium sulfate concentration respectively (without PLL) at the same pH and the CD measurements were repeated at least three times for each condition.

4.2.2 Atomic Force Microscopy (AFM) Imaging

AFM (NanoWizard II, JPK Instruments, Germany) imaging was performed to obtain the surface morphology and roughness of the different substrates used in this study. The adsorption of PLL (α-helix and β-sheet) and chemisorption of PEG (750 and 2000) were allowed to proceed for 1 hr. The substrates were then rinsed with MilliQ water and dried under vacuum overnight. Samples were

imaged using a silicon tip (Olympus AC240TS, Al reflex coated, tip radius 9±2 nm, resonant frequency 70 kHz) in the tapping mode in air. At least three samples and three different positions on each sample were imaged to characterize each type of substrate surface.

4.2.3 Surface Force Measurement in Aqueous Solution Using SFA

The interactions among PLL, PEG and different substrates were measured in various configurations by SFA, as shown in Figure 4.1c-4.1f. In a typical SFA experiment, freshly cleaved mica sheets (1-5 μm thickness) were used as main supporting substrate [52]. In order to prepare gold substrate, first, a precursor layer of chromium (~5 nm) was deposited on mica and then gold (40-45 nm) was deposited at a deposition rate of 0.2 Å/s using a Gomez electron beam evaporator. Two mica sheets were then glued on cylindrical glass disks with radius of $R=2$ cm. The multiple beam interferometry (MBI) technique was used to monitor the separation between the two interacting surfaces in different configurations as shown in Figure 4.1c-4.1f by using fringes of equal chromatic order (FECO) [52, 53]. The interaction force $F(D)$ between two curved surfaces in a crossed-cylinder configuration can be correlated to the interaction energy per unit area $W(D)$ between two parallel plates based on the Derjaguin approximation, $F(D)=2\pi RW(D)$, when $D \ll R$ and the range of interaction between the surfaces be much smaller than R [29, 54]. For deformable soft surfaces which show adhesion during separation, the pull-off or adhesion force, F_{ad}, is related to the adhesion energy per unit area by $F_{ad}=1.5\pi RW_{ad}$. [29] For SFA mesurements, at least

2 pairs of surfaces were prepared and studied for each condition, and at least 3 different positions were tested on each pair of surfaces.

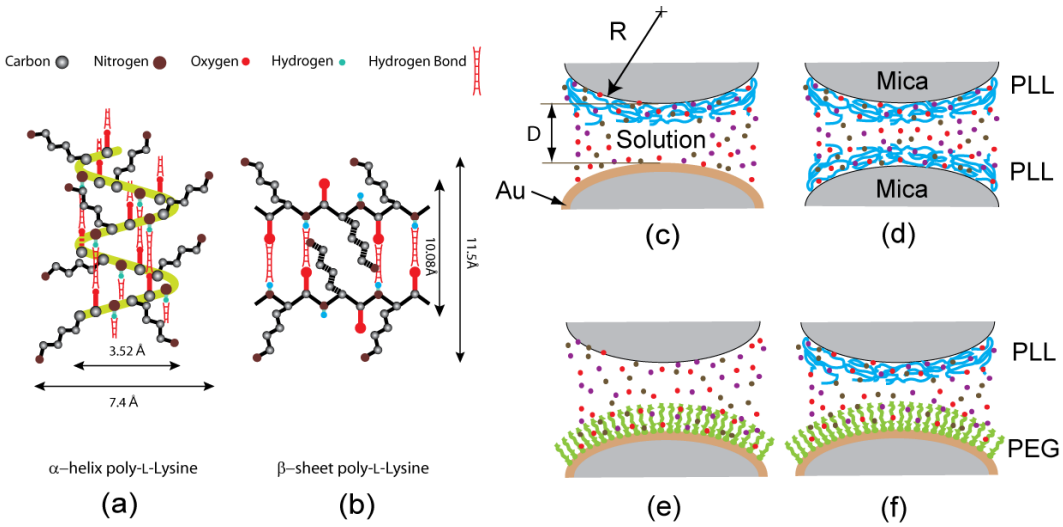

Figure 4.1 Illustration of PLL secondary structures: **a.** α-helix PLL [55], **b.** β-sheet PLL [56]. Schematic of various surface interaction configurations for surface force measurements using SFA: **c.** PLL layer coated on mica vs. Au, **d.** two PLL layers coated on mica surfaces, **e.** PEG layer chemisorbed on Au vs. mica, and **f.** PLL layer coated on mica vs. PEG layer chemisorbed on Au. Colourful dots in **c-f** represent different ions in the PB solution.

Four different configurations were used in this study to measure the interactions between PLL vs. Au, PLL vs. PLL, PEG vs. mica, and PLL vs. PEG, as show in Figure 4.1c-4.1f respectively. For the PLL adsorption and PEG chemisorption, the appropriate solution (0.1 mg/mL PLL in 10 mM PB with 5 mM sodium sulfate at pH 10.6 or 5 mM PEG in sodium phosphate buffered saline (PBS) at pH 7.4 with ionic strength of 3.5 M) was first dropped on mica and Au surface respectively and the surfaces were then kept in a sealed chamber at 100% relative humidity and 37°C for 1 hr to ensure sufficient adsorption of PLL or PEG. The surfaces were then rinsed with the PB solution (void of PLL) to remove

unbounded PLL or PEG and mounted into the SFA chamber with proper solution. During the measurements, the surfaces were driven to approach and separate at a constant rate of ~4 nm/s. The surfaces were kept in contact for 1 min under the maximum load (F/R ~ 10 mN/m) before separation. To study the salt concentration effect on the surface forces the solution between surfaces was replaced with PB solution with different sodium sulphate concentrations (5 mM to 50 and 500 mM).

4.3 Results and Discussions

4.3.1 Circular dichroism (CD)

Through increasing the solution pH from ~7 to 10.6 (37ºC) a complete transformation of PLL from the random coil to α-helix state was achieved [44]. This PLL α-helix solution was then heated to 70°C for 50 min in order to transform the α-helix PLL into a β-sheet conformation [47], which was retained upon cooling the solution to 37ºC. The change in PLL secondary structure was confirmed using CD, where α-helix structures exhibit a characteristic maximum peak at ~190 nm and two minimum peaks at ~205 and ~222 nm, and β-sheet structures exhibit a characteristic maximum and minimum peak at ~195 and ~215 nm, respectively [57, 58].

Figure 4.2 shows the CD spectra (molar ellipticity vs. wavelength [59]) of PLL in bulk solution, containing 5 mM Na_2SO_4, and hydrated adsorbed PLL in solutions containing different sodium sulfate concentrations (5, 50, and 500 mM). It was found that α-helix (Figure 4.2a) and β-sheet (Figure 4.2b) secondary

structures were maintained in the bulk solution, as well as, the hydrated adsorbed state regardless of the sodium sulfate concentration of the solution (Table 4.1). As shown in Figure 4.2, no considerable changes in peak position were observed, indicating that (1) the respective secondary structures were induced successfully through controlling solution conditions and (2) the different secondary structures of PLL persist upon adsorption on quartz and subsequent solution change. Previous studies have reported that a 3 nm shift in CD spectra peak position does not imply an overall difference in secondary structure [57, 59] thus the minor peak position shifts reported in Table 4.1 does not imply an overall change in the secondary structure. The spectra deconvolution based on a method reported by Whitmore et al [60] suggested that there would be at least 75% α-helix content in Figure 4.2a. Furthermore it was shown that ~94% of PLL chains could be formed in α-helix conformation at pH 10.6 [61]. As the basal plane of mica is chemically similar to quartz in aqueous solutions (i.e., mainly Si-O-Si structure), the secondary structures of PLL adsorbed on mica should also be maintained in the same solution conditions.

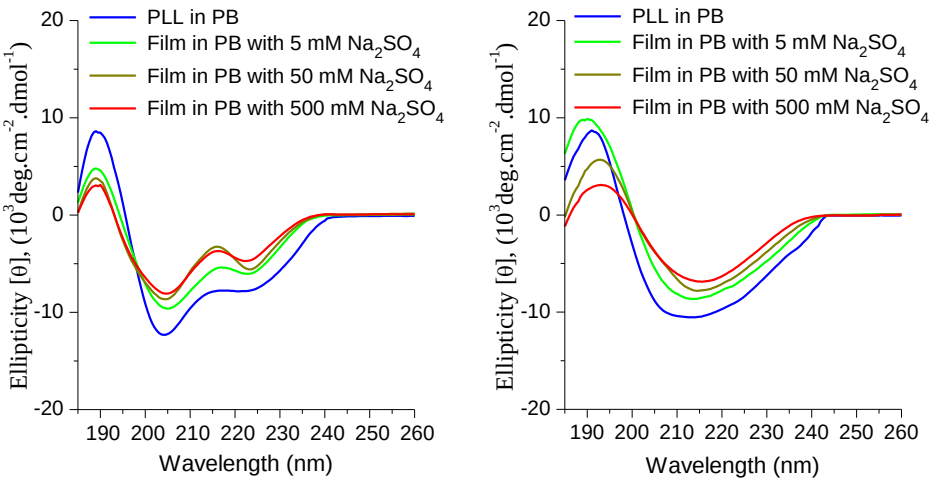

Figure 4.2 CD spectra of PLL in **a.** α-helix and **b.** β-sheet conformation in solution (10 mM potassium phosphate solution with 5 mM Na_2SO_4 at pH 10.6, T=37ºC) and adsorbed on quartz slides and hydrated with 10 mM potassium phosphate solution with 5, 50, and 500 mM Na_2SO_4 concentrations at pH 10.6, T=37ºC. Data represent the average of n=3 measurements.

Table 4.1 Position and intensity of peaks in the CD spectra of different secondary structures of PLL in bulk solution and adsorbed state. Data from 0.1 mg/mL PLL in 10 mM PB with 5mM Na_2SO_4 (bulk solution) and adsorbed PLL on quartz hydrated *via* 10 mM PB with 5, 50, and 500 mM Na_2SO_4 at pH 10.6 and 37ºC. Data represent the average of n=3 measurements.

Conformation		Peak 1 position [nm]	Intensity 10^3 [θ]	Peak 2 position [nm)]	Intensity 10^3 [θ]	Peak 3 position [nm)]	Intensity 10^3 [θ]
α-helix	solution	190.0	8.5	203.5	-13.2	223.0	-8.0
	quartz- 5	190.0	4.6	205.0	-9.6	223.0	-6.0
	quartz- 50	190.0	3.8	204.5	-8.7	223.5	-5.6
	quartz- 500	190.0	3.2	204.5	-8.1	222.5	-4.8
β-sheet	solution	192.0	9.0	214.0	-10.6	-	-
	quartz- 5	190.0	10.1	214.0	-8.7	-	-
	quartz- 50	192.5	5.7	213.5	-7.8	-	-
	quartz- 500	192.0	3.1	215.5	-6.9	-	-

4.3.2 AFM Measurements

AFM imaging was conducted to provide information about the surface structure and roughness of the different substrates and coatings used in this study. As shown in Figure 4.3a, mica has a root mean square (rms) roughness of 0.3±0.1 nm. The AFM imaging of PLL and PEG coatings was conducted in the dry state. From Figure 4.3e and 4.3f it could be seen that α-helix PLL spread over the mica surface while β-sheet PLL tends to form nanofibers. It should be noted that adsorbed PLL layers were washed with MilliQ water to remove the salts that might otherwise form crystals on the substrate surface and interfere with the AFM measurements. Both washing and drying of the PLL coated mica surfaces might change the adsorbed PLL surface coverage and morphology. The different film patterns observed from AFM imaging of dry α-helix and β-sheet PLL films implies that the secondary structures of PLL play a role in their adsorption to substrates. Deposition of Au on mica by electron beam evaporator formed a smooth surface with an rms of 0.5±0.1 nm (Figure 4.3b). It was found that chemisorption of PEG 750 and 2000 did not significantly increase the substrate surface roughness, with respective rms values of 0.7±0.1 and 0.8±0.1 nm (Figure 4.3c and 4.3d).

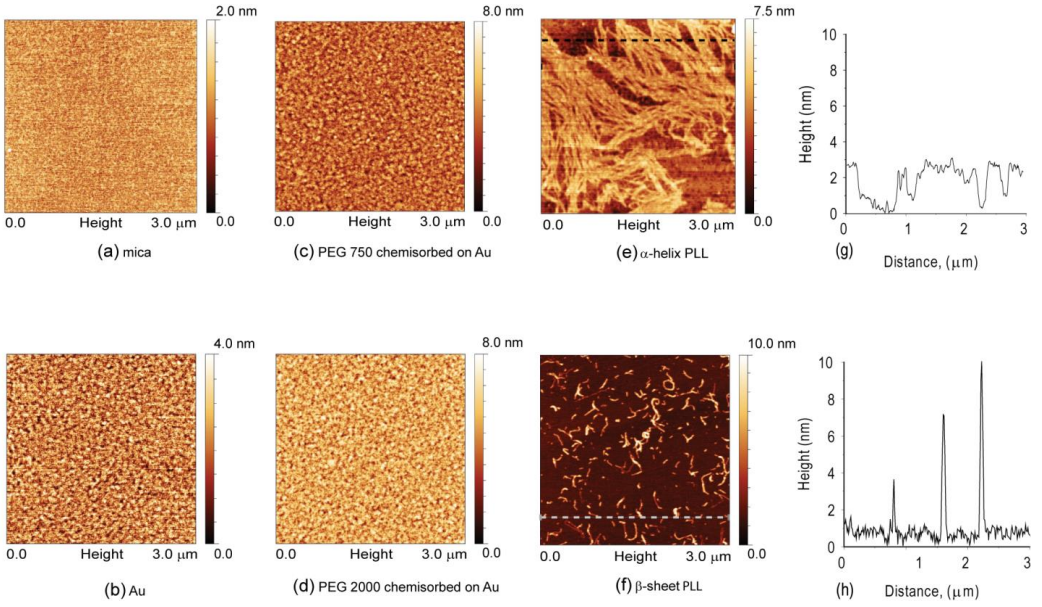

Figure 4.3 Representative topographical AFM images (height) of **a.** mica surface (rms=0.3±0.1 nm), **b.** Au surface (rms=0.5±0.1 nm), **c.** PEG 750 chemisorbed on Au (rms=0.7±0.1 nm), **d.** PEG 2000 chemisorbed on Au (rms=0.8±0.1 nm), **e.** α-helix PLL adsorbed on mica (rms=1.1±0.1 nm), **f.** β-sheet PLL adsorbed on mica (rms=1.3±0.1 nm), **g**. height profile of α-PLL, and **h**. height profile of β-sheet PLL. PEG and PLL solutions were incubated on mica and Au respectively for 1 hr. The absorbed surfaces were then washed with copious amounts of Milli-Q water and dried under vacuum overnight before imaging.

4.3.3 Surface Force Measurement

4.3.3.1 PLL-Au Interaction

To understand the effect of secondary structure on protein-substrate interaction, the interaction between the adsorbed α-helix or β-sheet PLL (on mica) and opposing Au surface were studied at different solution ionic strengths (Figure 4.4). The confined thickness (layer thickness confined between two substrates at the maximum load applied F/R = 10 mN/m) of α-helix PLL layer was 2.6±0.3 nm in solution containing 5 mM Na_2SO_4 and did not show a significant change upon increasing the salt concentration. In contrast, the confined thickness of β-sheet

PLL layer was 6.6±0.3 nm in solution containing 5 mM Na_2SO_4 and decreased to 5.7±0.3 and 4.8±0.3 nm by increasing the Na_2SO_4 concentration to 50 and 500 mM, respectively. Relatively more compressed conformation for the β-sheet PLL at higher ionic strength could be due to the reduction of the intramolecular and intermolecular (electrostatic) repulsion at higher salt concentrations, and may be greater than the α-helix PLL due to having a greater adsorbed amount, as previously reported [40]. It should be noted that van der Waals interactions between PLL and Au also play a role in the PLL adsorption [40]. Weak adhesion for the α-helix PLL vs. Au (F_{ad}/R ~-0.3±0.1, -0.2±0.1, and -0.1±0.1 mN/m or W_{ad} ~-57.3.9±6.4, -40.9±4.4, and -35.1±6.5 μJ/m^2 in solution containing 5, 50, and 500 mM Na_2SO_4 respectively) was measured as compared with the adhesion of β-sheet PLL vs. Au (F_{ad}/R ~-1.2±0.1, -0.7±0.1, and -0.3±0.1 mN/m or W_{ad} ~ -245.6±21.3, -143.3±10.4, and -48.1±7.5 μJ/m^2 in solution containing 5, 50, and 500 mM Na_2SO_4 respectively). Figure 4.6a summarizes the adhesion energy of α-helix and β-sheet PLL to Au as a function of Na_2SO_4 concentration. Such difference in the adhesion could be due to several main interactions. Firstly, the electrostatic interaction between Au and α-helix PLL may be less than that for Au and β-sheet PLL. The isoelectric point (IEP) of PLL in this study (with an average MW of PLL 22.5 kDa) is estimated to be ~12.2 and the PLL chain carries an average of 33.7 positive charges at pH 10.6 [62]. The zeta potential value for Au at pH 10.6 is -49.4 mV [63] and α-helix PLL zeta potential values are 4.6±0.4, 3.5±0.1, and 1.8±0.4 mV in solution containing 5, 50, and 500 mM Na_2SO_4 at pH 10.6 respectively [40], which suggests an electrostatic attraction contributing to

the adhesion between Au and α-helix PLL. The comparatively higher zeta potential values of β-sheet PLL (12.6±0.4, 7.4±0.1, and 5.6±0.4 mV in solution containing 5, 50, and 500 mM Na_2SO_4 at pH 10.6 respectively [40]) results in stronger electrostatic interaction with Au and contributes to the stronger adhesion between Au and β-sheet PLL. Moreover, secondary structure specific arrangement of lysine side chains in the β-sheet conformation may allow for increased interactions. As shown in Figure 4.1a and 4.1b, α-helix and β-sheet conformations represent a respective cylinder and plane geometry. It could be concluded that only a fraction of lysine side chains in α-helix PLL are available [64] to interact with the Au surface which results in a weak adhesion (Figure 4.4a, 4.4c, and 4.4e). It should also be noted that the flat surface geometry of β-sheet provides a large number of lysine side chains, which can constructively align on the Au surface and result in a stronger adhesion on Au surface.

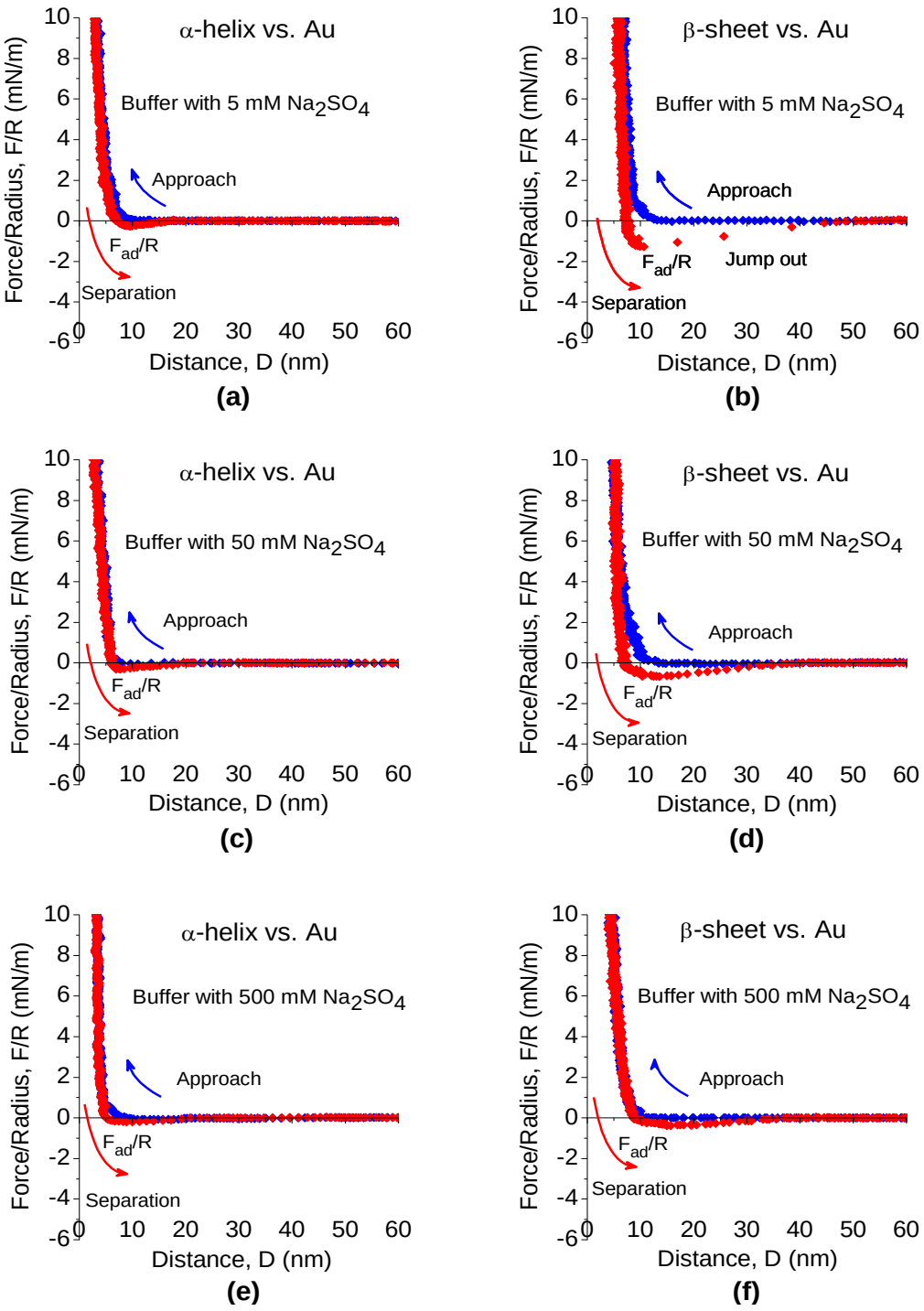

Figure 4.4 Representative force-distance profiles for the approach and separation of a layer of α-helix or β-sheet PLL interacting with a Au surface (corresponding to the schematic drawing in Figure 4.1c) in 10 mM potassium phosphate solution with 5, 50, and 500 mM Na_2SO_4 at pH 10.6, T=37ºC.

4.3.3.2 PLL-PLL Interaction

Figure 4.5 shows the force-distance profiles of interacting PLL layers with the same secondary structure at different salt concentrations. The confined thickness of α-helix PLL layer was 6.0±0.4 nm at 5 mM Na_2SO_4 concentration and did not show significant change upon increasing salt concentration. In contrast the confined thickness of β-sheet PLL layer decreased from 15.3±0.4 to 13.3±0.4 and 11.1±0.5 nm upon increasing salt concentration from 5 to 50 and 500 mM, respectively. For β-sheet PLL layers an increase in the salt concentration resulted in a decrease in the initial repulsion distance during approach, which could be due to the compression of the electrostatic repulsion between PLL molecules and a decreased range of repulsion with increasing ionic strength [38, 39]. It should be noted that some adsorbed PLL molecules might form aggregates on the substrate which could play a role in the interaction forces measured. Figure 4.6b shows the adhesion energy between two PLL layers during separation. Higher adhesion energy of β-sheet PLL as compared with α-helix PLL layers may be attributed to the previously mentioned constructive alignment of lysine side chains in the β-sheet conformation, where a larger number of lysine side chains from opposing PLL layers can interact in the β-sheet configuration and contribute to the formation of hydrogen bonding as well as interdigitation and interpenetration of these opposing chains. The salt influence on peptide-peptide interactions is normally classified into non-specific and specific interactions. Nonspecific ion-peptide interactions are independent of the ion type and occur mainly due to ionic strength [65] resulting in charge shielding [66]. Specific ion-peptide interactions, also known as Hofmeister effect [67], depend on the type of ions and ionic

strength [68]. It could be seen from the Figure 4.6b that adhesion energy depends on sodium sulfate concentration. The reduction of the adhesion energy at higher ionic strength is most likely due to reduced hydrogen bonding ability of the opposing $–NH_2$ groups of the lysine side chains (viz., non-specific ion-peptide interaction).

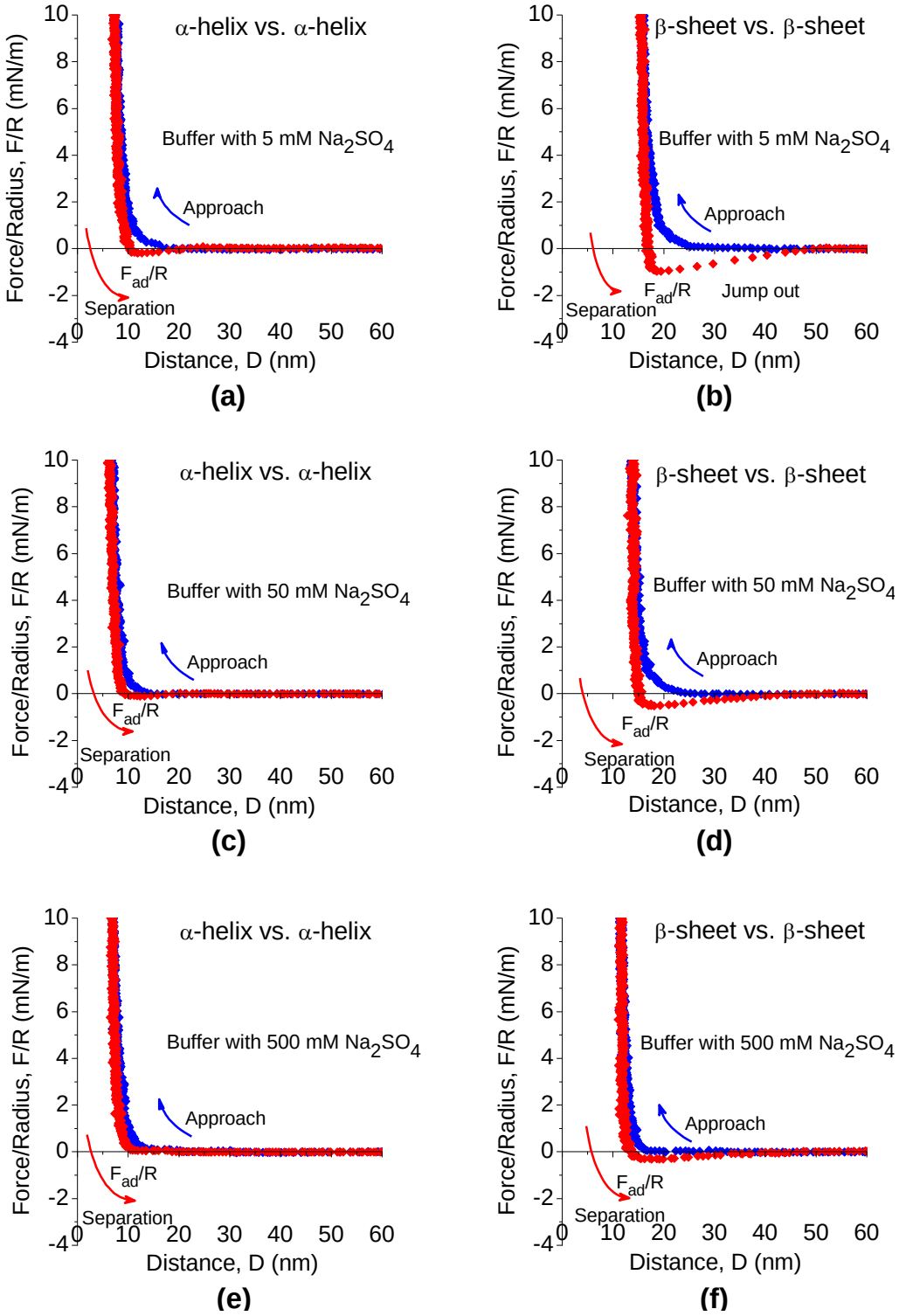

Figure 4.5 Force-distance profiles between two α-helix or β-sheet PLL layers (corresponding to the schematic drawing in Figure 4.1d) in 10 mM potassium phosphate solution with 5, 50, and 500 mM Na_2SO_4 at pH 10.6, T=37ºC.

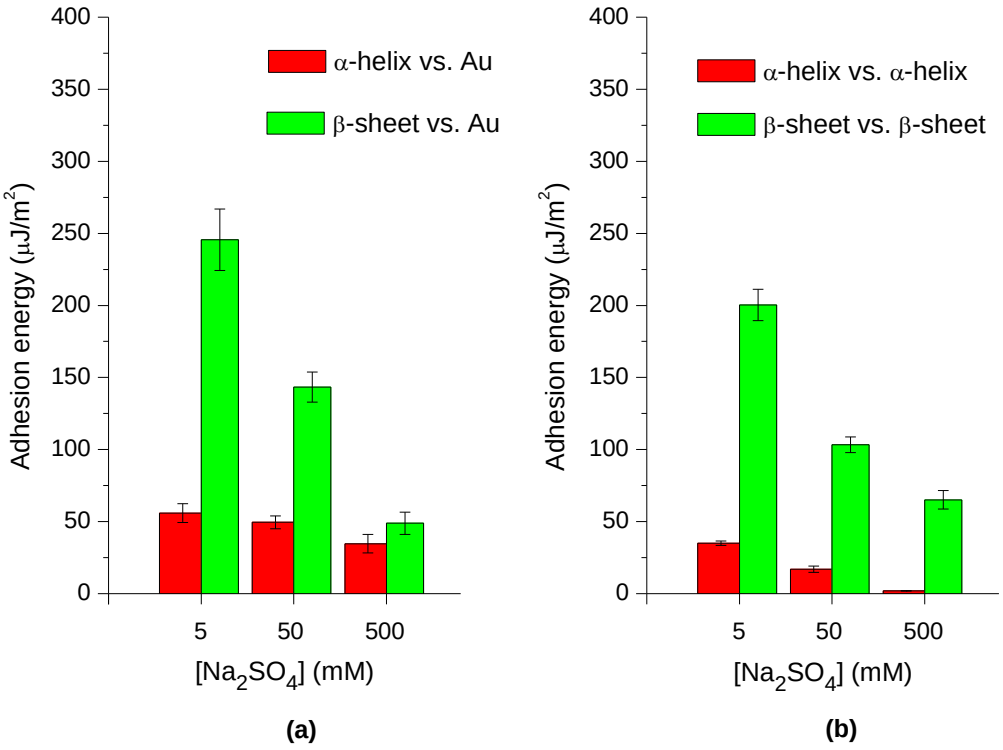

Figure 4.6 Adhesion energy between a. PLL of two different conformations and Au and b. two PLL surfaces in 10 mM potassium phosphate solution containing different concentrations of Na_2SO_4. Data are mean value ± standard deviation of 6 measurements.

The interaction between PLL and Au or two PLL layers of the same secondary structure during the approach process were analysed using the Alexander-de Gennes (AdG) scaling theory of steric interaction [69], electrical double layer interaction and van der Waals forces based on classical Derjaguin-Landau-Verwey-Overbeek (DLVO) theory [29]. Upon adsorption, PLL chains could distribute on the substrate and may locally form tails which could act like polymer brushes [38, 39]. The interactions between two brush bearing surfaces (symmetric configuration) and a brush and a substrate (asymmetric configuration) can be described by Equation 4.1 and Equation 4.2, respectively [70].

$$\frac{F(D)}{R} = \frac{16\pi kTL}{35s^3}\left[7(\frac{2L}{D})^{5/4} + 5(\frac{D}{2L})^{7/4} - 12\right] \qquad (4.1)$$

$$\frac{F(D)}{R} = \frac{8\pi kTL}{35s^3}\left[7(\frac{L}{D})^{5/4} + 5(\frac{D}{L})^{7/4} - 12\right] \qquad (4.2)$$

where k=1.381x10^{-23}m^2.kg.s^{-2}.K^{-1}, is Boltzmann constant, T is temperature, L is the PLL layer thickness, s is the average distance between PLL "grafting" or bonding sites, and D is the distance between the two curved surfaces. The fitted results for the steric interaction for PLL vs. PLL and PLL vs. Au are shown in Figures 4.7 and 4.8 respectively and the corresponding fitting parameters are summarized in Table 4.2. The repulsive force observed during the approach of two surfaces fits well using the AdG theory, suggesting that PLL chains are swollen and extended into the bulk solution and the repulsion is mainly due to the steric interaction between the swollen chains. The α-helix PLL layer thickness, L, varied between 6.5±0.3 and 7.3±0.3 nm (Figure 4.7 and Table 4.2), while the β-sheet PLL (Figure 4.8 and Table 4.2) layer thickness varied between 9.5±0.4 and 12.6±0.4 nm. Such differences in the PLL layer thicknesses may indicate that the secondary structure affects the adsorption behavior and adsorbed layer properties of peptides. The average distance between PLL grafting sites, s, was almost independent of the secondary structure of PLL.

The electrostatic double-layer and van der Waals forces between two crossed cylinders of radius R (configuration in SFA measurements) are given by Equations 4.3 and 4.4, respectively [29]. κ (inverse of Debye length) is given by Equation 4.5 [29]. It should be noted that Equation 4.3 was derived for the case of

symmetrical (e.g., 1:1 or 2:2) electrolytes. However, this theory still provides a good approximation for the mixed electrolytes used in this study [71]. For the asymmetric case of PLL (surface 1) and Au (surface 3) across aqueous solution (medium 2) the geometry independent constant (Z) and Hamaker constant (A_{123}) are given by Equations 4.6 and 4.7, respectively [72, 73]. For the symmetric case of two PLL surfaces (surface 1) across aqueous solution (medium 2), Z and A_{121} are given by Equations 4.8 and 4.9 respectively [29, 73].

$$\left.\frac{F(D)}{R}\right|_{EDL} = \kappa Z e^{-\kappa D} \qquad (4.3)$$

$$\left.\frac{F(D)}{R}\right|_{vdw} = -\frac{6A}{D^2} \qquad (4.4)$$

$$\kappa = \sqrt{\left(\sum \frac{\rho_j e^2 z_j^2}{\varepsilon_0 \varepsilon_2 kT}\right)} \qquad (4.5)$$

$$Z_{123} = 64\pi\varepsilon_0\varepsilon_2\left(\frac{kT}{ze}\right)^2 \tanh\left(\frac{ez\psi_3}{4kT}\right)\tanh\left(\frac{ez\psi_1}{4kT}\right) \qquad (4.6)$$

$$A_{123} \approx \frac{3h}{8\sqrt{2}} \frac{(n_1^2 - n_2^2)v_1 v_3}{\left(n_1^2 + n_2^2\right)^{1/2}\left(v_1 + \left(n_1^2 + n_2^2\right)^{1/2} v_3\right)} \approx \frac{3hv_e}{8\sqrt{2}} \frac{\left(n_1^2 - n_2^2\right)}{\left(n_1^2 + n_2^2\right)^{1/2}\left(1 + \left(n_1^2 + n_2^2\right)^{1/2}\right)} \qquad (4.7)$$

$$Z_{121} = 64\pi\varepsilon_0\varepsilon_2\left(\frac{kT}{ze}\right)^2 \tanh^2\left(\frac{ez\psi_1}{4kT}\right) \qquad (4.8)$$

$$A_{121} \approx \frac{3}{8\sqrt{2}} \frac{(n_1^2 - n_2^2)^2}{\left(n_1^2 + n_2^2\right)^{3/2}} \frac{hv_1 v_2}{(v_1 + v_2)} \approx \frac{3hv_e}{16\sqrt{2}} \frac{\left(n_1^2 - n_2^2\right)^2}{\left(n_1^2 + n_2^2\right)^{3/2}} \qquad (4.9)$$

In the above equations: ρ_j is number density of ion species j (ρ_j=6.022x10^{26} M_j, where M_j is the molarity of species j); e=1.602x10^{-19} C, is electron charge; z is electrolyte ion valence; ε_0=8.85x10^{-12} F.m^{-1} is vacuum permittivity; ε_2= 74.8 at 37°C, is relative permittivity of medium, water; k=1.381x10^{-23}m^2.kg.s^{-2}.K^{-1} is Boltzmann constant; ψ is surface potential; h=6.626x10^{-34} J.s, is Planck constant; υ is the main electronic absorption frequency in the UV (υ_e=3x10^{15} s^{-1}); and n is refractive index (n_1=1.48 for PLL [74] and n_2=1.33 for water). The Hamaker constants A_{123} and A_{121} were calculated as 3.3x10^{-20} and 0.6x10^{-20} J, respectively. The zeta potential value for α-helix PLL layer at pH 10.6 is 4.6±0.4, 3.5±0.1, and 1.8±0.4 mV in PB solutions containing 5, 50, and 500 mM sodium sulfate, respectively. For β-sheet PLL the zeta potential value is 12.6±0.4, 7.4±0.1, and 5.6±0.5 mV in PB solutions containing 5, 50, and 500 mM sodium sulfate, respectively [40]. Zeta potential value for Au at pH 10.6 is -49.4 mV [63]. The DLVO prediction is also shown in Figures 4.7 and 4.8, which show that DLVO forces play a role only at very close separation distances. It is noted that the surface potential of PLL adsorbed on mica was assumed to be the same as its zeta potential in bulk solution [75-77] and the actual PLL surface potential could be slightly different due to the impact of mica substrate. However the effect of such difference on the PLL surface interactions can be negligible due to the small Debye length (≤ 1.5 nm) of electric double layer and the dominant role of steric interaction.

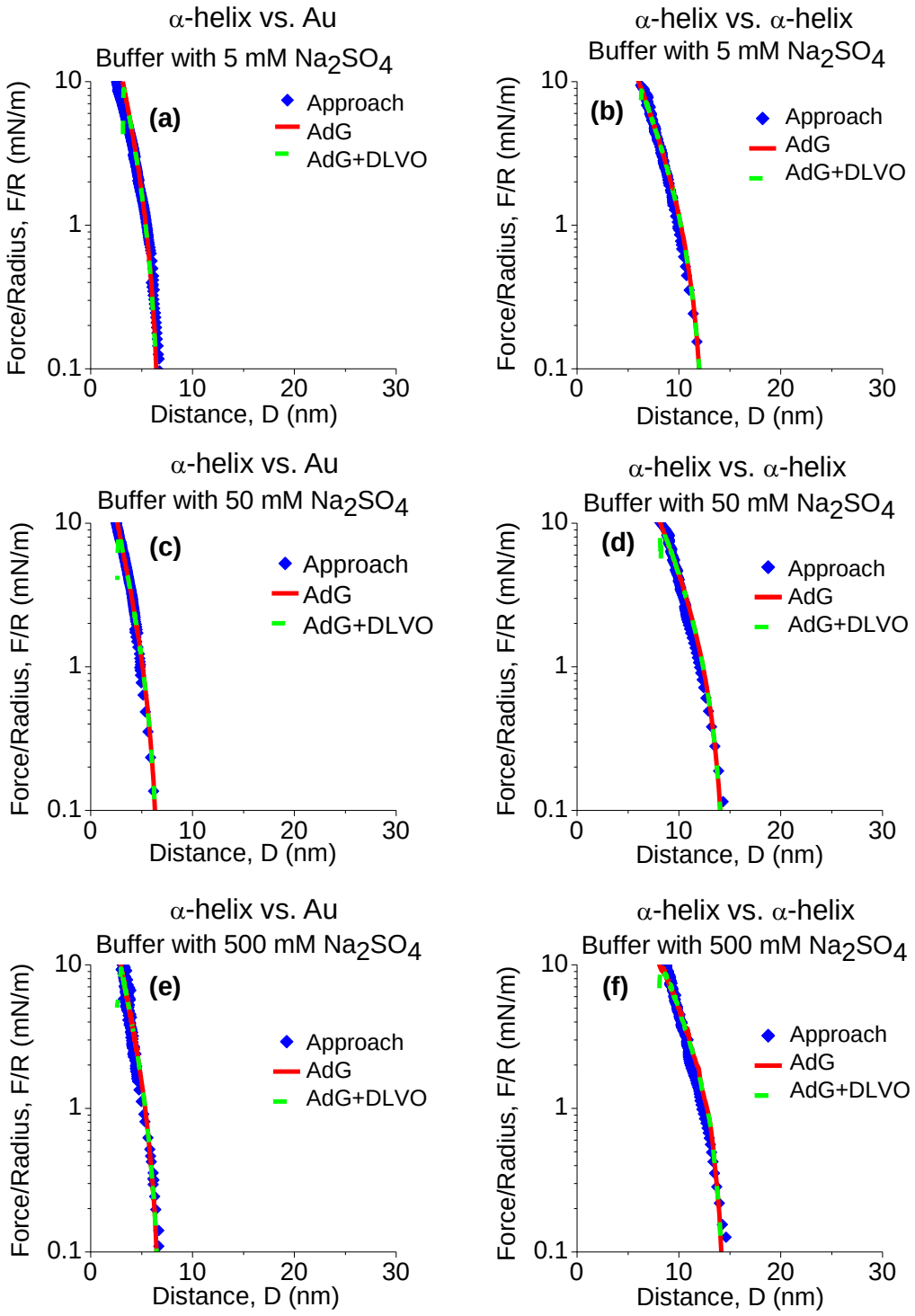

Figure 4.7 Theoretical force vs. distance curves incorporating steric repulsion and DLVO interactions and comparison with the experimental approaching force-distance profile for interaction of an α-helix PLL surface with Au (**a**, **c**, **e**) or another α-helix PLL surface (**b**, **d**, **f**) in 10 mM potassium phosphate solution with different concentrations of Na_2SO_4 at pH 10.6, T=37ºC. The surface potentials used for DLVO were -49 mV for Au and 4.6, 3.5, and 1.8 mV for α-helix PLL surface in solutions containing 5, 50, and 500 mM Na_2SO_4 respectively.

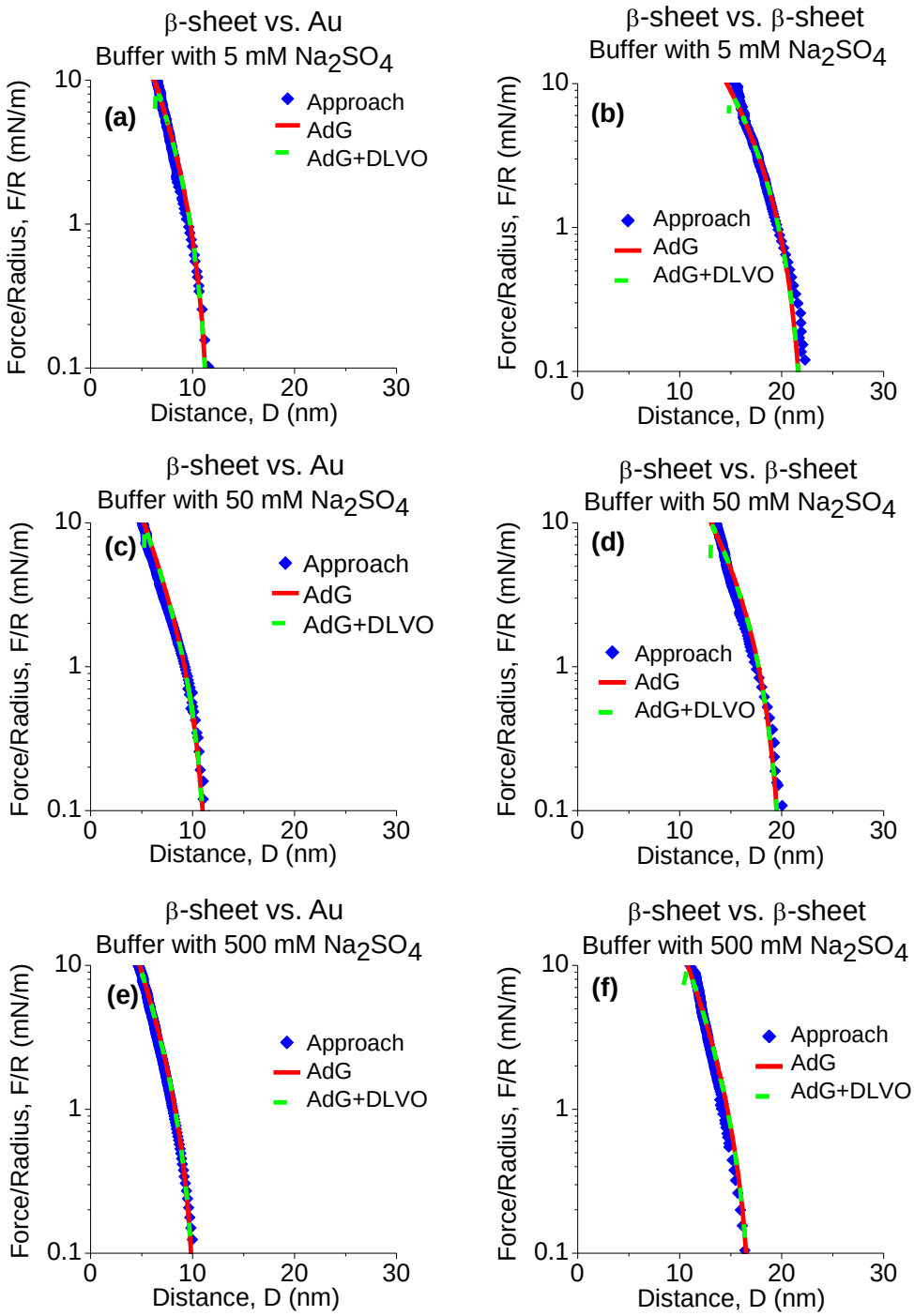

Figure 4.8 Theoretical force vs distance curves incorporating steric repulsion and DLVO interactions and comparison with the experimental approaching force vs distance profile for interaction of an β-sheet PLL surface and Au surface (a, c, e) or with another β-sheet PLL surface (b, d, f) in 10 mM potassium phosphate solution with 5, 50, and 500 mM Na_2SO_4 at pH 10.6, T=37ºC. The surface potentials used for DLVO were -49 mV for Au and 12.6, 7.4, and 5.6 mV for β-sheet PLL surface in PB solutions containing 5, 50, and 500 mM Na_2SO_4 respectively.

It should be also noted that although adsorbed PLL molecules could form tails locally [38, 39] the adsorbed α-helix and β-sheet PLL layers may not form uniform brush layer on mica. Meanwhile some adsorbed PLL molecules could form aggregates locally on the substrate contributing to the measured forces and change of confined PLL thickness. The force hysteresis upon loading/unloading in the SFA measurements (see Figures 4.4 and 4.5) suggests an attractive component of the interaction between or within PLL layers. An improved model will be needed to describe the complete interaction mechanism (i.e., combining steric effects, DLVO forces, structure changes of polymer chains due to inter and intra molecular forces under complex solution conditions, and time/rate dependent effects). Nevertheless, the above experiment results and analysis indicate that the repulsive forces measured during approach are mainly due to steric effects of the PLL layers.

4.3.3.3 PEG-mica Interaction

Force-distance profiles between a chemisorbed PEG layer (PEG 750 or PEG 2000) and a mica surface are shown in Figure 4.9. Both PEG 750 and 2000 layers show a purely repulsive force. No obvious force hysteresis was observed during the force measurements. The confined polymer thickness was 2.9±0.3 and 3.7±0.4 nm for chemisorbed PEG 750 and 2000 layers, respectively (Figure 4.9 and Table 4.2). These data (Figure 4.9) may be indicative of PEG brushes forming an elastic, hydrated, non-adhesive, and compressible layer that is due to the

underlying non-fouling properties of PEG coatings: excluded volume mechanism [33].

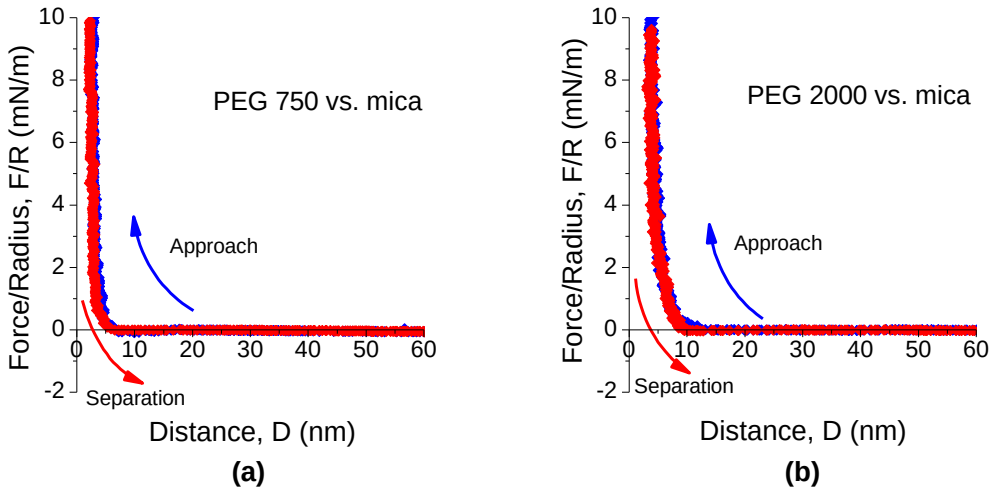

Figure 4.9 Force-distance profiles measured during the approach and separation of chemisorbed PEG layers on Au surface and a bare mica surface (corresponding to the schematic drawing in Figure 4.1e) in 10 mM potassium phosphate solution with 5 mM Na_2SO_4 at pH 10.6, T=37ºC.

Previous SFA studies of PEG systems have reported that repulsion between PEG modified surfaces has a steric origin [70, 78]. Alexander-de Gennes scaling theory (Equation 4.2) were used to further understand the nature of the repulsion between the chemisorbed PEG brushes and mica surface (asymmetric configuration). Figure 4.10 shows the measured repulsive force during approach of chemisorbed PEG 750 and 2000 surfaces and mica surface as well as the fitted curves using the AdG theory (Equation 2). The AdG theory could well describe the force-distance profile between PEG brushes and mica surface suggesting the steric nature of the observed repulsion. Flory radius, R_F, of PEG chains can be calculated using $R_F=aN^{\upsilon}$ where a is the monomer length (0.*35* nm for ethylene

glycol) [79], N is number of repeating units in a polymer chain, and υ is 0.6 for a good solvent [80]. R_F value for PEG 750 and 2000 were calculated as 1.9 and 3.4 nm, respectively. Chemisorbed PEG layer grafting regime could be obtained by comparing R_F and mean grafting distance between two PEG chains, s, where $s>>2R_F$ suggests the dilute non-overlapping mushroom regime, $s\sim2R_F$ the semidilute overlapping mushrooms, $s<2R_F$ the dilute brush regime, and $s<<2R_F$ the dense brush regime [81]. From the s values (2.3±0.2 and 4.3±0.2 nm for PEG 750 and 2000 respectively) obtained by fitting PEG force profile using AdG theory (Table 4.2) it was confirmed that the chemisorbed PEG 750 and 2000 layers formed dense brush regimes.

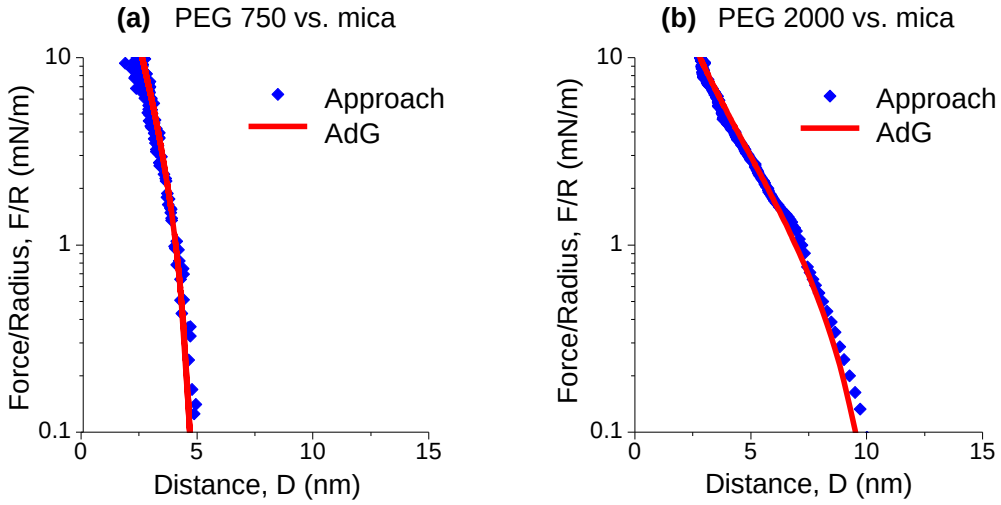

Figure 4.10 Force-distance profiles fitted using the AdG theory for interaction between chemisorbed PEG layers on Au and a bare mica surface in 10 mM potassium phosphate solution with 5 mM Na_2SO_4 at pH 10.6, T=37ºC.

4.3.3.4 PEG-PLL Interaction

The interaction profiles for α-helix and β-sheet PLL layers with PEG 750 and 2000 layers in PB solution (5 mM sodium sulphate) are summarized in Figure 4.11. It could be seen from Figure 4.11 that no hysteresis was observed during approach and separation of the PEG and PLL surfaces and that the adhesion observed during the separation of α-helix and β-sheet PLL from the Au surface was eliminated. This may be due to the hydrophilic nature of PEG chains in aqueous solutions and the resulting steric repulsion between PEG chains and PLL layers. Both chemisorbed PEG 750 and 2000 layers were equally capable in inhibiting any secondary structure specific interactions. The above interaction behaviour of PEG grafted chains with PLL layer is mainly attributed to the excluded volume mechanism of anti-fouling PEG coatings.

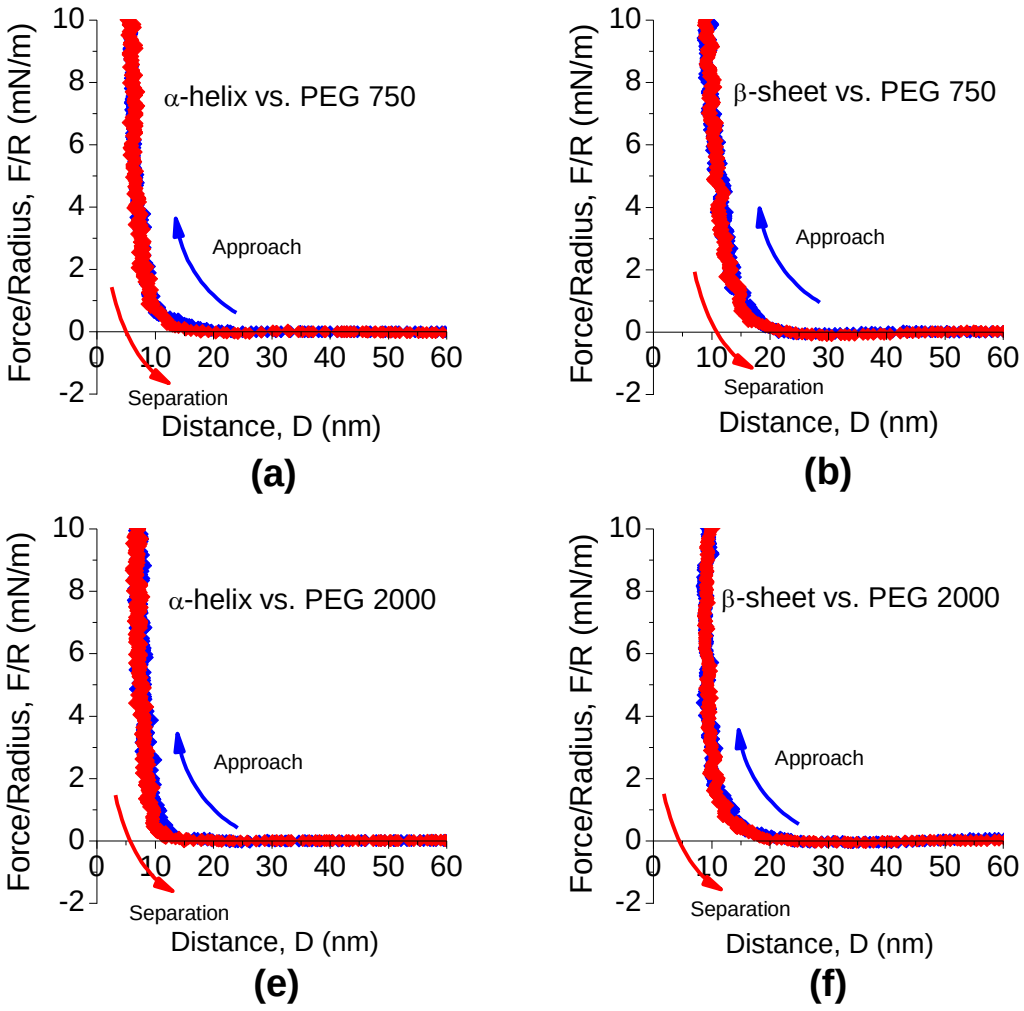

Figure 4.11 Representative approaching (in) and separating (out) normal force (normalized by the radius R of the surfaces) measured between a mica surface coated by α-helix (**a**, **c**) or β-sheet PLL (b, d) and a chemisorbed thiolated PEG MW 750 on Au (**a**, **b**), and chemisorbed thiolated PEG MW 2000 on Au (**c**, **d**) as a function of distance (corresponding to the schematic drawing in Figure 4.1f) at 10 mM potassium phosphate solution with 5 mM Na_2SO_4 at pH 10.6, T 37ºC.

Table 4.2 Confined thickness (CT) and fitted parameters of Alexnder-de Gennes theory for force-distance profiles of PLL or PEG layers in 10 mM potassium phosphate solution with different concentrations of Na_2SO_4 at pH 10.6, T 37ºC. Data are mean value ± standard deviation of 6 measurements.

Layers	[Na_2SO_4] (mM)		Asymmetric	Symmetric
α-helix PLL	5	L (nm)	7.1±0.3	6.8±0.3
		s (nm)	3.0±0.1	3.0±0.1
		CT (nm)	2.6±0.3	6.0±0.4
	50	L (nm)	7.2±0.3	6.5±0.3
		s (nm)	2.9±0.1	2.9±0.1
		CT (nm)	2.5±0.2	6.2±0.1
	500	L (nm)	7.3±0.3	6.9±0.4
		S (nm)	2.8±0.1	3.0±0.2
		CT (nm)	2.9±0.2	6.7±0.4
β-sheet PLL	5	L (nm)	12.3±0.3	12.6±0.4
		s (nm)	2.6±0.1	2.7±0.2
		CT (nm)	6.6±0.3	15.3±0.4
	50	L (nm)	11.2±0.4	10.5±0.4
		s (nm)	2.8±0.2	2.6±0.2
		CT (nm)	5.7±0.3	13.3±0.4
	500	L (nm)	10.3±0.4	9.5±0.4
		s (nm)	2.9±0.2	2.6±0.3
		CT (nm)	4.8±0.3	11.1±0.5
PEG 750	5	L (nm)	3.9±0.5	-
		s (nm)	2.3±0.2	-
		CT (nm)	2.2±0.3	-
PEG 2000	5	L (nm)	9.8±0.9	-
		s (nm)	4.3±0.2	-
		CT (nm)	3.7±0.4	-
α-helix PLL-PEG 750	5	CT (nm)	6.1±0.2	-
α-helix PLL-PEG 2000	5	CT (nm)	7.2±0.2	-
β-sheet PLL-PEG 750	5	CT (nm)	9.3±0.2	-
β-sheet PLL-PEG 2000	5	CT (nm)	10.1±0.4	-

4.4 Conclusion

PLL based α-helices and β-sheets were prepared to study the effect of secondary structure content of a protein on its interaction with different substrates. Through CD studies it was found that secondary structure of PLL was formed in solution and maintained upon adsorption on quartz surface. AFM imaging suggested that secondary structure specific interactions of PLL influenced the surface coverage and morphology of the adsorbed PLL. Surface forces study suggested that the secondary structure of PLL determines PLL layer thickness and surface adhesion. The stronger adhesion of β-sheet PLL vs. Au was attributed to the stronger electrostatic interaction of β-sheet PLL with Au surface as well as the flat surface geometry of the β-sheet PLL and the constructive alignment of the lysine side chains. Similar adhesion forces observed during surface forces measurement of β-sheet vs. β-sheet PLL was due to the hydrogen bonding between the opposing $–NH_2$ groups of the aligned lysine side chains. The decay in the adhesion energy upon increasing salt concentration was the result of weakened electrostatic interactions (PLL vs. Au system) and hydrogen bonding between $–NH_2$ groups of the opposing PLL side chains (PLL vs. PLL system). The interaction of PLL vs. Au and PLL vs. PLL layers were fitted using AdG and DLVO theories which suggested the dominance of steric repulsion during approach in all systems. The reversible repulsive force in the PEG vs. mica system revealed that the chemisorbed PEG layers act as a brush layer of swollen chains (as suggested by AdG fitting) which could eliminate the secondary structure effect of PLL to the point that no adhesion was observed between PLL and PEG layers.

4.5 References

[1] Anderson, JM, Bonfield, TL, and Ziats, NP. Protein adsorption and cellular adhesion and activation on biomedical polymers. Int. J. Artif. Organs, 1990;13:375-382.

[2] Andrade, JD and Hlady, V. Plasma protein adsorption: the big twelve. Ann. N. Y. Acad. Sci., 1987;516:158-172.

[3] Nath, N, Hyun, J, Ma, H, and Chilkoti, A. Surface engineering strategies for control of protein and cell interactions. Surf. Sci., 2004;570:98-110.

[4] Pankowsky, DA, Ziats, NP, Topham, NS, Ratnoff, OD, and Anderson, JM. Morphologic characteristics of adsorbed human plasma-proteins on vascular grafts and biomaterials. J. Vasc. Surg., 1990;11:599-606.

[5] Shen, M, Garcia, I, Maier, RV, and Horbett, TA. Effects of adsorbed proteins and surface chemistry on foreign body giant cell formation, tumor necrosis factor alpha release and procoagulant activity of monocytes. J. Biomed. Mater. Res., Part A, 2004;70A:533-541.

[6] Hlady, V, VanWagenen, RA, and Andrade, JD. Total internal reflection intrinsic fluorescence (TIRIF) spectroscopy applied to protein adsorption, in Surface and Interfacial Aspects of Biomedical Polymers J.D. Andrade, Editor. 1985, Plenum Press, New York, NY, USA, . 81-119.

[7] Collier, TO and Anderson, JM. Protein and surface effects on monocyte and macrophage adhesion, maturation, and survival. J. Biomed. Mater. Res., 2002;60:487-496.

[8] Evans-Nguyen, KM, Fuierer, RR, Fitchett, BD, Tolles, LR, Conboy, JC, and Schoenfisch, MH. Changes in adsorbed fibrinogen upon conversion to fibrin. Langmuir, 2006;22:5115-5121.

[9] Heuberger, M, Drobek, T, and Spencer, ND. Interaction forces and morphology of a protein-resistant poly(ethylene glycol) layer. Biophys. J., 2005;88:495-504.

[10] Hu, W-J, Eaton, JW, Ugarova, TP, and Tang, L. Molecular basis of biomaterial-mediated foreign body reactions. Blood, 2001;98:1231-1238.

[11] Lu, DR and Park, K. Effect of surface hydrophobicity on the conformational changes of adsorbed fibrinogen. J. Colloid Interface Sci., 1991;144:271-281.

[12] Absolom, DR, Zingg, W, Policova, Z, and Neumann, AW. Determination of the surface tension of protein coated materials by means of the advancing solidification front technique. ASAIO J., 1983;29:146-151.

[13] Andrade, JD, Hlady, VL, and Vanwagenen, RA. Effects of plasma-protein adsorption on protein conformation and activity. Pure Appl. Chem., 1984;56:1345-1350.

[14] Dadsetan, M, Jones, JA, Hiltner, A, and Anderson, JM. Surface chemistry mediates adhesive structure, cytoskeletal organization, and fusion of macrophages. J. Biomed. Mater. Res., Part A, 2004;71A:439-448.

[15] Statz, AR, Meagher, RJ, Barron, AE, and Messersmith, PB. New peptidomimetic polymers for antifouling surfaces. J. Am. Chem. Soc., 2005;127:7972-7973.

[16] Dalsin, JL and Messersmith, PB. Bioinspired antifouling polymers. Materials Today, 2005;8:38-46.

[17] Vladkova, TG. Surface engineered polymeric biomaterials with improved biocontact properties. Int. J. Polym. Sci., 2010;2010:1-22.

[18] Ball, V. Adsorption behavior of different polypeptides in the 3 kDa molecular weight range at an Si0.8Ti0.2O2-aqueous solution interface from low ionic strength solutions. Colloids Surf., B, 2004;33:129-142.

[19] Yang, Q, Kaul, C, and Ulbricht, M. Anti-nonspecific protein adsorption properties of biomimetic glycocalyx-like glycopolymer layers: effects of glycopolymer chain density and protein size. Langmuir, 2010;26:5746-5752.

[20] Chen, SF, Li, LY, Zhao, C, and Zheng, J. Surface hydration: Principles and applications toward low-fouling/nonfouling biomaterials. Polymer, 2010;51:5283-5293.

[21] Jordan, CE and Corn, RM. Surface plasmon resonance imaging measurements of electrostatic biopolymer adsorption onto chemically modified gold surfaces. Anal. Chem., 1997;69:1449-1456.

[22] Ramsden, JJ and Prenosil, JE. Effect of ionic-strength on protein adsorption-kinetics. J. Phys. Chem., 1994;98:5376-5381.

[23] Norde, W and Lyklema, J. The adsorption of human plasma albumin and bovine pancreas ribonuclease at negatively charged polystyrene surfaces: I. Adsorption isotherms. Effects of charge, ionic strength, and temperature. J. Colloid Interface Sci., 1978;66:257-265.

[24] Elgersma, AV, Zsom, RLJ, Lyklema, J, and Norde, W. Kinetics of single and competitive protein adsorption studied by reflectometry and streaming potential measurements. Colloids Surf., 1992;65:17-28.

[25] Meder, F, Daberkow, T, Treccani, L, Wilhelm, M, Schowalter, M, Rosenauer, A, Mädler, L, and Rezwan, K. Protein adsorption on colloidal alumina particles functionalized with amino, carboxyl, sulfonate and phosphate groups. Acta Biomater., 2012;8:1221-1229.

[26] Wong, SY, Han, L, Timachova, K, Veselinovic, J, Hyder, MN, Ortiz, C, Klibanov, AM, and Hammond, PT. Drastically lowered protein adsorption on microbicidal hydrophobic/hydrophilic polyelectrolyte multilayers. Biomacromolecules, 2012;13:719-726.

[27] Deligianni, DD, Katsala, N, Ladas, S, Sotiropoulou, D, Amedee, J, and Missirlis, YF. Effect of surface roughness of the titanium alloy Ti-6Al-4V on human bone marrow cell response and on protein adsorption. Biomaterials, 2001;22:1241-1251.

[28] Leckband, D and Israelachvili, J. Molecular basis of protein function as determined by direct force measurements. Enzyme Microb. Technol., 1993;15:450-459.

[29] Israelachvili, JN. Force- Measuring Techniques, in Intermolecular and surface forces. 2010, Academic Press: San Diego. 223-252.

[30] Leckband, D and Israelachvili, J. Intermolecular forces in biology. Q. Rev. Biophys., 2001;34:105-267.

[31] Unsworth, LD, Sheardown, H, and Brash, JL. Protein resistance of surfaces prepared by sorption of end-thiolated poly(ethylene glycol) to gold: Effect of surface chain density. Langmuir, 2005;21:1036-1041.

[32] Valentini, M, Napoli, A, Tirelli, N, and Hubbell, JA. Precise determination of the hydrophobic/hydrophilic junction in polymeric vesicles. Langmuir, 2003;19:4852-4855.

[33] Lee, JH, Lee, HB, and Andrade, JD. Blood compatibility of polyethylene oxide surfaces. Prog. Polym. Sci., 1995;20:1043-1079.

[34] Li, LY, Chen, SF, Zheng, J, Ratner, BD, and Jiang, SY. Protein adsorption on oligo(ethylene glycol)-terminated alkanethiolate self-assembled monolayers: The molecular basis for nonfouling behavior. J. Phys. Chem. B, 2005;109:2934-2941.

[35] Abe, T, Kurihara, K, Higashi, N, and Niwa, M. Direct Measurement of Surface Forces between Monolayers of Anchored Poly(L-glutamic acid). J. Phys. Chem., 1995;99:1820-1823.

[36] Hayashi, S, Abe, T, Higashi, N, Niwa, M, and Kurihara, K. Polyelectrolyte Brush Layers Studied by Surface Forces Measurement: Dependence on pH and Salt Concentrations and Scaling. Langmuir, 2002;18:3932-3944.

[37] Kurihara, K, Abe, T, Higashi, N, and Niwa, M. Steric forces between brush layers of poly(l-glutamic acid) and their dependence on secondary structures as determined by FT-IR spectroscopy. Colloids. Surf. A Physicochem. Eng. Asp., 1995;103:265-272.

[38] Klein, J and Luckham, PF. Long-range attractive forces between 2 mica surfaces in an aqueous polymer solution. Nature, 1984;308:836-837.

[39] Luckham, PF and Klein, J. Forces between mica surfaces bearing adsorbed polyelectrolyte, poly-L-lysine, in aqueous media. J. Chem. Soc., Faraday Trans. 1 F, 1984;80:865-878.

[40] Binazadeh, M, Zeng, H, and Unsworth, LD. Effect of peptide secondary structure on adsorption and adsorbed film properties. Acta Biomater., 2013;9:6403-6413.

[41] Binazadeh, M, Kabiri, M, and Unsworth, LD. Poly(ethylene glycol) and Poly(carboxy betaine) Based Nonfouling Architectures: Review and Current Efforts, in Proteins at Interfaces III: State of the Art, T. Horbett, J.L. Brash, and W. Norde, Editors. 2012. 621-643.

[42] Barbosa, RV, Moraes, MAR, Gomes, AS, and Soares, BG. EVA-based graft-copolymers as compatibilizing agents for polymer blends. J. Macromol. Sci., Part A: Pure Appl. Chem., 1995;A32:663-669.

[43] Du, YJ and Brash, JL. Synthesis and characterization of thiol-terminated poly(ethylene oxide) for chemisorption to gold surface. J. Appl. Polym. Sci., 2003;90:594-607.

[44] Chiou, J-S, Tatara, T, Sawamura, S, Kaminoh, Y, Kamaya, H, Shibata, A, and Ueda, I. The [alpha]-helix to [beta]-sheet transition in poly(L-lysine): Effects of anesthetics and high pressure. Biochim. Biophys. Acta, Protein. Struct. Mol. Enzymol., 1992;1119:211-217.

[45] Kingshott, P, Thissen, H, and Griesser, H. Effects of cloud-point grafting, chain length, and density of PEG layers on competitive adsorption of ocular proteins J. Biomaterials, 2002;23:2043.

[46] Dormidontova, EE. Role of competitive PEO-water and water-water hydrogen bonding in aqueous solution PEO behavior. Macromolecules, 2002;35:987-1001.

[47] Chittchang, M, Alur, HH, Mitra, AK, and Johnston, TP. Poly(L-lysine) as a model drug macromolecule with which to investigate secondary structure and membrane transport, part I: physicochemical and stability studies. J. Pharm. Pharmacol., 2002;54:315-323.

[48] Yang, H, Fung, SY, Pritzker, M, and Chen, P. Modification of Hydrophilic and Hydrophobic Surfaces Using an Ionic-Complementary Peptide. PLoS One, 2007;2.

[49] Van, J-N, Menezes, JL, and Sharma, M. Wettability alteratio due to interactions with oil-based muds and mud components. in 63rd Annual Technical Conference and Exhibition of the Society of Petroleum Engineers. 1988. Houston TX: Society of Petroleum Engineers.

[50] Israelachvili, JN. Van der Waals Forces between Particles and Surfaces, in Intermolecular and surface forces. 2010, Academic Press: San Diego. 253-289.

[51] Wolkers, WF, van Kilsdonk, MG, and Hoekstra, FA. Dehydration-induced conformational changes of poly--lysine as influenced by drying rate and carbohydrates. Biochim. Biophys. Acta, Gen. Subj., 1998;1425:127-136.

[52] Israelachvili, JN. Thin film studies using multiple-beam interferometry. J. Colloid Interface Sci., 1973;44:259-272.

[53] Zeng, H, Tian, Y, Anderson, TH, Tirrell, M, and Israelachvili, JN. New SFA techniques for studying surface forces and thin film patterns induced by electric fields. Langmuir, 2008;24:1173-1182.

[54] Faghihnejad, A and Zeng, H. Fundamentals of Surface Adhesion, Friction, and Lubrication, in Polymer adhesion, friction, and lubrication, H. Zeng, Editor. 2013, John Wiley & Sons: Hoboken, New Jersey. 1-57.

[55] Andrews, DW and Ottensmeyer, FP. Electron-microscopy of the poly-L-Lysine alpha-helix. Ultramicroscopy, 1982;9:337-348.

[56] Demirdoven, N, Cheatum, CM, Chung, HS, Khalil, M, Knoester, J, and Tokmakoff, A. Two-dimensional infrared spectroscopy of antiparallel beta-sheet secondary structure. J. Am. Chem. Soc., 2004;126:7981-7990.

[57] Parson, WW. Circular Dichroism, in Modern Optical Spectroscopy: With Exercises and Examples from Biophysics and Biochemistry. 2009, Springer: New York. 307-334.

[58] Miles, AJ, Whitmore, L, and Wallace, BA. Spectral magnitude effects on the analyses of secondary structure from circular dichroism spectroscopic data. Protein Sci., 2005;14:368-374.

[59] Greenfield, NJ. Using circular dichroism spectra to estimate protein secondary structure. Nat. Protoc., 2006;1:2876-2890.

[60] Whitmore, L and Wallace, BA. Protein secondary structure analyses from circular dichroism spectroscopy: Methods and reference databases. Biopolymers, 2008;89:392-400.

[61] Myer, YP. The pH-Induced Helix-Coil Transition of Poly-L-lysine and Poly-L-glutamic Acid and the 238-mμ Dichroic Band. Macromolecules, 1969;2:624-628.

[62] Putnam, C. Protein calculator v3.3 2006 March 28, 2006; Available from: http://www.scripps.edu/~cdputnam/protcalc.html.

[63] Giesbers, M, Kleijn, JM, and Stuart, MAC. The electrical double layer on gold probed by electrokinetic and surface force measurements. J. Colloid Interface Sci., 2002;248:88-95.

[64] Grigsby, JJ, Blanch, HW, and Prausnitz, JM. Effect of secondary structure on the potential of mean force for poly--lysine in the [alpha]-helix and [beta]-sheet conformations. Biophys. Chem., 2002;99:107-116.

[65] Staahlberg, J, Joensson, B, and Horvath, C. Combined effect of coulombic and van der Waals interactions in the chromatography of proteins. Anal. Chem., 1992;64:3118-3124.

[66] Boström, M, Tavares, FW, Bratko, D, and Ninham, BW. Specific ion effects in solutions of globular proteins: comparison between analytical models and simulation. J Phys Chem B Condens Matter Mater Surf Interfaces Biophys, 2005;109:24489-94.

[67] Hofmeister, F. Zur Lehre von der Wirkung der Salze. Arch. Exp. Path. Pharm., 1888;24:247-260.

[68] Melander, WR, El Rassi, Z, and Horváth, C. Interplay of hydrophobic and electrostatic interactions in biopolymer chromatography : Effect of salts on the retention of proteins. J. Chromatogr. A, 1989;469:3-27.

[69] de Gennes, PG. Polymers at an interface; a simplified view. Adv. Colloid Interface Sci., 1987;27:189-209.

[70] Zhang, L, Zeng, H, and Liu, Q. Probing molecular and surface interactions of comb-type polymer polystyrene-graft-polyethylene oxide (PS-g-PEO) with an SFA. J. Phys. Chem. C, 2012;116:17554-17562.

[71] Chan, DYC. A simple algorithm for calculating electrical double layer interactions in asymmetric electrolytes-Poisson-Boltzmann theory. J. Colloid Interface Sci., 2002;245:307-310.

[72] Gregory, J. Interaction of unequal double-layers at constant charge. J. Colloid Interface Sci., 1975;51:44-51.

[73] Kristiansen, K, Zeng, H, Wang, P, and Israelachvili, JN. Microtribology of Aqueous Carbon Nanotube Dispersions. Adv. Funct. Mater., 2011;21:4555-4564.

[74] Vörös, J. The Density and Refractive Index of Adsorbing Protein Layers. Biophys. J., 2004;87:553-561.

[75] Dougherty, GM, Rose, KA, Tok, JBH, Pannu, SS, Chuang, FYS, Sha, MY, Chakarova, G, and Penn, SG. The zeta potential of surface-functionalized metallic nanorod particles in aqueous solution. Electrophoresis, 2008;29:1131-1139.

[76] Li, YQ, Tao, NJ, Pan, J, Garcia, AA, and Lindsay, SM. Direct measurement of interaction forces between colloidal particles using the scanning force microscope. Langmuir, 1993;9:637-641.

[77] Schweiss, R, Pleul, D, Simon, F, Janke, A, Welzel, PB, Voit, B, Knoll, W, and Werner, C. Electrokinetic Potentials of Binary Self-Assembled Monolayers on Gold: Acid−Base Reactions and Double Layer Structure. J. Phys. Chem. B, 2004;108:2910-2917.

[78] Claesson, PM and Golander, CG. Direct measurments of steric interactions between mica surfaces covered with electrostatically bound low molecular weight polyethylene oxide. J. Colloid Interface Sci., 1987;117:366-374.

[79] Hansen, PL, Cohen, JA, Podgornik, R, and Parsegian, VA. Osmotic properties of poly(ethylene glycols): Quantitative features of brush and bulk scaling laws. Biophys. J., 2003;84:350-355.

[80] Teraoka, I. Thermodynamics of Dilute Polymer Solutions, in Polymer Solutions: An Introduction to Physical Properties. 2002, John Wiley & Sons, Inc.: New York. 69-89.

[81] Unsworth, LD, Tun, Z, Sheardown, H, and Brash, JL. Chemisorption of thiolated poly(ethylene oxide) to gold: surface chain densities measured by ellipsometry and neutron reflectometry. J. Colloid Interface Sci., 2005;281:112-121.

5. Conclusions and Future Work

5.1 Major conclusions

In this work the effect of secondary structure of PLL, solution condition, and PEG grafting on PLL adsorption to an Au surface was investigated. CD results showed that secondary structure of PLL persists upon adsorption from solutions of different ionic strengths to Au, PEG 750, and 2000 layers chemisorbed on Au and quartz surfaces; which could be due to the hydrophilic nature of Au, PEG, and quartz surfaces and structure stabilizing property of PEG chains.

PLL adsorption studied by QCM-D revealed that secondary structure regulated the interaction between the PLL and Au surface and further affected adsorption rate, extent, and layer viscosity. Higher extent of adsorption in case of β-sheet PLL could be due to stronger intermolecular interactions among β-sheet PLLs. Noticeably higher viscosity of α-helix layers, compared with β-sheet PLL at the same physicochemical condition revealed the stiffer α-helix PLL adsorbed layer structure due to the secondary structure specific hydrogen bonding patterns between the amino acids residues of the PLL chain which resulted in a more compact α-helix PLL adsorbed layer structure. The interactions between PLL and Au in aqueous solutions (mainly electrostatic and van der Waals) were dependent on specific conformation of the PLL chain and presentation of local charges in solutions (secondary structure effect) and reduced upon an increase of the ion concentration and resulted in a decrease in the adsorbed amount.

Chemisorption of thiolated PEG chains on Au surface is diffusion limited at θ condition and produces brushes of highly extended chains of grafted PEG 750

and 2000. It was found that the chain density values were inversely proportional to the PEG MW (final chemisorbed PEG mass was almost independent of the polymer MW). Changing buffer from PBS (3.5 M, pH 7.4) to 10mM PB (5 mM Na_2SO_4, pH 10.6) further hydrated the chemisorbed PEG chains (salt effect). It is probable that some non-hydrogen bonded water molecules were associated with the highly extended chains of grafted polymers and incorporated into the hydration number calculation without being directly bonded to the polymer chains.

Final adsorbed amount of PLL onto chemisorbed PEG 2000 layer was almost independent of the secondary structure. It is thought lower viscosity of chemisorbed PEG 2000 layer (as compared with chemisorbed PEG 750 layer) contributes to its better overall performance by reducing the viscosity difference between PLL solution and PEG chemisorbed layer. Passivation of Au surface *via* chemisorption of PEG 750 and 2000 drastically suppressed rigidity of the adsorbed layer by elimination of direct interaction between unmodified Au surface and peptide chains resulting in similar layer viscosity for adsorbed PLL layers regardless of PLL secondary structure.

AFM imaging revealed the secondary structure specific surface coverage and morphology of the adsorbed PLL on Au substrate. Surface forces study suggested that the secondary structure of PLL determines its adsorbed layer thickness and surface adhesion. The stronger adhesion of β-sheet PLL vs. Au was attributed to the stronger electrostatic interaction of β-sheet PLL with Au surface as well as the flat surface geometry of the β-sheet PLL and the constructive

alignment of the lysine side chains. Adhesion forces observed during surface force measurement of β-sheet vs. β-sheet PLL was due to the hydrogen bonding between the opposing $–NH_2$ groups of the aligned lysine side chains. The decay in the adhesion energy upon increasing salt concentration was the result of weakened electrostatic interactions (PLL vs. Au system) and hydrogen bonding between $–NH_2$ groups of the opposing PLL side chains (PLL vs. PLL system). The interaction of PLL vs. Au and PLL vs. PLL layers were fitted using AdG and DLVO theories which suggested the dominance of steric repulsion during approach in all systems. The reversible repulsive force in the PEG vs. mica system revealed that the chemisorbed PEG layers act as a brush layer of swollen chains (as suggested by AdG fitting) which could eliminate the secondary structure effect of PLL to the point that no adhesion was observed between PLL and PEG layers.

5.2 Suggestions for future work

Results of this work provide new information about the adsorption mechanisms of proteins and could be used to develop better materials/coatings to control the non-specific adsorption of proteins. Future studies are required to further improve our understanding of the protein-surface interaction mechanisms. For the next step, secondary structures of peptides formed by different amino acids (other than poly L-Lysine chain) could be used to understand the primary structure influence. The effect of protein tertiary structures could also be studied by synthesis of a peptide chain which has different secondary structure domains. Surface forces studies of

immobilized proteins could also provide new information on the affinity of different proteins to the engineered surfaces.